Material Characterization of Lithium Ion Batteries for Crash Safety

by

Larie Alecia Brandy Dixon

B.S., North Carolina State University (2005)

Submitted to the Department of Mechanical Engineering
in partial fulfillment of the requirements for the degrees of

Naval Engineer

and

Master of Science in Mechanical Engineering

at the

MASSACHUSETTS INSTITUTE OF TECHNOLOGY

June 2015

Author ..... Signature redacted
Department of Mechanical Engineering
May 8, 2015

Certified by ..... Signature redacted .....
Tomasz Wierzbicki
Professor
Thesis Supervisor

Accepted by ..... Signature redacted .....
David E. Hardt
Chairman, Department Committee on Graduate Students

Material Characterization of Lithium Ion Batteries for Crash Safety

by

Larie Alecia Brandy Dixon

Submitted to the Department of Mechanical Engineering
on May 8, 2015, in partial fulfillment of the
requirements for the degrees of
Naval Engineer
and
Master of Science in Mechanical Engineering

Abstract

The safety of lithium-ion batteries is extremely important due to their widespread use in consumer products such as laptops and cell phones. Several cases of thermal runaway in lithium ion batteries that resulted in fires have been reported recently. And in the case of vehicle batteries, deformation during a crash event could cause an internal short circuit, leading to thermal runaway, fires, or toxic gas release. While much is understood about lithium-ion batteries, no comprehensive computational models exist to test and optimize these batteries before manufacture.

The objective of this research was to characterize the mechanical properties of three types of lithium-ion batteries through cell and interior component mechanical testing. Prismatic, elliptic, and pouch cells were tested using hemispherical punches to obtain load-displacement curves. Elliptic and pouch cells were also compression tested. Uniaxial, biaxial, and compression tests were performed on the interior components of elliptic and pouch cells. The test results were then used by Impact and Crashworthiness Laboratory team members to create, validate, and refine computational models.

This research resulted in many conclusions involving the lithium-ion cells, their interior components, and efforts to model the failure of cells. At the cell level, the effect of liquid presence, strain rate, separator type, and test location was studied. The level of experience in sample preparation and testing methods was an important result for interior component material characterization, as was the varied force-displacement results for different cell types. But most importantly, this work demonstrated that the material characterization of lithium-ion battery cells through mechanical testing could be used to create, calibrate, and validate cell numerical simulation models.

Thesis Supervisor: Tomasz Wierzbicki
Title: Professor

Acknowledgments

This thesis was completed with the support of many individuals. I would like to sincerely thank the following:

Professor Tomasz Wierzbicki for his leadership, guidance, and enthusiasm.

Dr. Elham Sahraei for her direction and collaboration on almost all aspects of this project.

The members of the Impact and Crashworthiness Laboratory for their instruction and assistance with testing events.

My husband, Michael Schafer, for his encouragement, support, and love.

Contents

1 Introduction **15**

1.1 Background 15

1.2 Summary of Impact and Crashworthiness Laboratory (ICL) Battery Research 17

1.3 Objective 18

1.4 Testing Equipment 18

1.5 General Description of Sample Preparation 21

2 Prismatic Battery Cells **25**

2.1 Test Details 26

2.2 Test Observations and Results 27

2.3 Summary and Application of Test Results 29

3 Elliptic Battery Cells **31**

3.1 Cell Tests 32

3.1.1 First Testing Event 33

3.1.2 Second Testing Event 37

3.2 Interior Component Tests 45

3.2.1 Uniaxial Test Details and Results 48

3.2.2 Biaxial Punch Test Details and Results 59

3.2.3 Compression Test Details and Results 66

3.2.4 Summary and Application of Test Results 69

4 Pouch Battery Cells **79**

4.1 Cell Tests 80

4.1.1 Pouch Dry Cell 80

4.1.2 Pouch Discharged Cell 86

4.2 Interior Component Tests 90

4.2.1 Uniaxial Test Details and Results 92

4.2.2 Biaxial Test Details and Results 97

4.2.3 Compression Test Details and Results 100

4.3 Summary and Application of Test Results 102

5 Conclusion **107**

5.1 Summary of Results 107

5.2 Conclusions 110

List of Figures

1-1 Examples of Lithium-ion Battery Cell Types 16
1-2 Lithium-ion Battery Structure 17
1-3 Instron Test Machine Model 5944 [2] 19
1-4 Instron Test Machine with Biaxial Punch 20
1-5 Typical Test Set-up on MTS Loading Frame 21
1-6 Uniaxial Sample Preparation 22
1-7 Aluminum Guiding Block 22
1-8 Biaxial Sample Preparation 23

2-1 Prismatic Battery 26
2-2 Punches and Enclosure for Prismatic Battery Tests 27
2-3 Prismatic Battery Force Results 28
2-4 Damage to Prismatic Cells 28
2-5 Prismatic Battery Resistance and Force Results 29

3-1 Elliptic Battery 31
3-2 Elliptic Cell Flat Plate Compression Test Setup 32
3-3 Elliptic Cell Punch Indentation Test Setup 33
3-4 Elliptic Cell transverse Compression Test Results 34
3-5 Compressed Elliptic Dry Cell 35
3-6 Compressed Elliptic Wet Cell 1 35
3-7 Compressed Elliptic Wet Cell 2 36
3-8 Elliptic Cell Hemispherical Punch Test Results from First Test Event 37
3-9 Elliptic Cell Damage from Punch Test 37

3-10 Elliptic Cell Axial Compression Test Setup 38
3-11 Elliptic Cell Hemispherical Punch Test Results 39
3-12 Elliptic Dry Cell 2 Hemispherical Punch Test Results 40
3-13 Elliptic Wet Cell 2 Hemispherical Punch Test Results 40
3-14 Elliptic Wet Cell Hemispherical Punch Test Results at Varying Rates 41
3-15 Elliptic Wet Cell Hemispherical Punch Test Results for 20 mm/min Rate Test 42
3-16 Elliptic Cell Axial Compression Test Results 43
3-17 Elliptic Cell Damage from Axial Compression Test 43
3-18 Elliptic Dry Cell Axial Compression Test Results 44
3-19 Elliptic Wet Cell Axial Compression Test Results 45
3-20 Copper Foil Sheets 46
3-21 Aluminum Foil Sheets 47
3-22 Elliptic Copper Uniaxial Test Results 48
3-23 Elliptic Copper Uniaxial Test Samples 49
3-24 Elliptic Aluminum Uniaxial Test Results- Rolling Direction 50
3-25 Elliptic Aluminum Uniaxial Test Results- 90° Direction 50
3-26 Elliptic Aluminum Uniaxial Test Samples 51
3-27 Elliptic Coated Metal Samples 52
3-28 Rolling Direction of Coated Sheets 53
3-29 Elliptic Anode Uniaxial Test Results- Rolling Direction 54
3-30 Elliptic Anode Uniaxial Test Results- 90° Direction 54
3-31 Elliptic Anode Uniaxial Test Samples 55
3-32 Elliptic Cathode Uniaxial Test Results- Rolling Direction 56
3-33 Elliptic Cathode Uniaxial Test Results- 90° Direction 56
3-34 Elliptic Cathode Uniaxial Test Samples 57
3-35 Elliptic Copper and Anode Uniaxial Test Comparison 58
3-36 Elliptic Aluminum and Cathode Uniaxial Test Comparison 58
3-37 Elliptic Copper Biaxial Test Results 59
3-38 Elliptic Copper Biaxial Test Samples 60

3-39 Elliptic Aluminum Biaxial Test Results 61
3-40 Elliptic Aluminum Biaxial Test Sample 5 61
3-41 Elliptic Anode Biaxial Test Results 62
3-42 Elliptic Cathode Biaxial Test Results 63
3-43 Elliptic Coated Metal Biaxial Test Samples 63
3-44 Elliptic Copper and Anode Biaxial Test Comparison 64
3-45 Elliptic Aluminum and Cathode Biaxial Test Comparison 64
3-46 Elliptic Copper Biaxial Retest Results 65
3-47 Elliptic Copper and Anode Biaxial Retest Comparison 66
3-48 Elliptic Coated Metal Compression Test Samples 67
3-49 Elliptic Anode Compression Test Results 68
3-50 Elliptic Cathode Compression Test Results 68
3-51 Elliptic Cell Model 72
3-52 Damaged Elliptic Cell Model 72
3-53 Elliptic Cell Hemispherical Punch Simulation and Test Results 72
3-54 Elliptic Anode Biaxial Punch Test Model 73
3-55 Elliptic Anode Biaxial Punch Simulation Contour Plots 74
3-56 Elliptic Anode Biaxial Punch Modeling Results 75
3-57 Elliptic Cathode Biaxial Punch Test Model 76
3-58 Elliptic Cathode Biaxial Punch Simulation Contour Plots 76
3-59 Elliptic Cathode Biaxial Punch Modeling Results 77

4-1 Pouch Battery 79
4-2 Pouch Dry Cell Compression Test Setup 80
4-3 Pouch Dry Cell Compression Test Results 81
4-4 Pouch Dry Cell Hemispherical Punch Test Setup 82
4-5 Pouch Dry Cell Hemispherical Punch Test 3 83
4-6 Location of Edge Indentations on Pouch Dry Cell 83
4-7 Pouch Dry Cell Hemispherical Punch Test Results at Varying Locations 84
4-8 Pouch Dry Cell Hemispherical Punch Test Results at Varying Rates . 85

4-9 Pouch Dry Cell Hemispherical Punch Test Results at Three Strain Rates 85
4-10 Interior Damage to Pouch Dry Cell 86
4-11 Pouch Discharged Cell Hemispherical Punch Test Setup 87
4-12 Pouch Discharged Cell Hemispherical Punch Test Results 88
4-13 Discharged Pouch Cell Hemispherical Punch Test Results at Varying Rates 89
4-14 Dry and Discharged Pouch Cell Hemispherical Punch Test Results at Varying Rates 90
4-15 Dry Pouch Cell Before and After Outer Shell Removal 91
4-16 Machine Direction of Coated Sheets from Pouch Cell 92
4-17 Pouch Anode Uniaxial Test Results- Rolling Direction 93
4-18 Pouch Anode Uniaxial Test Results- 90° Direction 94
4-19 Pouch Anode Uniaxial Test Samples 94
4-20 Pouch Cathode Uniaxial Test Results- Rolling Direction 95
4-21 Pouch Cathode Uniaxial Test Results- 90° Direction 96
4-22 Pouch Cathode Uniaxial Test Samples 97
4-23 Pouch Cathode Biaxial Punch Test Results 98
4-24 Pouch Anode Biaxial Test Sample 6 98
4-25 Pouch Cathode Biaxial Punch Test Results 99
4-26 Pouch Cathode Biaxial Test Sample 1 100
4-27 Pouch Anode Compression Test Results 101
4-28 Pouch Cathode Compression Test Results 101
4-29 Pouch Cell Model 103
4-30 Damaged Pouch Cell Model 103
4-31 Pouch Cell Hemispherical Punch Simulation and Test Results 104
4-32 Pouch Cell Hemispherical Punch Simulation on Cell Edge 105
4-33 Pouch Cell Hemispherical Punch Simulation and Test Results 105

List of Tables

2.1 Measured Dimensions and Voltages of Prismatic Cells 25

3.1 Elliptic Cell Sheet Thicknesses 47
3.2 Elliptic Cell Test Results 70
3.3 Elliptic Cell Interior Component Test Results 71

4.1 Pouch Cell Sheet Thicknesses 92
4.2 Pouch Cell Test Results 102
4.3 Pouch Cell Interior Component Test Results 102

5.1 Prismatic Cell Hemispherical Punch Test Results 108
5.2 Elliptic Cell Test Results 108
5.3 Pouch Cell Test Results 108
5.4 Elliptic Cell Interior Component Test Results 109
5.5 Pouch Cell Interior Component Test Results 109

Chapter 1

Introduction

1.1 Background

Lithium-ion batteries were introduced commercially by Sony in 1991, and over the past two decades, these batteries have become a part of daily life [1]. The reason is simple: the high energy density of lithium-ion batteries means smaller, lighter batteries and smaller, more powerful consumer electronics. Lithium-ion batteries also have a low self-discharge rate and no memory effect, meaning their energy capacity will not diminish over time if recharged without being fully discharged [9].

Because of the significant advantages of lithium-ion batteries, they are used in a variety of applications, from small electronics such as cell phones to electric vehicles and airplanes. And due to their varied uses, lithium-ion batteries come in an assortment of shapes and sizes. Examples of the cell types of lithium-ion batteries include cylindrical, pouch, and prismatic. Cylindrical cells are the most common type of packaging for batteries and feature a metal cylinder with positive and negative tabs on each end. Pouch cells have a flexible, thin sheet enclosure and achieve a 90-95% packing efficiency [10]. Prismatic cells are generally smaller than pouch cells, have a metal housing made of steel or aluminum, and are used in cell phones as well as vehicle applications. In Figure 1-1, cylindrical, prismatic, and pouch cells are illustrated.

(a) Cylindrical [6]

(b) Prismatic [3]

(c) Pouch [8]

Figure 1-1: Examples of Lithium-ion Battery Cell Types

All lithium-ion batteries have alternating layers of negative electrode, anode, and positive electrode, cathode, and a separator between the layers that allows lithium-ions to flow between them. Anode and cathode layers are metal foils with a coating on both sides. The anode is commonly a copper foil coated with graphite, and the cathode is typically made from an aluminum foil coated with some type of lithium metal oxide. The separator is a thin polymer sheet, usually either polypropylene, polyethylene or a layered structure of the two polymers. These anode, cathode, and separator layers are either rolled or stacked, housed in an enclosure, and surrounded by an electrolyte such as lithium hexafluorophosphate (LiPF6) dissolved in a solution. Figure 1-2 shows a simple diagram of a lithium-ion battery cell structure [4]. Individual battery cells are then connected and housed together to form battery packs.

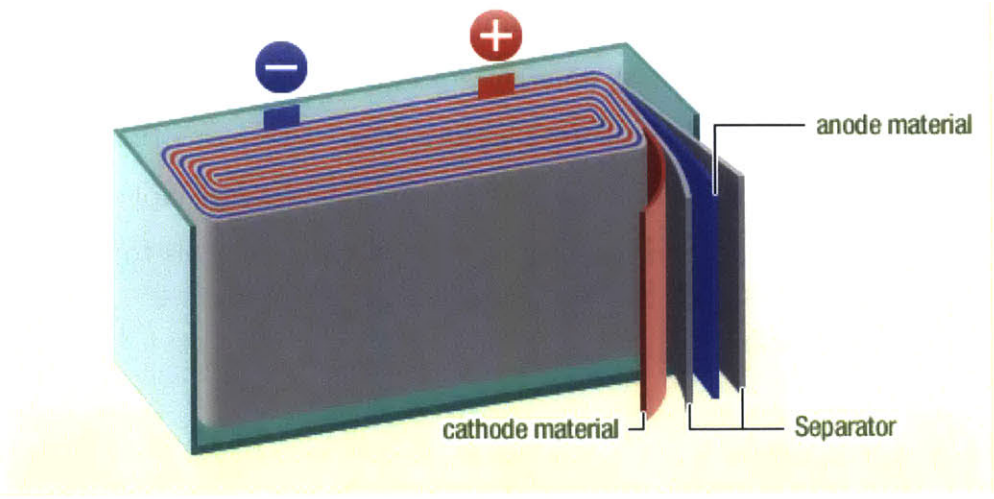

Figure 1-2: Lithium-ion Battery Structure

The safety of lithium-ion batteries is extremely important due to their widespread use in consumer products. Recently, several computer companies have recalled their products due to lithium-ion battery fires caused by overheating [7, 5]. And in the case of vehicle batteries, deformation during a crash event could cause an internal short circuit, leading to thermal runaway, fires, or toxic gas release. While much is understood about lithium-ion batteries, no comprehensive computational models exist to predict their safety and optimize these batteries before manufacture.

1.2 Summary of Impact and Crashworthiness Laboratory (ICL) Battery Research

The overall battery research of the Impact and Crashworthiness Laboratory (ICL) at MIT has been focused on understanding the lithium-ion battery's mechanical properties so that individual battery cells and battery packs can be characterized during crash events. This work began in 2010 with the mechanical testing of small cylindrical and pouch cells to develop a finite element model of a lithium-ion cell using representative volume elements (RVE). The first RVE models used a crushable foam to represent the interior of the battery [13, 12, 16], but subsequent models incorporated the characteristics of the individual layers [14, 17]. Mechanical testing of batteries

by the ICL included compression, indentation, and three-point bending of different sizes and types of batteries and at different states of charge (SOC). Tensile, biaxial punch, compression and other tests were performed on battery interior components, including individual anode, cathode, separator, and multilayer samples. All test results were incorporated into new or existing computational models to further refine and validate them.

1.3 Objective

The objective of this research was to characterize the mechanical properties of Lithium-ion batteries through mechanical testing of three types of battery cells, elliptic, prismatic, and pouch, and their interior components. Elliptic cells are a type of cylindrical cell with a more rectangular shape. All three cell types were tested with hemispherical punches, and the pouch and elliptic cells were compressed using cylindrical punches or flat plates. The interior copper, aluminum, cathode, and anode sheets of elliptic and pouch cells were subjected to uniaxial tension, biaxial punch, and compression testing. The results were used to further refine and validate high-level, robust, and accurate computational tools to predict strength, energy absorption, and the onset of electric short circuit of batteries under real-world crash loading situations.

The material characterization of the separator material for each cell type was performed concurrently by another ICL team member, Xiaowei Zhang. The interior separator sheets were subjected to uniaxial tension, biaxial punch, and compression testing. The results of this testing were also incorporated into the ICL cell models.

1.4 Testing Equipment

For testing conducted in the ICL, two machines, Instron Test Machine Model 5944 and MTS Loading Frame, were primarily used. Uniaxial and biaxial testing of the anode, cathode, and other interior cell components was completed with the Instron

machine, while the MTS machine was used for whole cell compression and indentation tests. The MTS machine was also used for interior component compression tests.

The Instron machine was fitted with a 100 N load cell and two 2 kN pneumatic grips with 25 mm by 32 mm rubber grip faces for uniaxial tests. For biaxial testing, a mount was developed by Xiaowei Zhang of the ICL to hold circular samples, and a smooth spherical metal punch with a diameter of 25 mm was attached to the Instron machine. Bluehill© 3 software measured the force and displacement during testing with the Instron machine. Figure 1-3 shows the Instron Test Machine Model 5944 and the pneumatic grip. The Instron machine with biaxial punch attachments is in Figure 1-4.

(a) Instron Test Machine with Grips (b) Close-up View of Grip

Figure 1-3: Instron Test Machine Model 5944 [2]

Figure 1-4: Instron Test Machine with Biaxial Punch

The MTS Loading Frame is a displacement-controlled 200 kN machine with a crosshead speed range of 0.1 mm/min to 1000 mm/min. The MTS machine was fitted with flat plates and flat cylindrical punches for compression tests and hemispherical punches for indentation tests. Testworks© 4 software measured the force and recorded the displacement.

In addition to the two test machines mentioned above, other equipment was used to conduct testing of cells and interior components. An Imaging Retiga 1300i digital camera and Vic-Snap™ and Vic-2D™ digital image correlation (DIC) software recorded and calculated the displacement or strain from specimens that were speckled with paint. For full cell tests, a RadioShack© 46-Range Digital Multimeter and Meterview software recorded voltage and resistance, and the Omega© HH176 thermometer with 5SRTC thermocouple and Temp Monitor software measured temperature. In order to ensure safety during full cell tests, an enclosure with ventilation

fan and an extension rod for the MTS machine were also used. Figure 1-5 shows a typical test set-up with a battery cell in the enclosure on the MTS Loading Frame, the multimeter connected to the battery, and the camera recording the test.

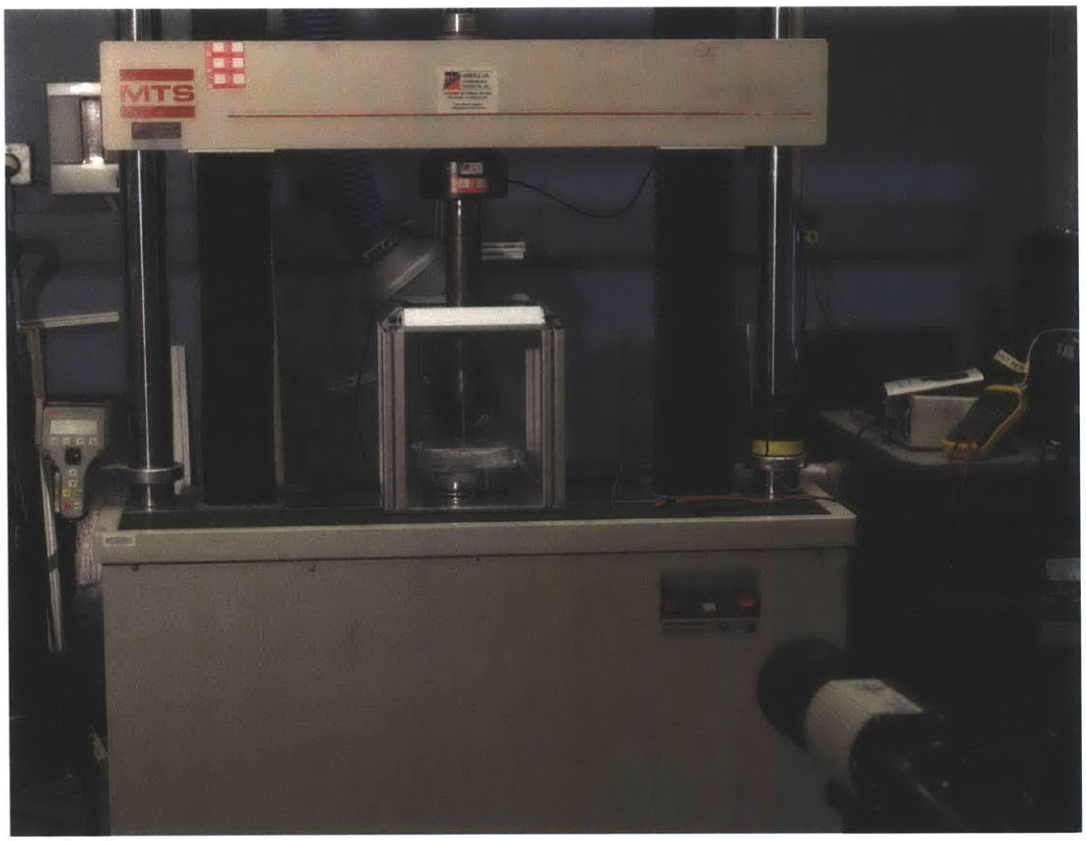

Figure 1-5: Typical Test Set-up on MTS Loading Frame

1.5 General Description of Sample Preparation

For uniaxial testing of the batteries' interior components, the samples were prepared by cutting small strips of each material. Many different methods of cutting with different types of X-Acto© knifes were examined. The best method was cutting the samples with a straight-edge X-Acto© knife between two sheets of lined graph paper, using a metal ruler as a straight-edge. This method was also used in separator testing by Sheidaei et al [15]. All strips were cut 10 mm in width and 85 mm in length. Figure 1-6 shows coated metal samples after cutting between graph paper.

Figure 1-6: Uniaxial Sample Preparation

The grip closure pressure of the Instron machine caused the cathode and anode samples to crack inside the grips. In order to avoid this issue, paper tape was placed on the ends of the samples. The tape was the same width as the grips and was placed on the sample to ensure the sample area inside the grips was covered. A simple aluminum guiding block, Figure 1-7, was machined to assist in applying tape to the samples.

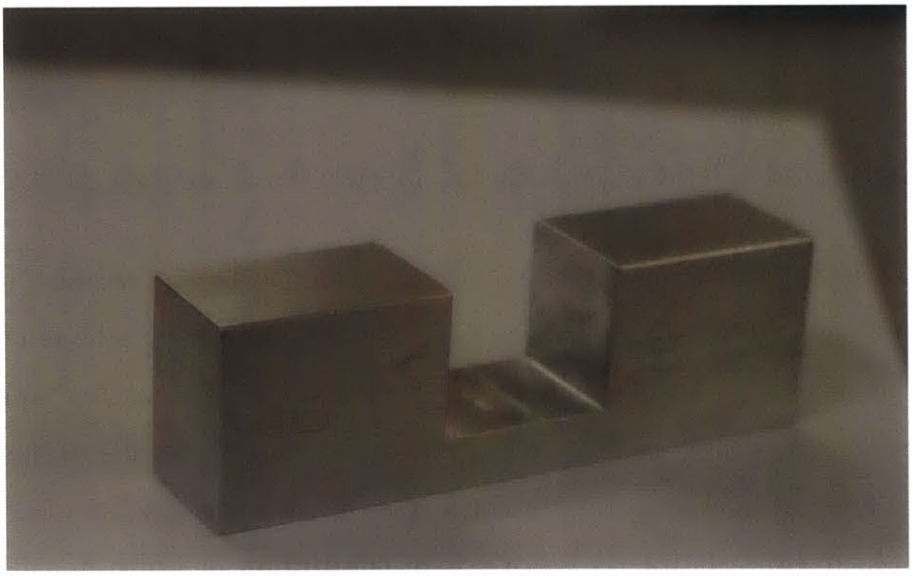

Figure 1-7: Aluminum Guiding Block

The fixture for biaxial testing required circular samples with a 45 mm diameter, so the sheets of battery component material were cut into circular shapes using either a straight-blade X-Acto © knife and a metal cylinder as a mold or a circular metal punch and hammer. The sheets were sandwiched between paper during cutting with the knife. Figure 1-8 shows the preparation of biaxial samples using the metal punch and hammer.

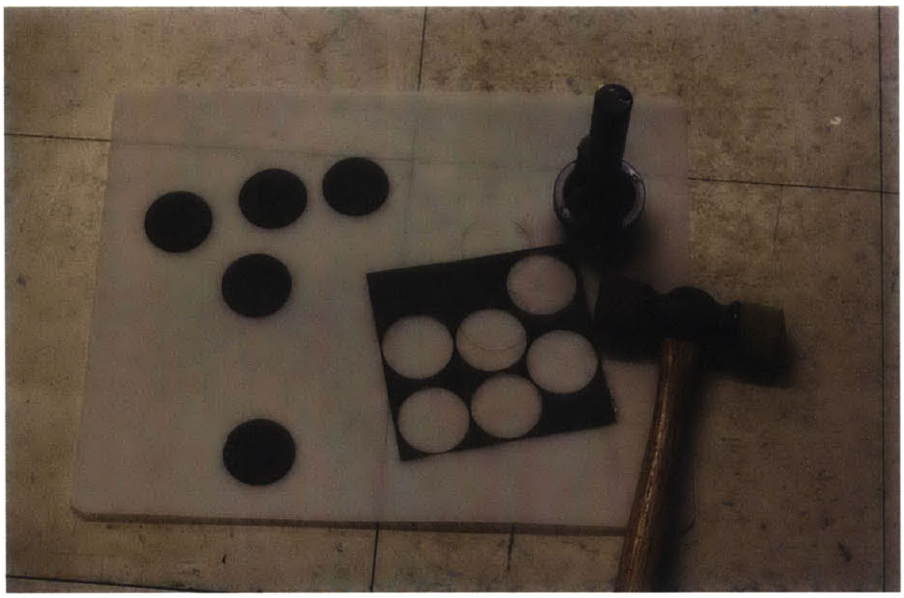

Figure 1-8: Biaxial Sample Preparation

For compression testing, a circular metal punch of 16 mm diameter and hammer were used to cut samples from the battery component sheets. The sheets were layered between paper during sample preparation to prevent flaking of coated metal sheets. The sheets were also marked to ensure samples could be aligned during testing.

Chapter 2

Prismatic Battery Cells

As mentioned in Chapter 1, prismatic lithium-ion battery cells usually have an aluminum housing and a layered or rolled cathode, anode, and separator internal structure. For this research, three discharged prismatic batteries were tested with three different hemispherical punches. No interior component testing was conducted. Table 2.1 contains the measured dimensions and voltages of the three batteries, and Figure 2-1 shows the battery with approximate dimensions. Each cell had a slightly bulged shape, with a measured thickness in the center of approximately 32 mm.

Battery	**Length (mm)**	**Width (mm)**	**Thickness (mm)**	**Voltage (mV)**
1	90.84	147.78	27.04	2.0
2	90.88	147.75	27.01	2.6
3	90.95	147.78	27.00	2.8

Table 2.1: Measured Dimensions and Voltages of Prismatic Cells

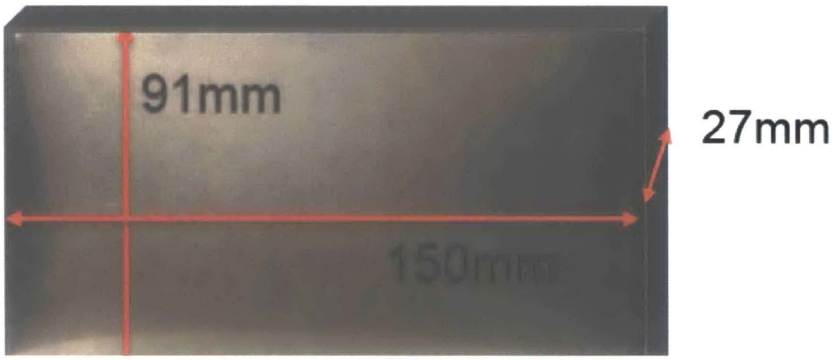

Figure 2-1: Prismatic Battery

2.1 Test Details

Using the MTS Loading Frame and three hemispherical punches with diameters of 12.5 mm, 28.575 mm, and 44.45 mm, the prismatic cells were indented at a rate of 1.0 mm/min. The multimeter was attached to the cell leads to measure resistance. The resistance measurement for this testing was used as a method to observe short circuit, but the resistance measurement values were not considered relevant due to the interaction between the prismatic battery and the multimeter. And because these batteries were discharged but still contained electrolyte, safety precautions included wearing masks, gloves, and goggles, using an enclosure fitted with exhaust fan, and placing each cell in a plastic bag. In addition, SOLUSORB®, a solvent absorbent, was positioned near enclosure in case of electrolyte leakage. The three hemispherical punches and the enclosure of the test set-up are shown in Figure 2-2.

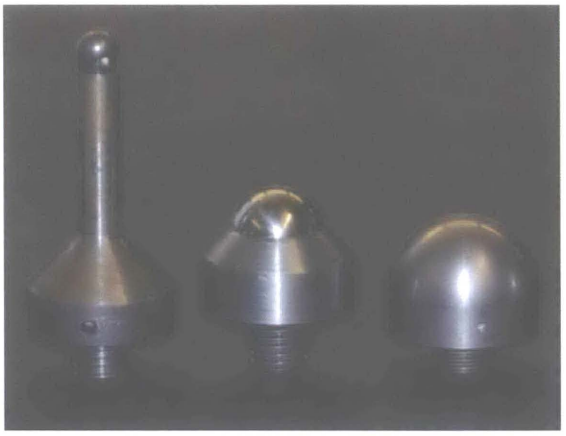

(a) Hemispherical Punches

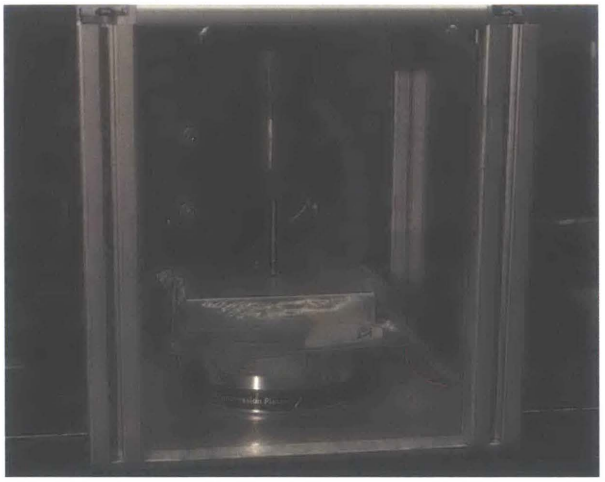

(b) Test Enclosure

Figure 2-2: Punches and Enclosure for Prismatic Battery Tests

2.2 Test Observations and Results

Cells 1, 2, and 3 were indented with the hemispherical punches of diameters 12.5 mm, 28.575 mm, and 44.45 mm, respectively. Figure 2-3 displays the resulting force versus crosshead displacement for all three cells. The graph shows that increasing punch diameter correlated with increasing maximum force. This result was expected since a larger punch diameter meant that a larger area of the cell was being compressed. The punch with the smallest diameter, 12.5 mm, had a maximum force of 4.7 kN at a crosshead of 4.6 mm. The punch with 28.575 mm diameter had a maximum force of 13.8 kN at 6.3 mm, and the largest punch with a diameter of

44.45 mm had a maximum force of 29.5 kN at 7.5 mm. The damage to each cell is displayed in Figure 2-4.

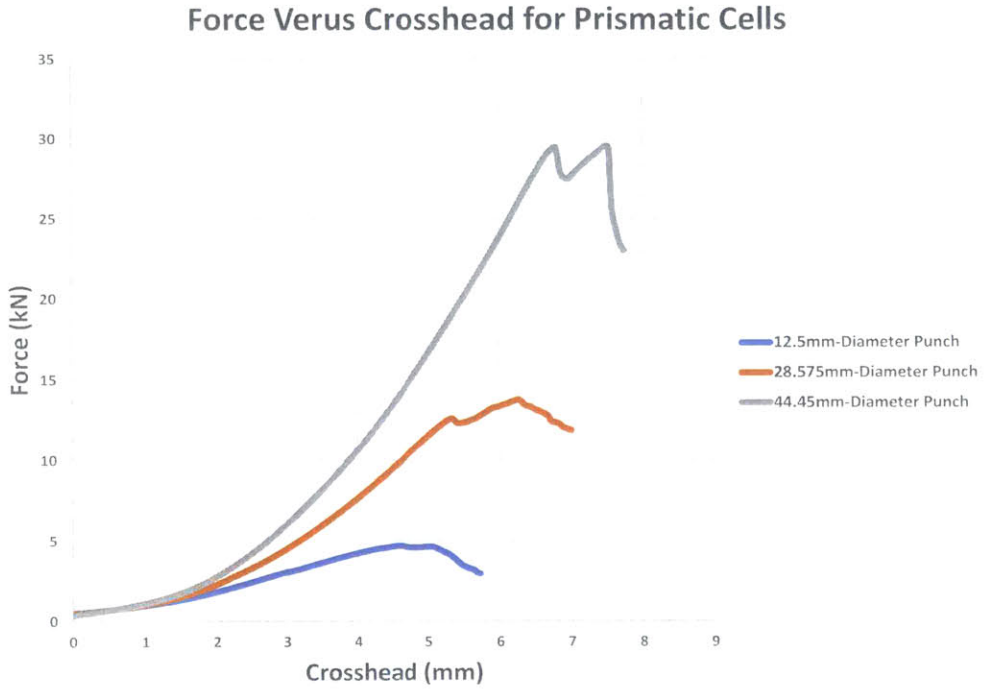

Figure 2-3: Prismatic Battery Force Results

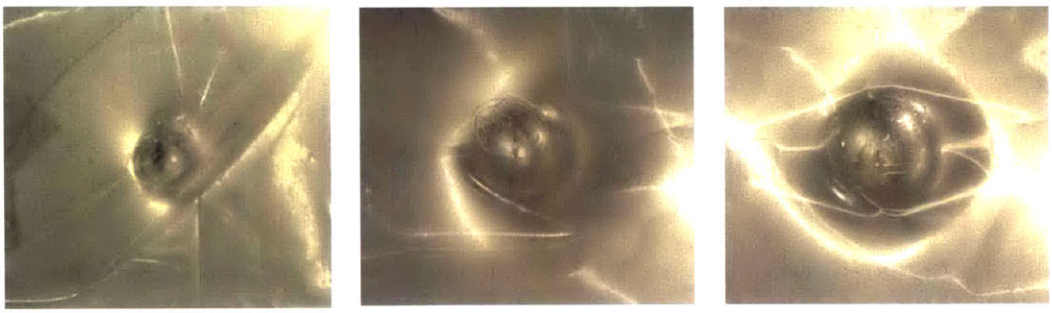

(a) Cell 1 (b) Cell 2 (c) Cell 3

Figure 2-4: Damage to Prismatic Cells

For all three cells, a drop in resistance coincided with a peak in force and represents the short-circuit of the cell. For the 12.5 mm diameter punch test, the resistance drop occurred before the peak load. Because the cells were discharged prior to the testing, damage could have existed in the cell and produced this early short circuit through

non-mechanical means. Another explanation could be that the small diameter punch produced localized damage and a short circuit before the punch breaks through the housing and cell layers completely. No conclusions could be drawn from this one test event. Figure 2-5 is a graph of the resistance and force versus crosshead displacement results.

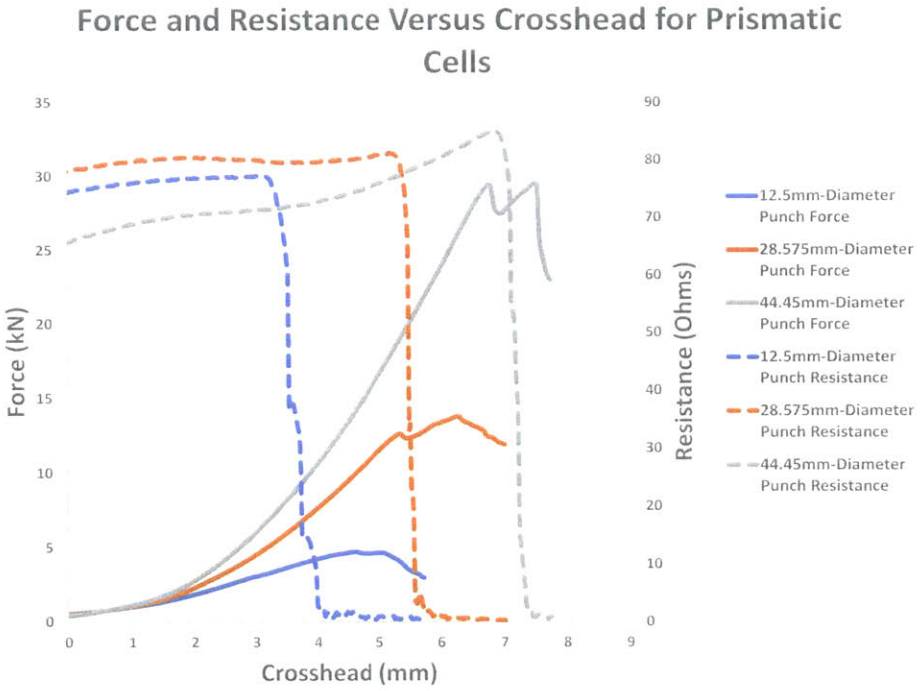

Figure 2-5: Prismatic Battery Resistance and Force Results

2.3 Summary and Application of Test Results

The hemispherical tests of the prismatic cells showed increasing maximum force and crosshead with increasing punch diameter. The prismatic cell tests also exhibited short circuit near the point of maximum force. The interior component tests and cell modeling was not completed during the course of this research but will be performed in the future.

Chapter 3

Elliptic Battery Cells

Elliptic lithium-ion battery cells are a type of cylindrical cells with a rolled interior component structure, called the jellyroll, and metal housing. Elliptic cells have the shape of a flattened cylindrical cell. Eleven elliptic cells and sheets of copper and aluminum foil, cathode, and anode were donated by ICL sponsors for testing. The cells were compression and hemispherical punch tested, and the interior component sheets were uniaxial, biaxial, and compression tested. Figure 3-1 shows the battery with approximate dimensions.

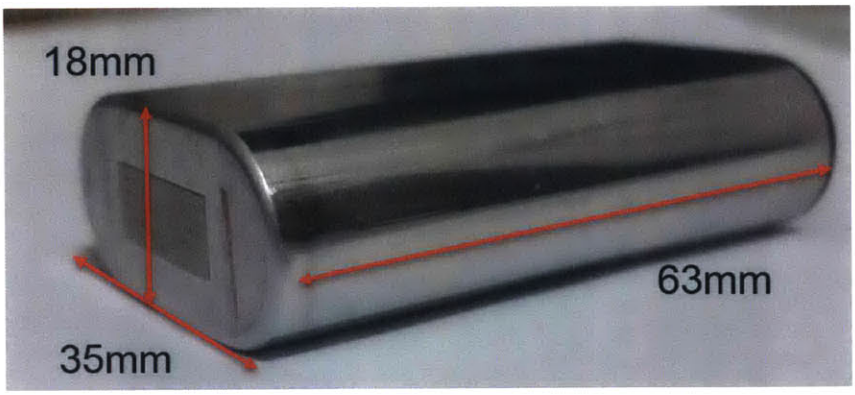

Figure 3-1: Elliptic Battery

3.1 Cell Tests

The cell tests were conducted in two separate testing events, with six cells tested in the first event and five tested in the second. The eleven elliptic cells included five with no electrolyte and six filled with polycarbonate instead of electrolyte. The polycarbonate was an inert liquid filler used for safety purposes. The cells with no electrolyte were referred to as "dry", and the polycarbonate cells were the "wet" cells.

Two types of tests were performed on the elliptic cells: flat plate compression in both the transverse and axial directions and punch indentation using a 12.5 mm diameter hemispherical punch. The MTS Loading Frame with test enclosure was used for both test types. In addition, the wet cells were placed inside plastic bags with SOLUSORB® in case of polycarbonate leakage. The flat plate compression and indentation punch test setups are shown in Figures 3-2 and 3-3.

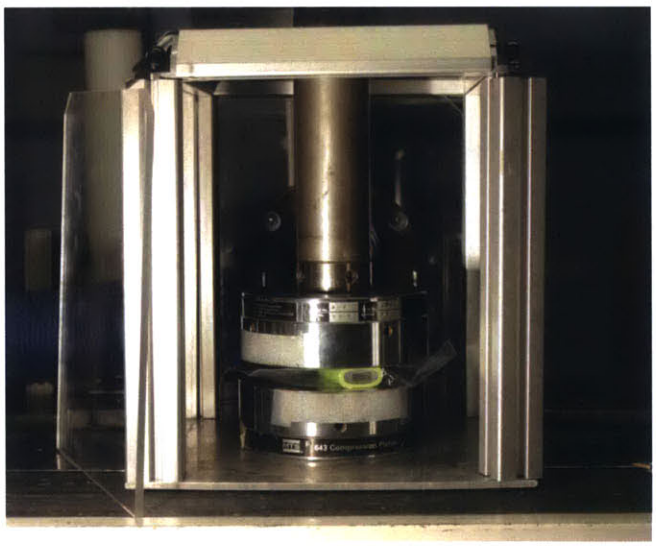

Figure 3-2: Elliptic Cell Flat Plate Compression Test Setup

Figure 3-3: Elliptic Cell Punch Indentation Test Setup

3.1.1 First Testing Event

During the first testing event, two dry cells and four wet cells were tested. One dry cell and three wet cells were compression tested in the transverse direction, and one dry cell and one wet cell was punch tested. One of the wet cell compression tests was discarded because the cell was either not placed in the middle of the plates or the cell moved during the testing due to polycarbonate leakage. All tests were conducted at a rate of 1 mm/min.

The results of the compression tests in the transverse direction are shown in Figure 3-4. The maximum force was similar for two cells, 141 kN for one wet cell and 137 kN for the dry cell. The maximum crosshead was also consistent between these cells, with a crosshead of 6.7 mm for the wet cell and 6.5 mm for the dry cell. The other wet cell had a lower maximum force of 118 kN at a crosshead of 6.4 mm. This cell may have moved slightly during testing due to electrolyte leakage.

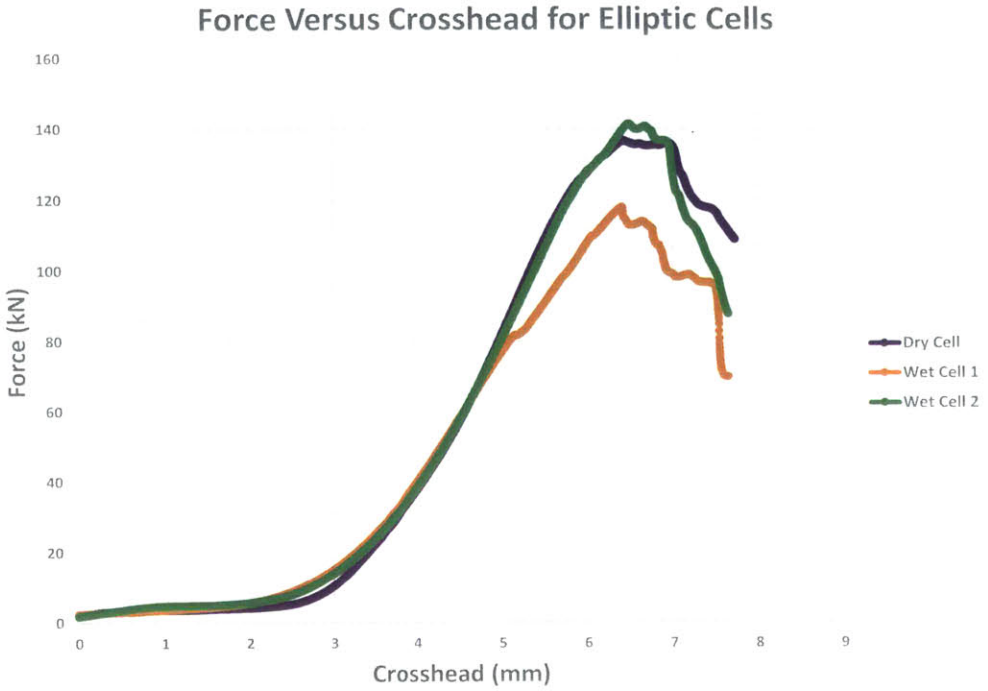

Figure 3-4: Elliptic Cell transverse Compression Test Results

Following the compression tests, the metal housing was removed from each battery, and the jellyroll was unrolled to view the resulting damage and determine the type of separator. Figure 3-5 shows the compressed elliptic dry cell and the unrolled jellyroll, with fracture lines in two directions. The separator was determined to be a trilayer polymer separator. The first wet cell, which had the lowest force measurement, is displayed in Figure 3-6. This cell had fracture lines in one direction and a single layer polymer. Figure 3-7 shows the unrolled jellyroll of the second compressed wet cell, which also had fracture lines in only one direction. The separator of the second wet cell was trilayer polymer.

(a) Compressed Cell

(b) Unrolled Jellyroll

Figure 3-5: Compressed Elliptic Dry Cell

(a) Jellyroll

(b) Unrolled Jellyroll

Figure 3-6: Compressed Elliptic Wet Cell 1

(a) Jellyroll

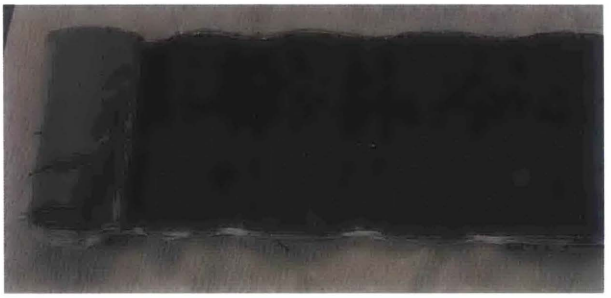

(b) Unrolled Jellyroll

Figure 3-7: Compressed Elliptic Wet Cell 2

Figure 3-8 shows the results of the first set of hemispherical punch tests on elliptic cells. The dry cell had a higher maximum force of 8.3 kN and crosshead of 5.8 mm, while the wet cell had a maximum force of 6.5 kN and crosshead of 5.6 mm. These cells were also opened, and they both had trilayer separators. Because of the large difference in force, the hemispherical punch tests were repeated in the second series of cell tests. Figure 3-9 shows the resulting damage to the cell.

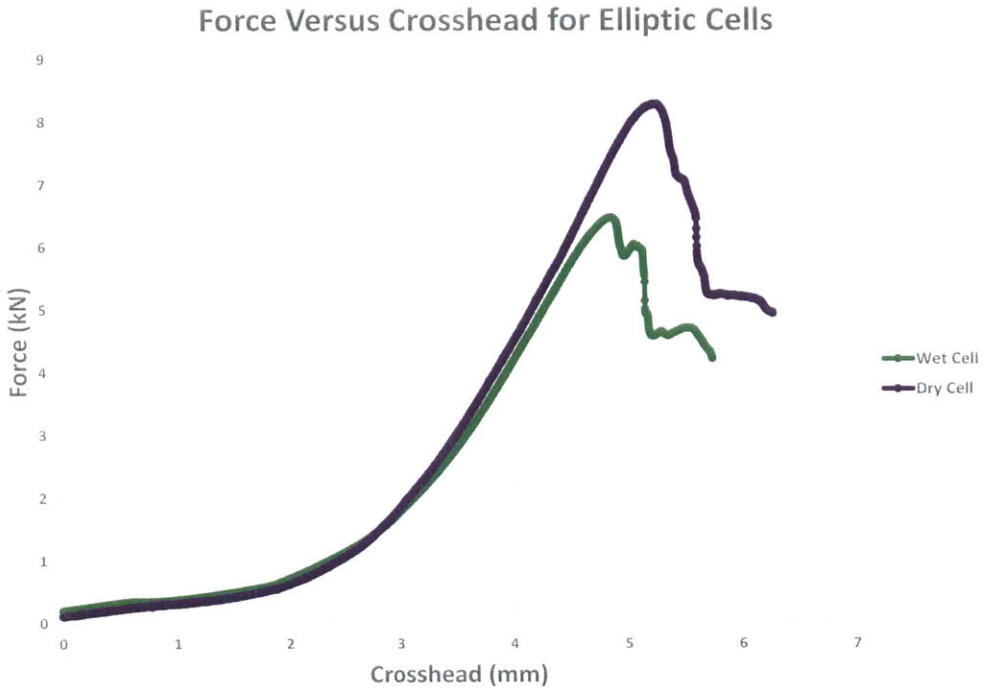

Figure 3-8: Elliptic Cell Hemispherical Punch Test Results from First Test Event

Figure 3-9: Elliptic Cell Damage from Punch Test

3.1.2 Second Testing Event

The second testing event involved hemispherical punch tests at two speeds and flat plate compression tests in the axial direction. The punch tests were repeated using one wet and one dry cell at a rate of 1 mm/min. The punch test was also

conducted at a rate of 20 mm/min on a dry cell. Finally, one wet and one dry cell was compression tested in the axial direction using the MTS flat plate fixtures.

Unlike the first set of tests, the cells were attached to a multimeter, and the resistance was recorded. The cells did not contain electrolyte, so the voltage could not be measured. The resistance measurement was used as a method to observe short circuit of the cell. As in the prismatic cell tests, the actual resistance measurement was not significant, only the drop in resistance. Figure 3-10 shows the test setup for the axial compression tests.

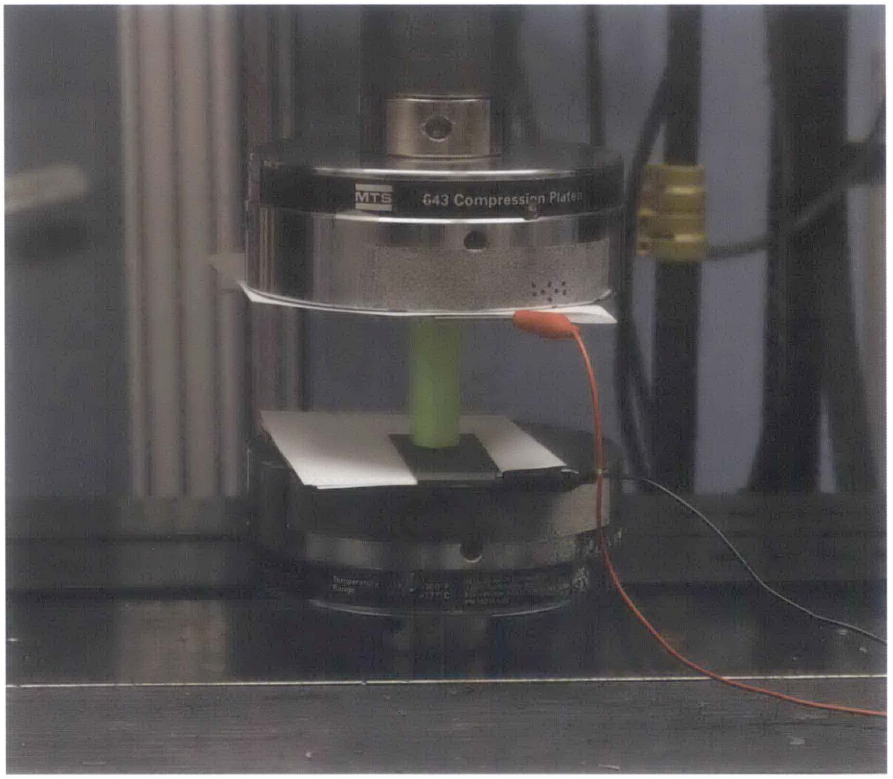

Figure 3-10: Elliptic Cell Axial Compression Test Setup

The results from the second set of punch tests are shown with the first set in Figure 3-11. The second dry cell had the highest maximum force of 8.8 kN with a crosshead of 5.4 mm. The second wet cell had a maximum force of 7.7 kN with a crosshead of 5.1 mm. While this force is lower than the dry cell, the difference is not as great as the difference between wet and dry cell force measurements in the first set of elliptic cell punch tests.

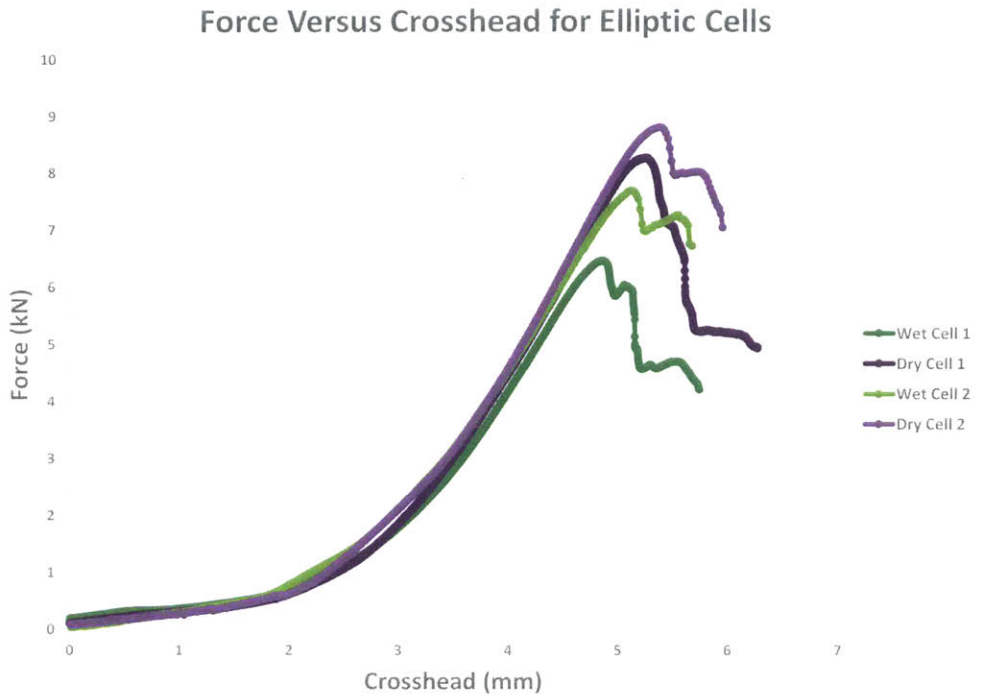

Figure 3-11: Elliptic Cell Hemispherical Punch Test Results

The force and resistance measurements for the second set of hemispherical punch tests are shown in Figures 3-12 and 3-13. Both graphs show a sharp drop in resistance just before the maximum force. This is similar to the timing of the resistance drop in the 12.5 mm diameter hemispherical punch test of the prismatic cells.

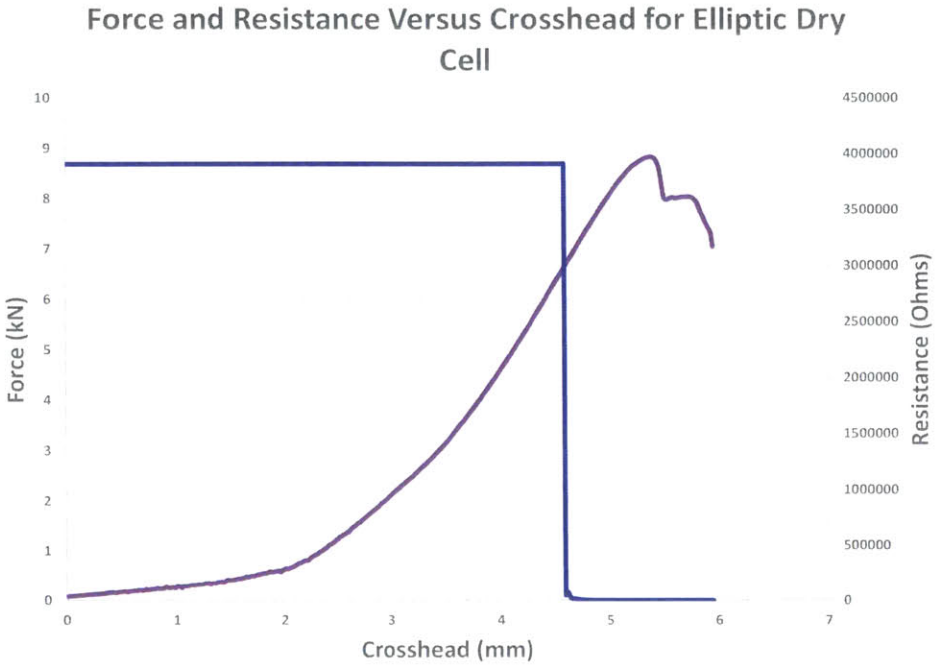

Figure 3-12: Elliptic Dry Cell 2 Hemispherical Punch Test Results

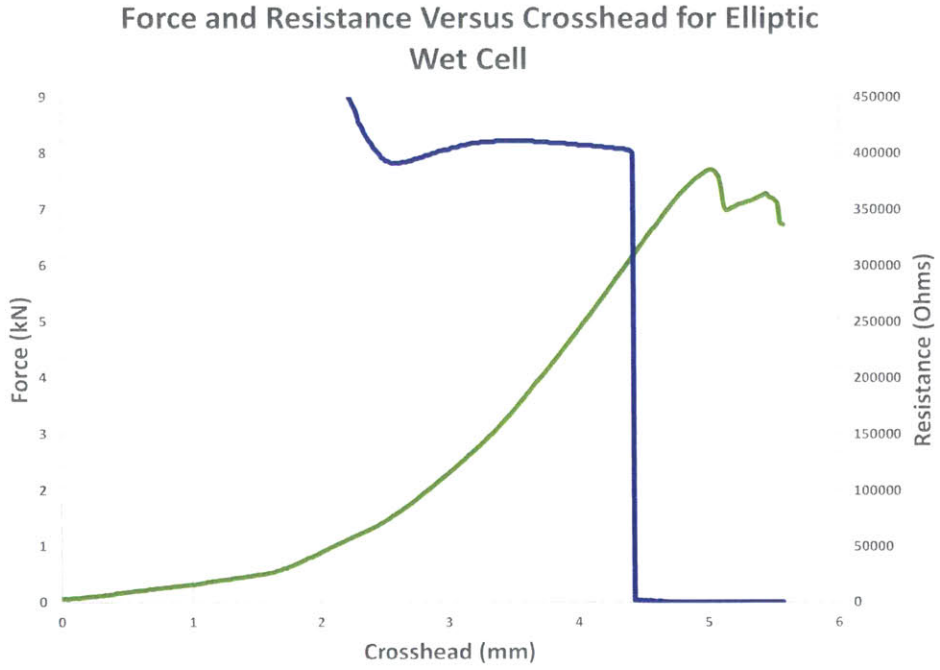

Figure 3-13: Elliptic Wet Cell 2 Hemispherical Punch Test Results

To compare the effects of increasing strain rate, the hemispherical punch test was repeated on a wet elliptic cell at a rate of 20 mm/min. The results were graphed in Figure 3-14 with the previous punch test results from Figure 3-11. The maximum force for the punch test at 20 mm/min was 6.7 kN at crosshead of 4.9 mm. This is higher than the maximum force of 6.5 kN for the 1 mm/min punch test of Wet Cell 1, but lower than the maximum force of 7.7 kN for Wet Cell 2.

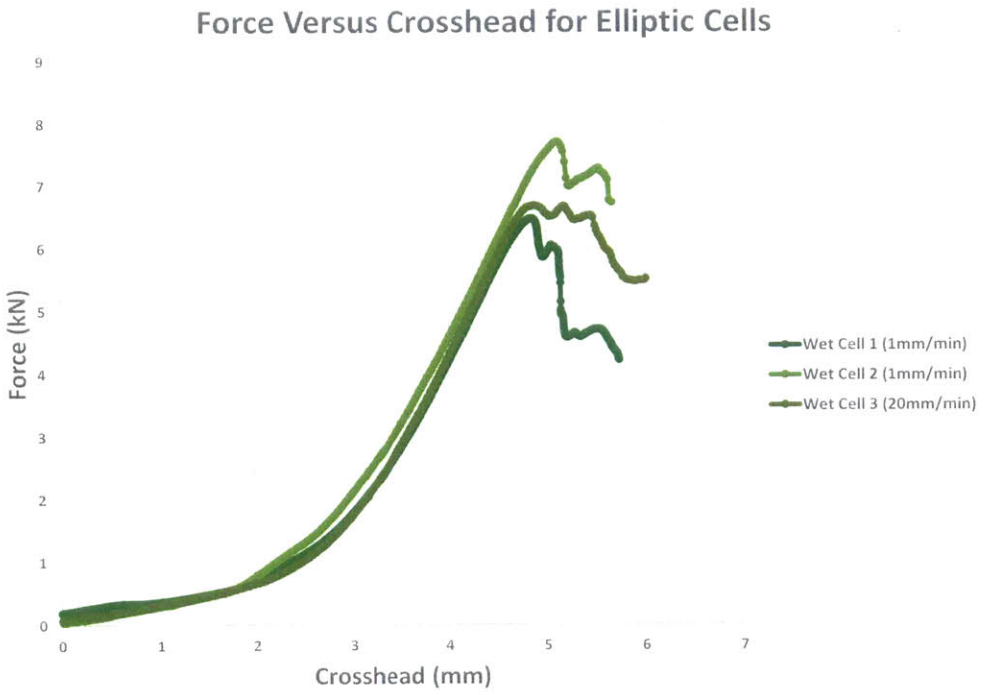

Figure 3-14: Elliptic Wet Cell Hemispherical Punch Test Results at Varying Rates

Figure 3-15 shows the force and resistance measurements for the 20 mm/min punch test of the elliptic wet cell. The most dramatic drop in resistance was prior to the maximum force, similar to previous hemispherical tests. However, because the multimeter could only record measurements at 1 Hz and the MTS software recorded force measurements at 20 Hz, the resistance measurements were not as accurate as the force measurements.

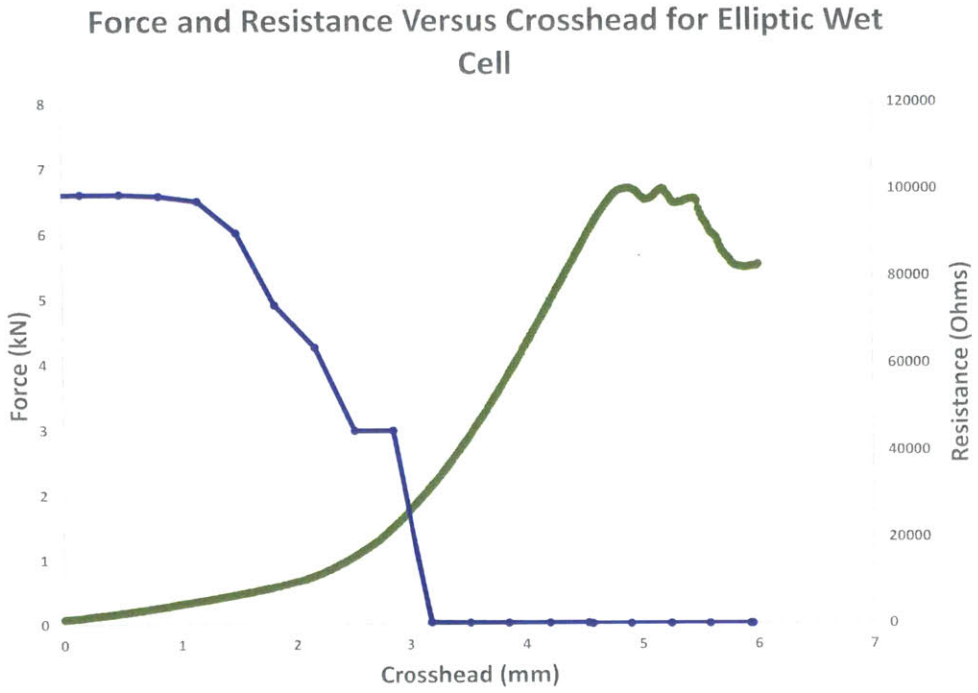

Figure 3-15: Elliptic Wet Cell Hemispherical Punch Test Results for 20 mm/min Rate Test

Figure 3-16 shows the results from the axial flat plate compression tests of the elliptic cells. The dry cell had a slightly higher maximum force of 10.0 kN with crosshead of 7.0 mm, and the wet cell had a maximum force of 9.6 kN with crosshead of 5.2 mm. While the maximum force measurements were similar, the wet cell reached its maximum force at a 26% lower crosshead. Figure 3-17 displays the elliptic cells after axial compression testing.

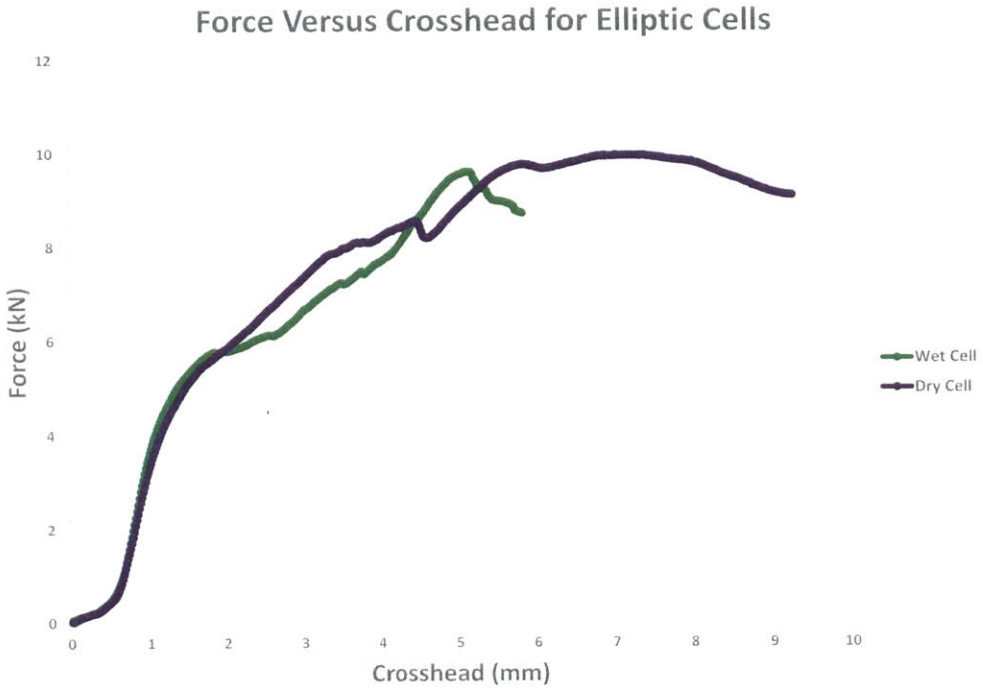

Figure 3-16: Elliptic Cell Axial Compression Test Results

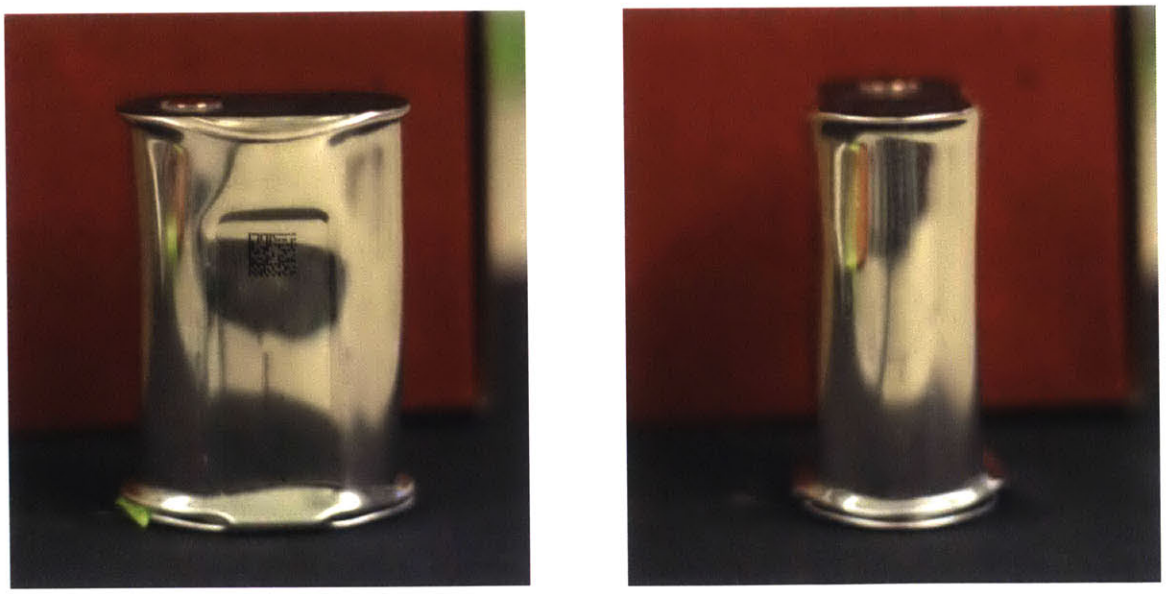

(a) Front View of Cell

(b) Side View of Cell

Figure 3-17: Elliptic Cell Damage from Axial Compression Test

The resistance was also recorded during the axial compression tests. Figure 3-18 and 3-19 show the force and resistance results for both the wet and dry cells. The drop in resistance was observed around the second inflection point in the graph and well before the maximum force.

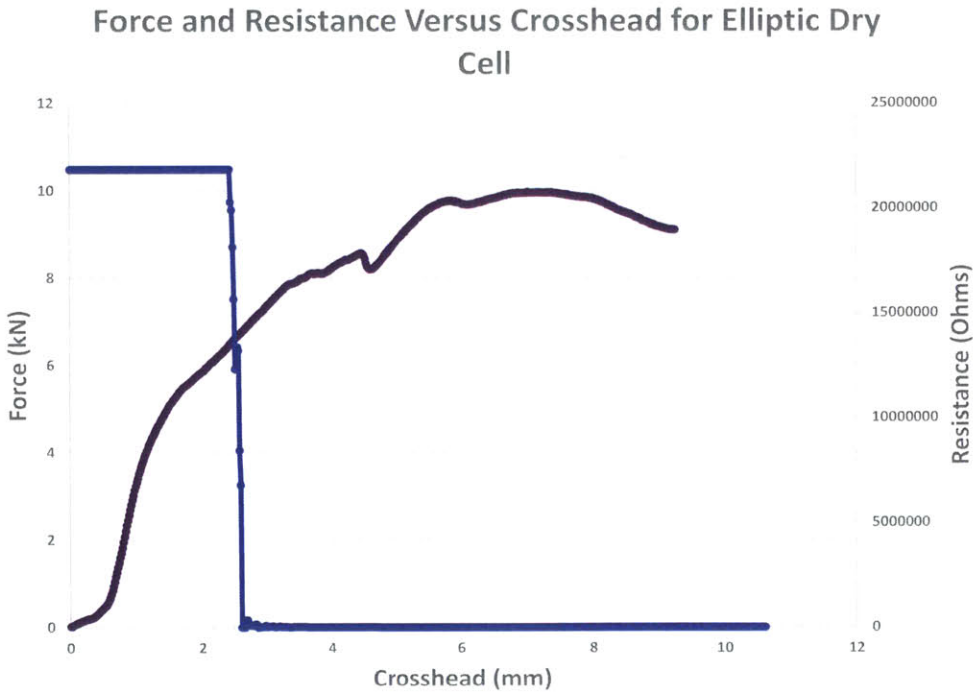

Figure 3-18: Elliptic Dry Cell Axial Compression Test Results

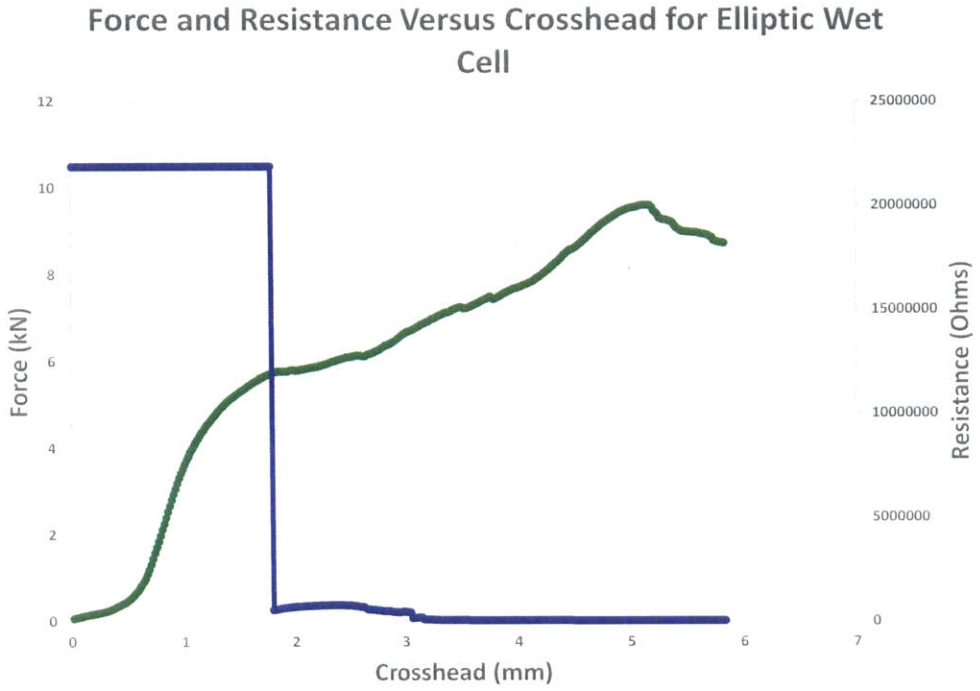

Figure 3-19: Elliptic Wet Cell Axial Compression Test Results

3.2 Interior Component Tests

ICL sponsors provided sheets of copper, aluminum, anode, and cathode from the elliptic cells. The sheets were inspected prior to testing. The copper and aluminum foil sheets had existing damage, including dimpling and wrinkles, possibly from handling. Figure 3-20 shows the copper sheets, and Figure 3-21 shows the aluminum sheets. The anode and cathode sheets had little noticeable damage. The thickness of each sheet of anode, cathode, copper, and aluminum was also measured, and the measurements are listed in Table 3.1. Some variation between sheets and within each sheet was noticed in measuring the thickness of the bare metal.

(a) Copper Foil Sheet

(b) Close-up View of Sheets

Figure 3-20: Copper Foil Sheets

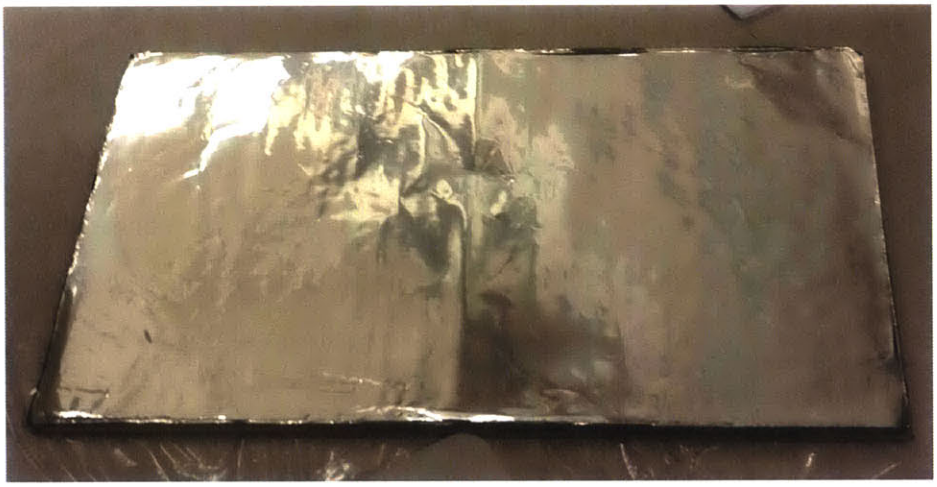

(a) Aluminum Foil Sheet

(b) Close-up View of Sheet

Figure 3-21: Aluminum Foil Sheets

Component	**Thickness (μm)**
Copper	12-16
Aluminum	16-23
Anode	141
Cathode	128

Table 3.1: Elliptic Cell Sheet Thicknesses

3.2.1 Uniaxial Test Details and Results

The copper and aluminum sheets were cut into strips 85 mm long and 10 mm wide using lined paper and an X-Acto© knife. Samples from the sheets were cut and tested in both the rolling and 90° directions to determine whether the materials were isotropic or anisotropic. The samples were tested using the Instron machine fitted with the pneumatic grips at a rate of 0.2 mm/min.

Based on previous ICL tests of copper sheets [11], the copper was expected to be isotropic. The results of the copper tests showed no anisotropy, so the resulting graph for the copper sheets, Figure 3-22, is in the rolling direction only. The maximum force for the copper samples was approximately 32 N, and the maximum extension varied from 2.5 mm to 3.0 mm. Figure 3-23 shows the samples before and after testing.

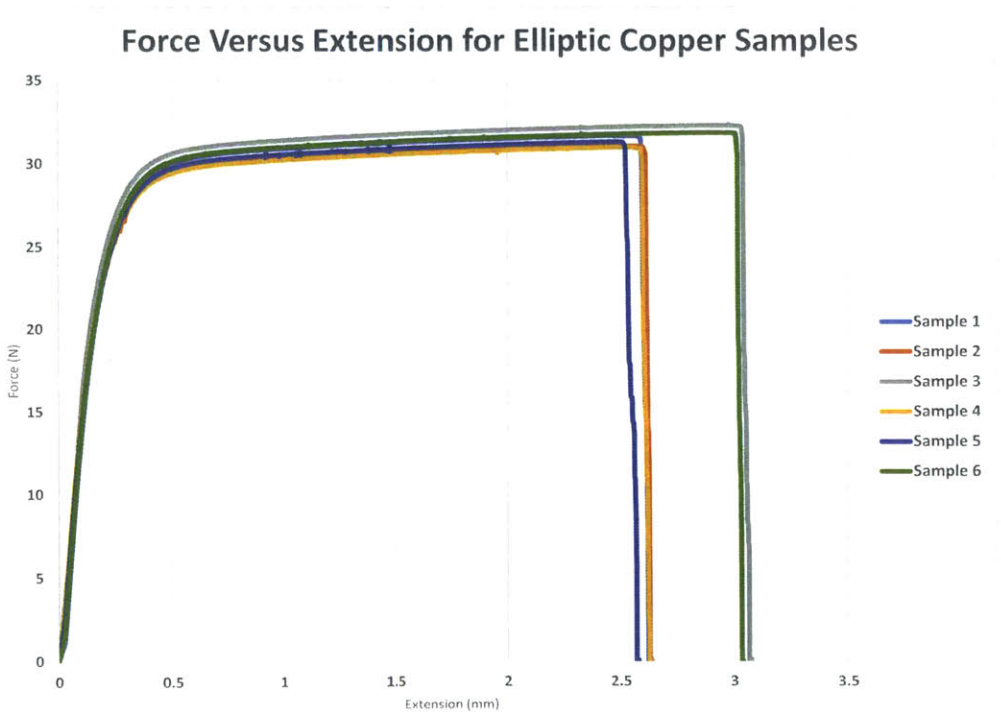

Figure 3-22: Elliptic Copper Uniaxial Test Results

(a) Samples Before Testing

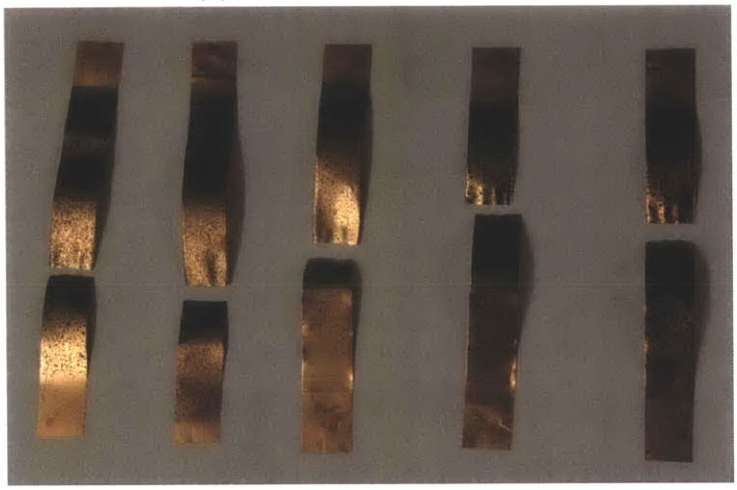

(b) Samples After Testing

Figure 3-23: Elliptic Copper Uniaxial Test Samples

The uniaxial test results for the the aluminum samples in the rolling direction are displayed in Figure 3-24. In the rolling direction, the aluminum samples showed a maximum force of 30.4 N and maximum extension of 0.97 mm. In the 90° direction, the maximum force was 29.7 N with a maximum extension of 1.1 mm. The aluminum sheets were expected to be anisotropic based on previous ICL testing of other aluminum sheets. While the aluminum samples showed slight anisotropy with a larger variation of maximum extension measurements and slightly lower force, the average values in both the rolling and 90° were 30 N for maximum force and 0.8 mm for

maximum extension. Figure 3-26 shows the elliptic aluminum samples in the machine direction before and after testing.

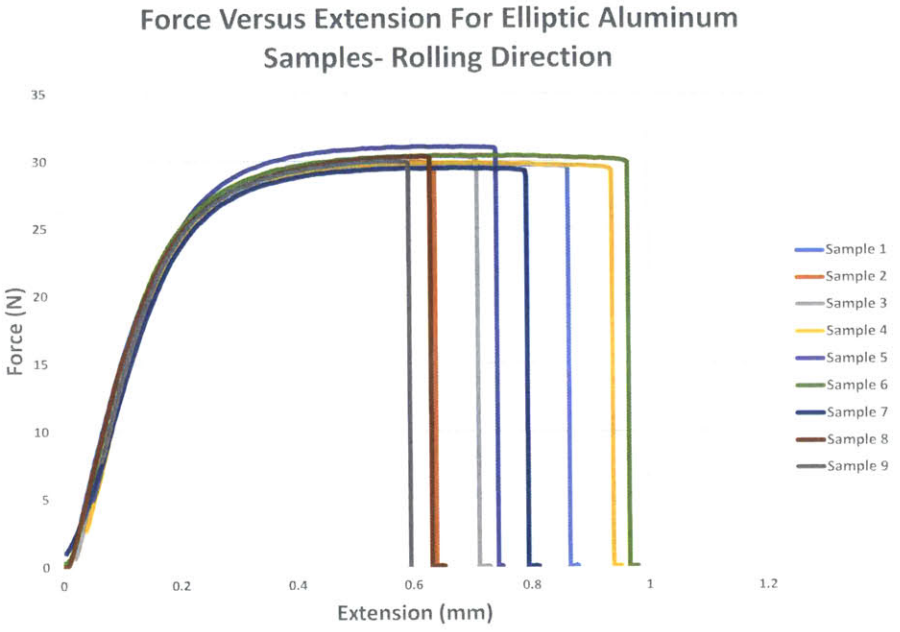

Figure 3-24: Elliptic Aluminum Uniaxial Test Results- Rolling Direction

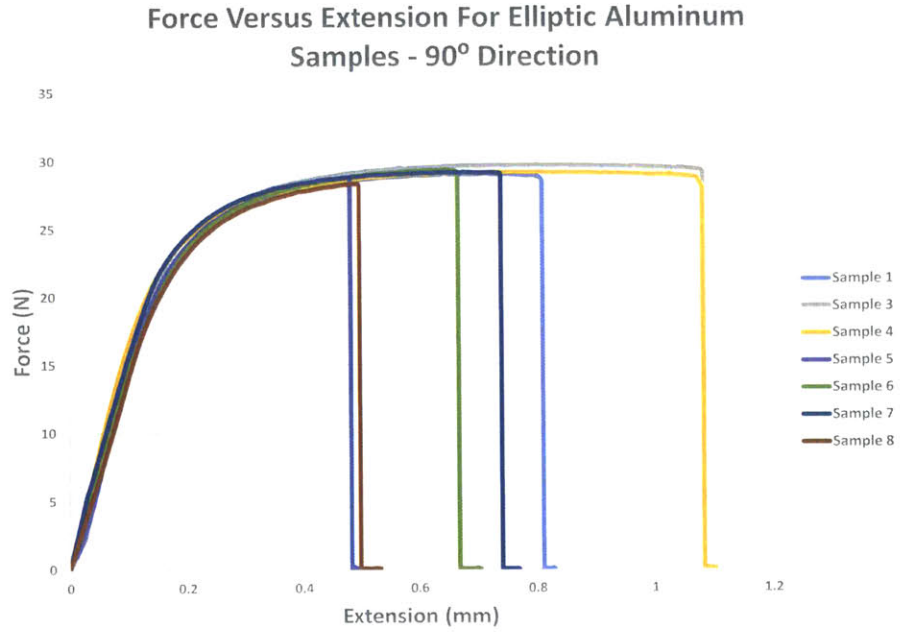

Figure 3-25: Elliptic Aluminum Uniaxial Test Results- 90° Direction

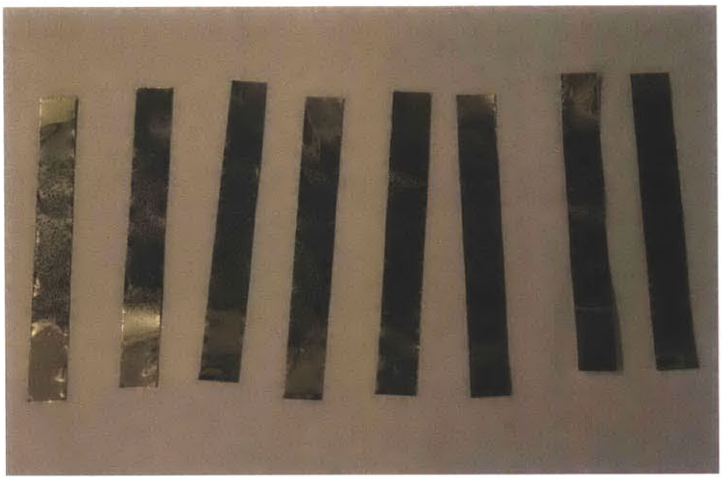

(a) Samples Before Testing

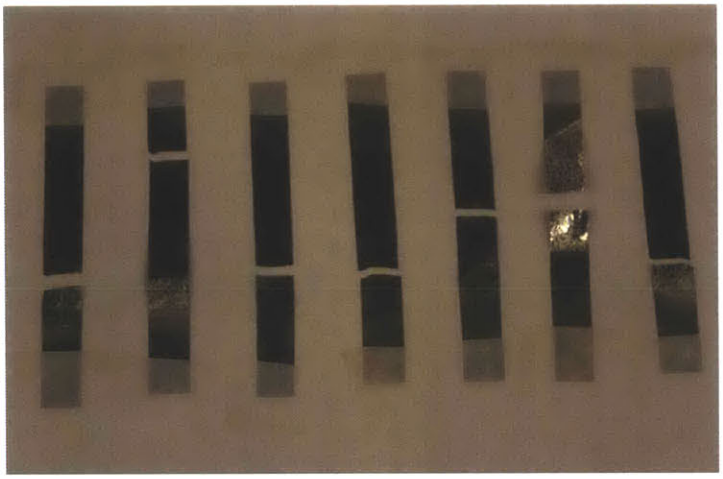

(b) Samples After Testing

Figure 3-26: Elliptic Aluminum Uniaxial Test Samples

The sheets of anode and cathode material were also cut into strips 85 mm long and 10 mm wide. During the first set of tests, the anode and cathode samples broke inside the grips due to the grip pressure. Because the grip pressure could not be adjusted, other methods were explored to improve the testing procedure. First, the edges of the grips were padded with different materials, and second, general purpose masking tape was applied directly to the samples. Neither of these methods corrected the issue. Finally a paper tape with the same width as the grips was applied to the samples, and this method eliminated sample breakage inside the grips. A small aluminum block was machined to allow exact placement of the paper tape to each sample. Figure 3-27

shows a sample which broke inside the Instron machine grips and a taped sample in the Instron machine grips.

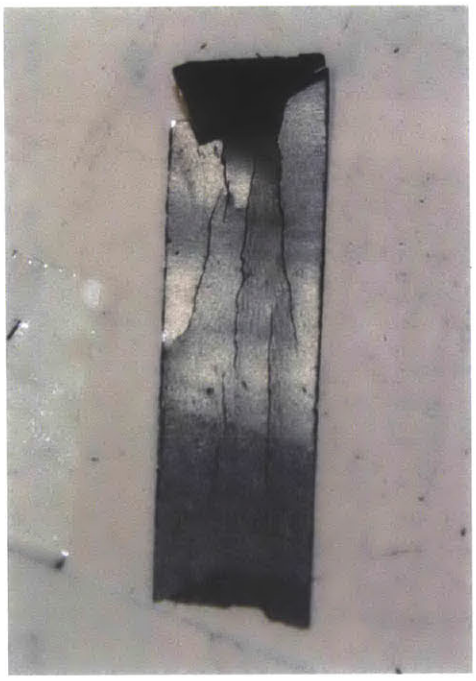

(a) Broken Coated Metal Sample

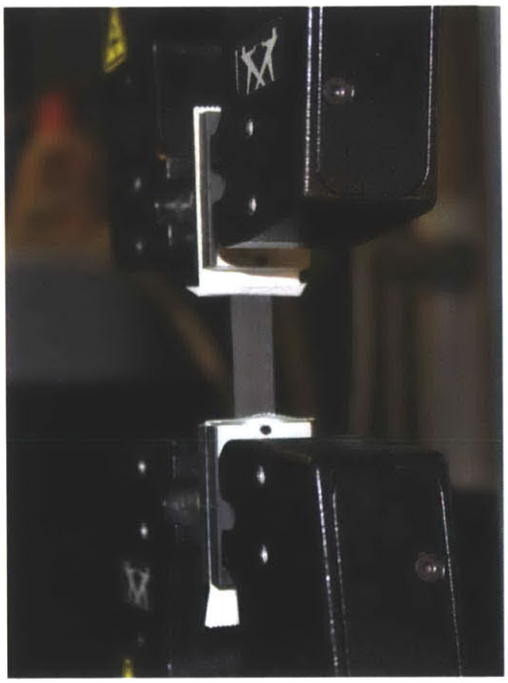

(b) Taped Sample in Instron Machine

Figure 3-27: Elliptic Coated Metal Samples

As with the copper and aluminum, anode and cathode samples in both the rolling and 90° direction were cut. Because a rolling direction for the metal foil was not obvious due to the coating, a rolling direction was assumed. The rolling direction of the coated metal sheets is illustrated in Figure 3-28

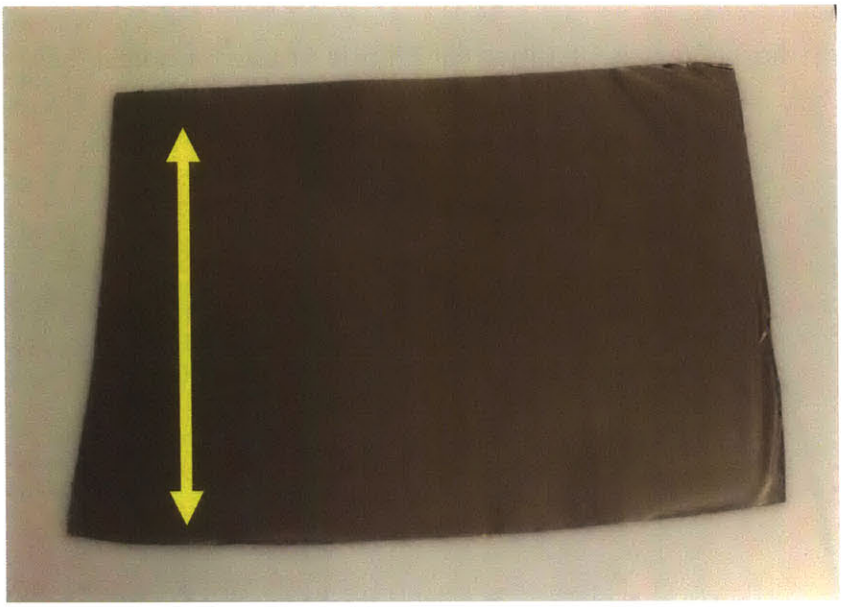

Figure 3-28: Rolling Direction of Coated Sheets

Figure 3-29 shows the results of the anode sample tests in the rolling direction, and Figure 3-30 shows the results in the 90° direction. In the rolling direction, a maximum force of approximately 36 N was observed for the anode samples with a maximum extension of 1.37 mm. While in the 90° direction, approximately 36 N maximum force for the cathode samples was seen with a maximum extension of 0.66 mm. The elliptic anode uniaxial samples are shown in Figure 3-31.

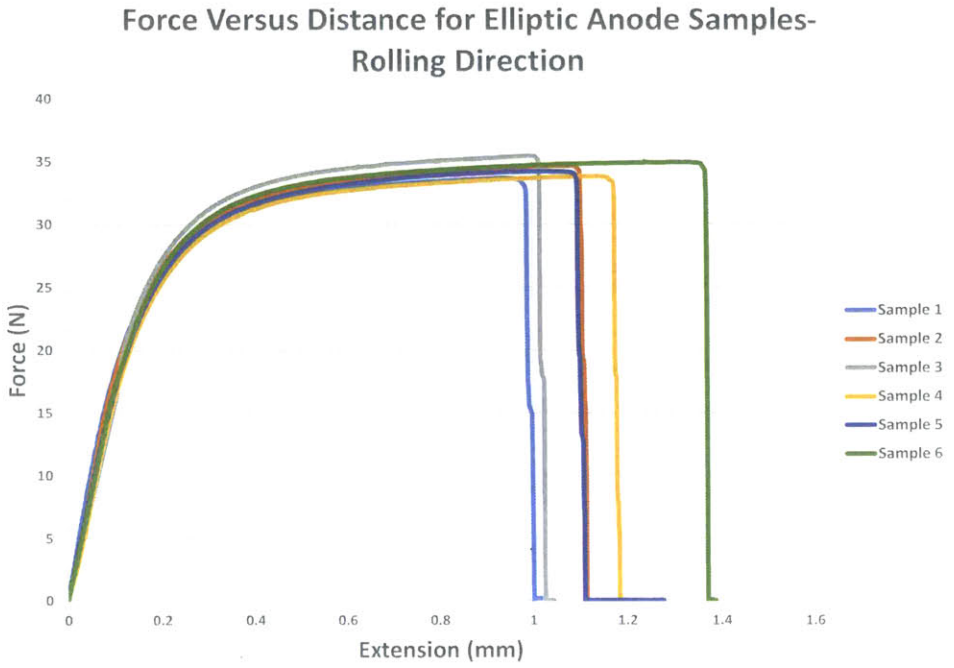

Figure 3-29: Elliptic Anode Uniaxial Test Results- Rolling Direction

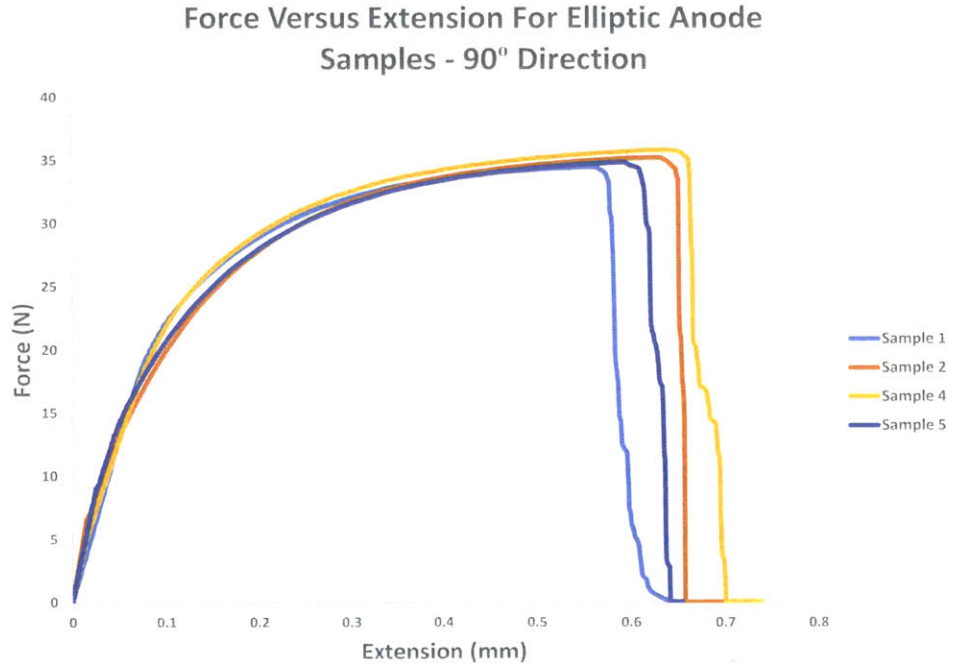

Figure 3-30: Elliptic Anode Uniaxial Test Results- 90° Direction

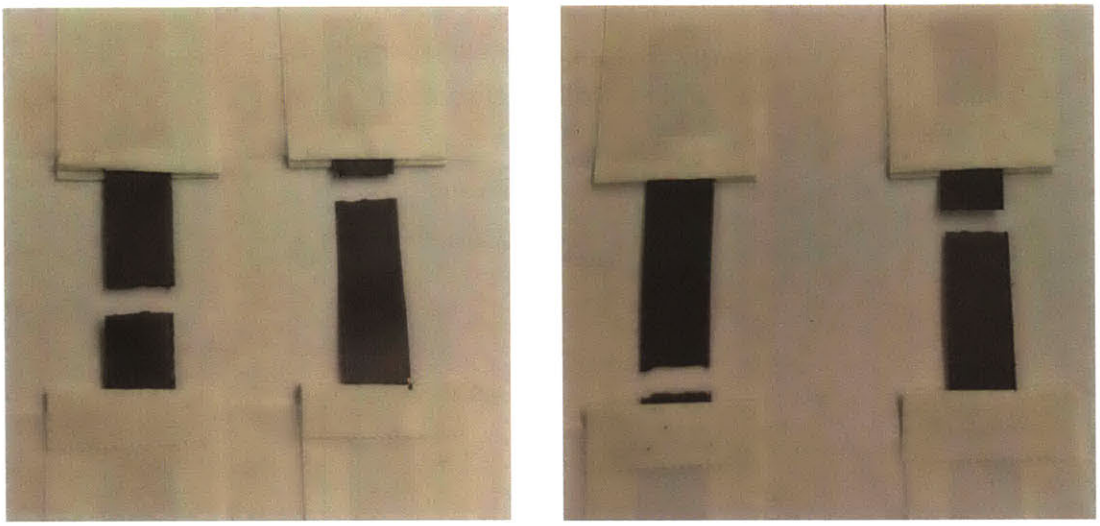

(a) Machine Direction (b) 90° Direction

Figure 3-31: Elliptic Anode Uniaxial Test Samples

In the 90° direction, tearing of the samples was observed. Because of this tearing and the fact that uniaxial tests in both directions had similar maximum force results, it was suspected that the cutting of the samples produced edge defects. Samples in the 90° direction were retested, and the results were consistent with the results of the rolling direction tests. Therefore, the anode sheets did not show any anisotropy.

As shown in the results of the cathode uniaxial tests in the rolling direction, Figure 3-32, a maximum force of approximately 37 N occurred with a maximum extension of 0.26 mm. In the 90° direction, Figure 3-33, a maximum force of 39 N with maximum extension of 0.33 mm was observed. The force measurements for both directions are similar, but the extension measurements for the 90° direction are larger than those for the rolling direction. Figure 3-34 shows the elliptic cathode samples after uniaxial testing.

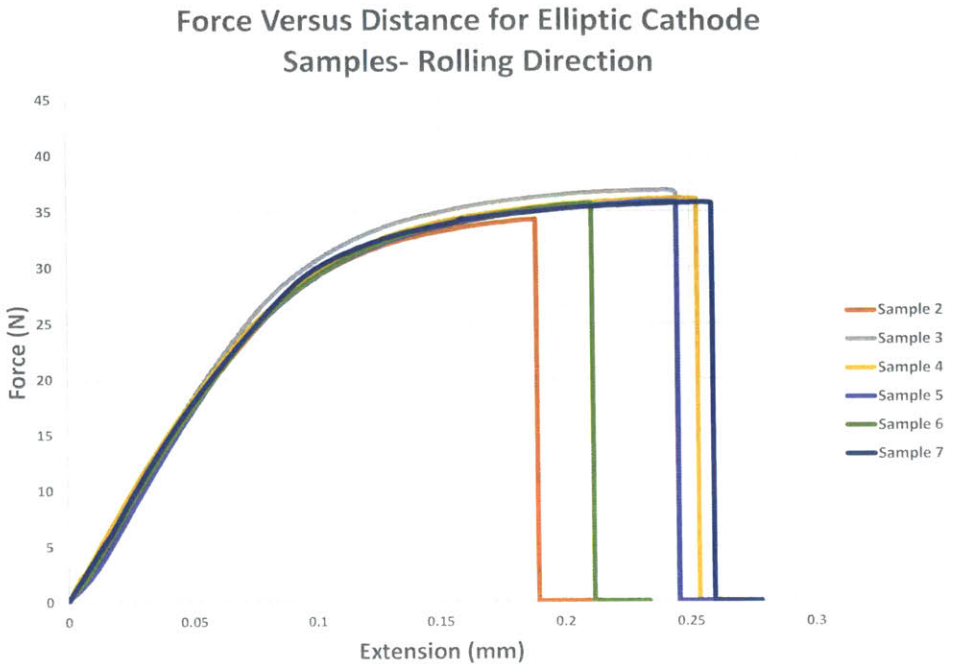

Figure 3-32: Elliptic Cathode Uniaxial Test Results- Rolling Direction

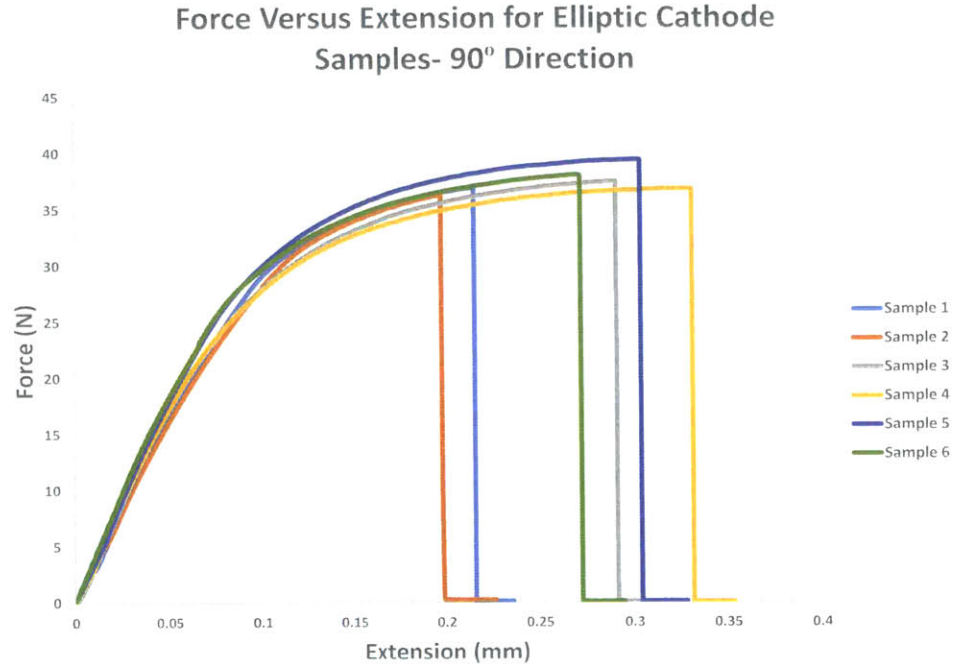

Figure 3-33: Elliptic Cathode Uniaxial Test Results- 90° Direction

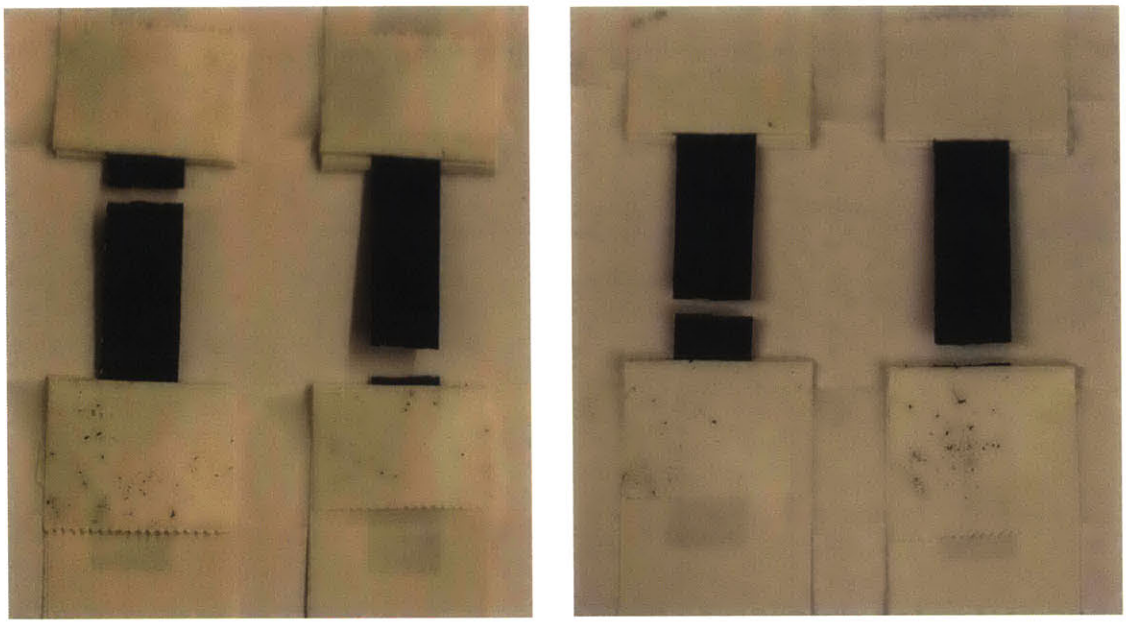

(a) Machine Direction (b) 90° Direction

Figure 3-34: Elliptic Cathode Uniaxial Test Samples

To compare the copper and anode samples and aluminum and cathode samples with each other, a representative sample was chosen for each sample type and displayed in Figures 3-35 and 3-36. Sample 3 from the copper tests and Sample 4 from the the 90° direction of the aluminum tests were chosen, along with Sample 6 from the rolling direction anode tests and Sample 5 from the 90° direction cathode tests. Both figures show that the bare metals have higher extension and lower force measurements than the coated metals.

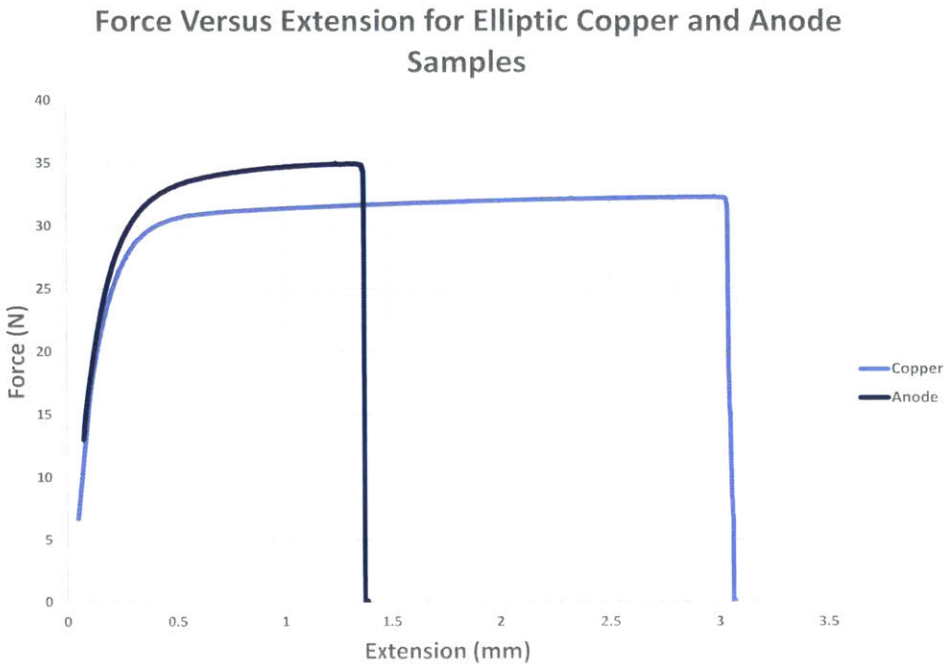

Figure 3-35: Elliptic Copper and Anode Uniaxial Test Comparison

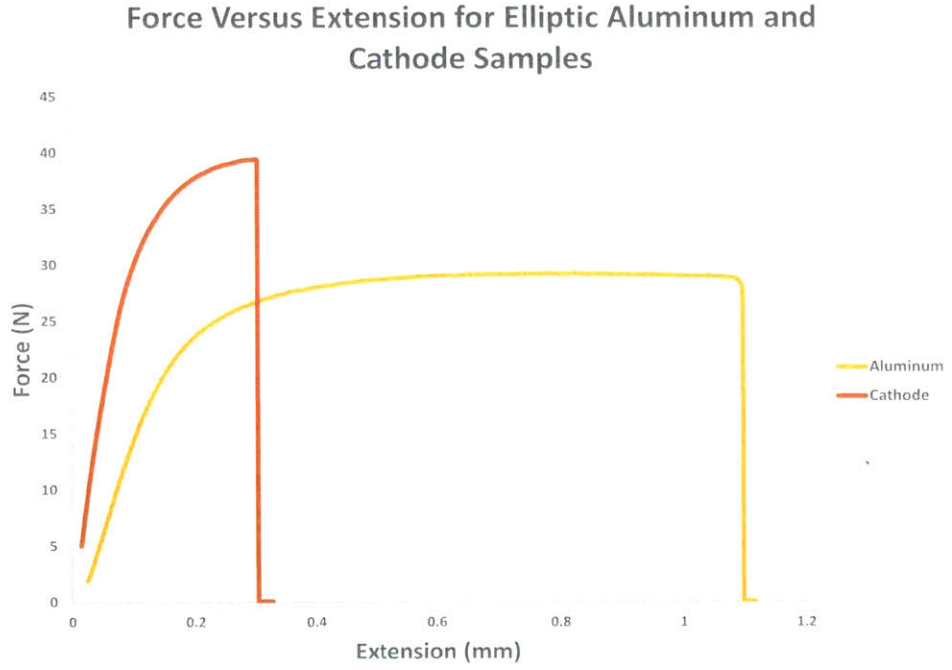

Figure 3-36: Elliptic Aluminum and Cathode Uniaxial Test Comparison

3.2.2 Biaxial Punch Test Details and Results

The sheets of copper, aluminum, anode, and cathode were cut into circular samples with diameters of 45 mm. The samples were loaded into a mount between two circular metal plates and tightened with screws. The samples were then tested using the Instron machine fitted with a spherical punch at a rate of 1 mm/min. Figures 3-37 through 3-42 below show the results of the biaxial punch tests.

As seen in Figure 3-37, Elliptic Copper Samples 1-4 had significantly lower maximum force and extension measurements compared with Samples 5 and 6. Samples 1, 3, and 4 broke in the middle of the sample and along the edge of the sample mount. This meant that the mount was over-tightened, and the results were not accurate. And Sample 2 was under-tightened, resulting in slippage of the sample. Because of the problems with sample loading, only Samples 5 and 6 could be used for further analysis. And based on these two samples, the maximum force for the copper samples was approximately 49 N with a maximum extension of 3.3 mm.

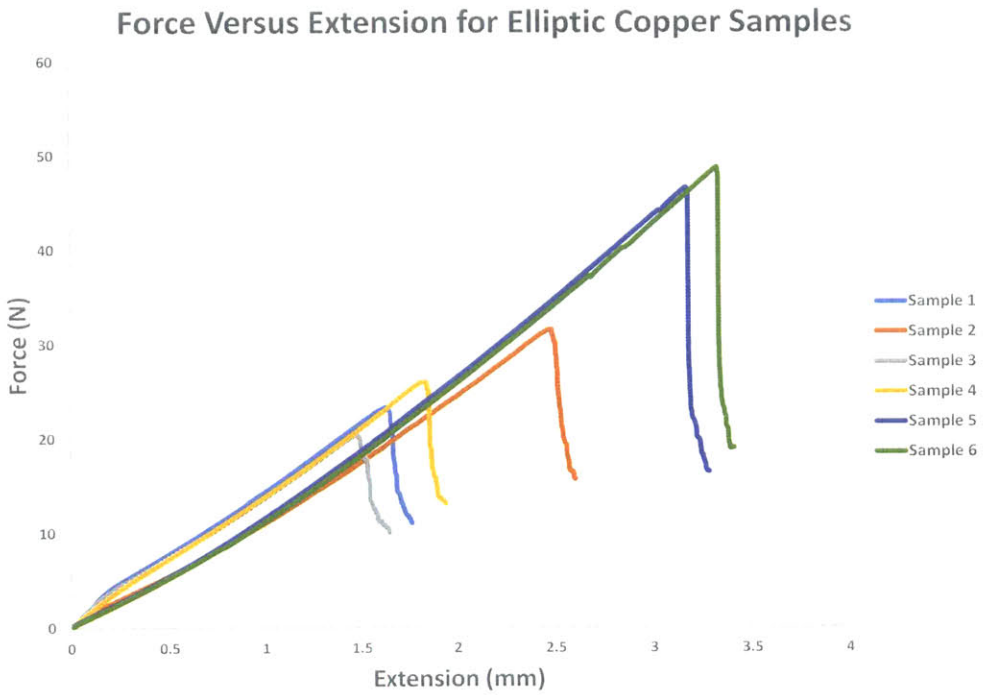

Figure 3-37: Elliptic Copper Biaxial Test Results

Figure 3-38 shows Samples 2 and 5 from the elliptic copper biaxial tests. Sample 2 was not properly tightened and slipped in the mount. Sample 5 was properly tightened. The location of the crack was not in the center of Sample 5. This correlated to a non-zero friction coefficient between the sample and the punch since a center crack would indicate no friction.

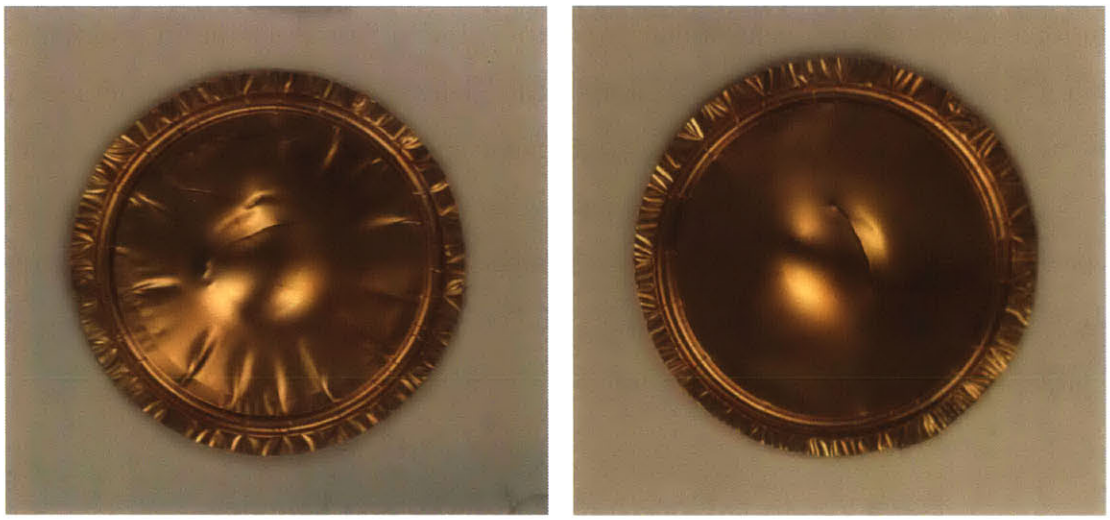

(a) Sample 2 (b) Sample 5

Figure 3-38: Elliptic Copper Biaxial Test Samples

The biaxial test results of the aluminum samples in Figure 3-39 show similar problems with sample loading. Samples 2 and 3 were over-tightened and broke along the edge of the sample mount, and Samples 6 and 8 were under-tightened and slipped. This only leaves Samples 5 and 7 as viable test results. Using these samples, the approximate maximum force for the elliptic aluminum samples was 16 N with a maximum extension of 2.0 mm. Sample 5 in Figure 3-40 had a crack near the center of the sample, indicating a small friction coefficient between the punch and aluminum sample.

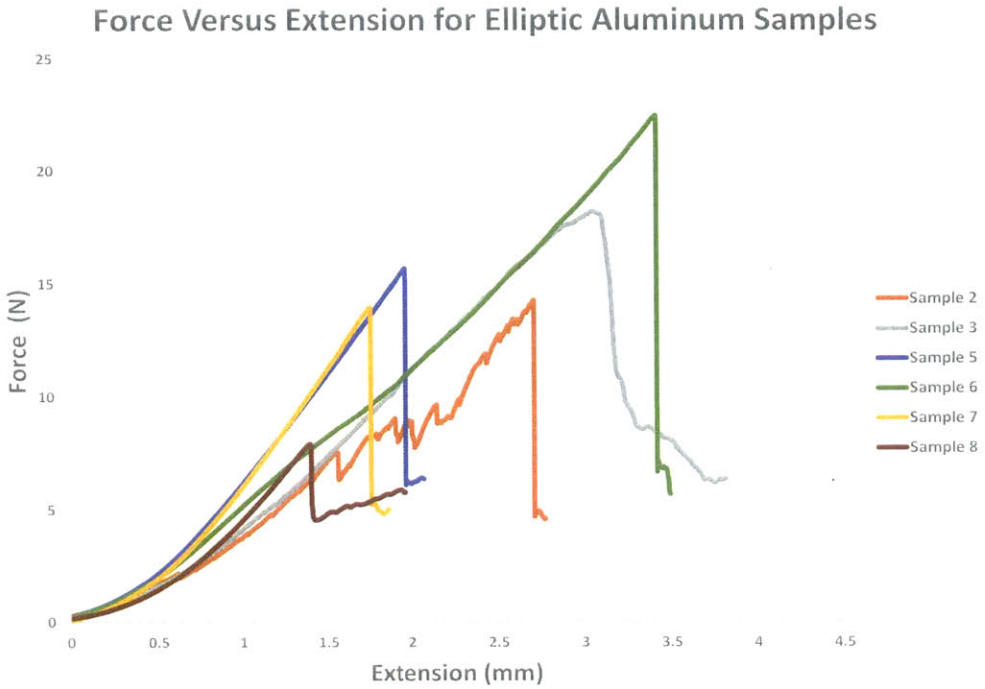

Figure 3-39: Elliptic Aluminum Biaxial Test Results

Figure 3-40: Elliptic Aluminum Biaxial Test Sample 5

Figures 3-41 and 3-42 show the biaxial test results of the elliptic anode and cathode tests. Signs of slipping were noted in Samples 4, 5, and 6, so the Sample 7 result was considered the most accurate for the elliptic anode samples. The maximum force for the elliptic anode samples was approximately 56 N with a maximum extension of

4.2 mm. For the cathode samples, the approximate maximum force was 14 N, and maximum extension was 1.6 mm.

Figure 3-43 shows Sample 7 from the anode biaxial tests and Sample 3 from the cathode biaxial tests. The crack in the anode sample was more off-center than the crack in the anode sample. This indicates that the friction coefficient between the punch and anode sample was larger than the friction coefficient between the punch and cathode.

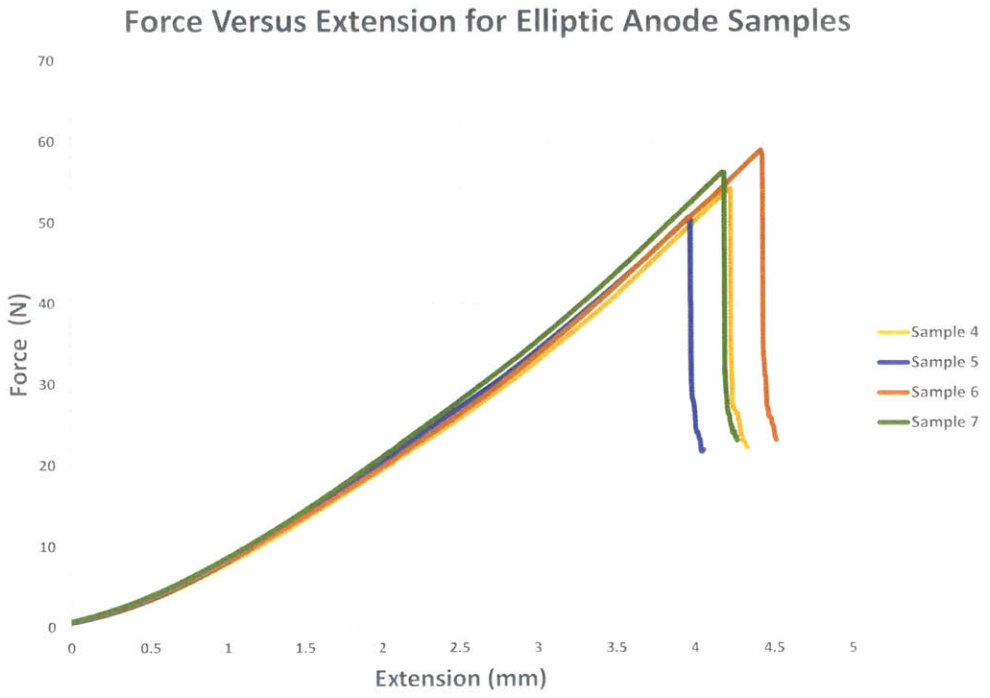

Figure 3-41: Elliptic Anode Biaxial Test Results

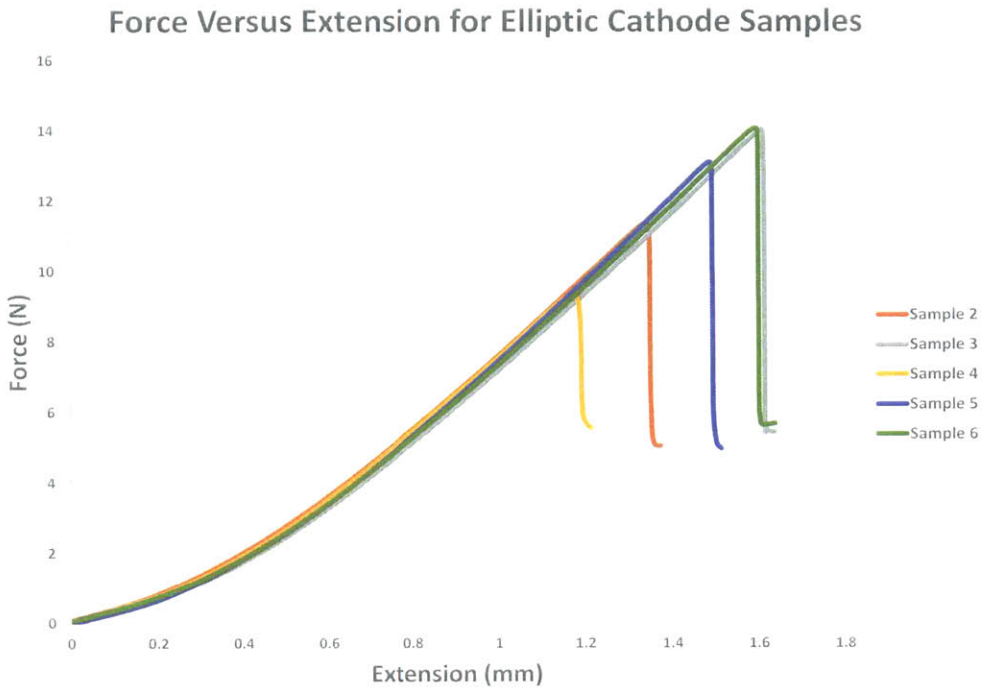

Figure 3-42: Elliptic Cathode Biaxial Test Results

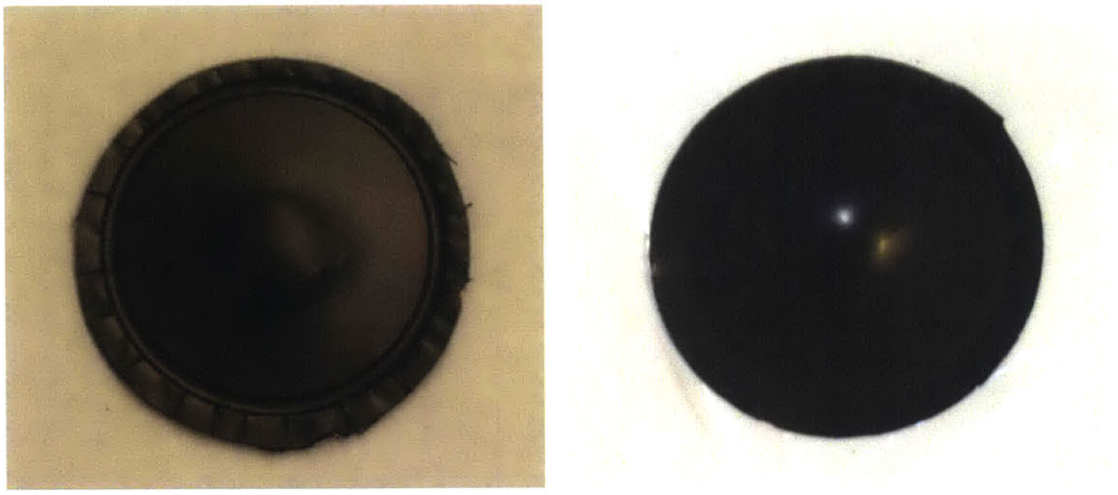

(a) Anode Sample 7 (b) Cathode Sample 3

Figure 3-43: Elliptic Coated Metal Biaxial Test Samples

Using the samples from each sheet type with the maximum force and extension measurements, Figures 3-44 and 3-45 were created to compare the copper and anode and aluminum and cathode samples. The anode samples have higher force and

extension than the bare copper samples. However, the bare aluminum samples had higher force and extension compared with the cathode samples.

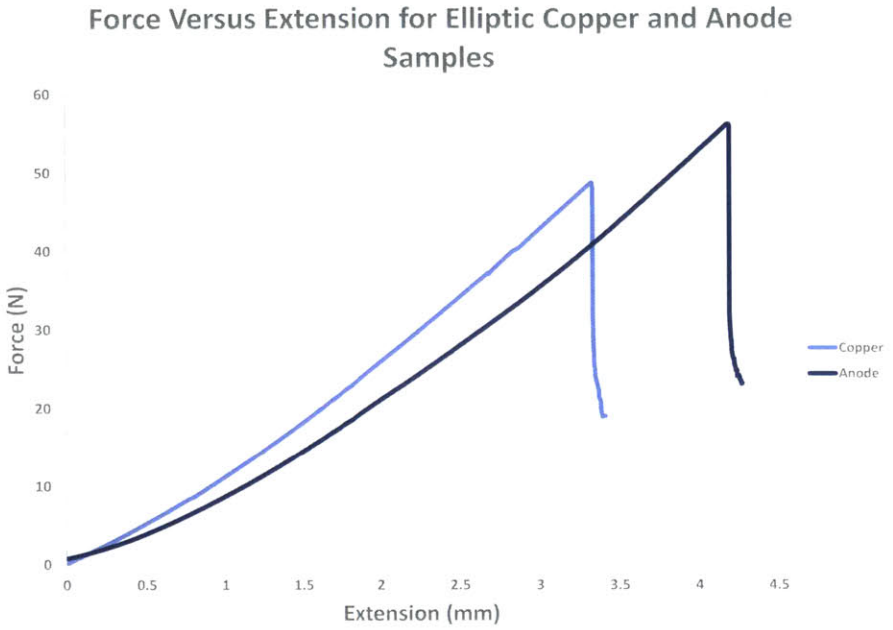

Figure 3-44: Elliptic Copper and Anode Biaxial Test Comparison

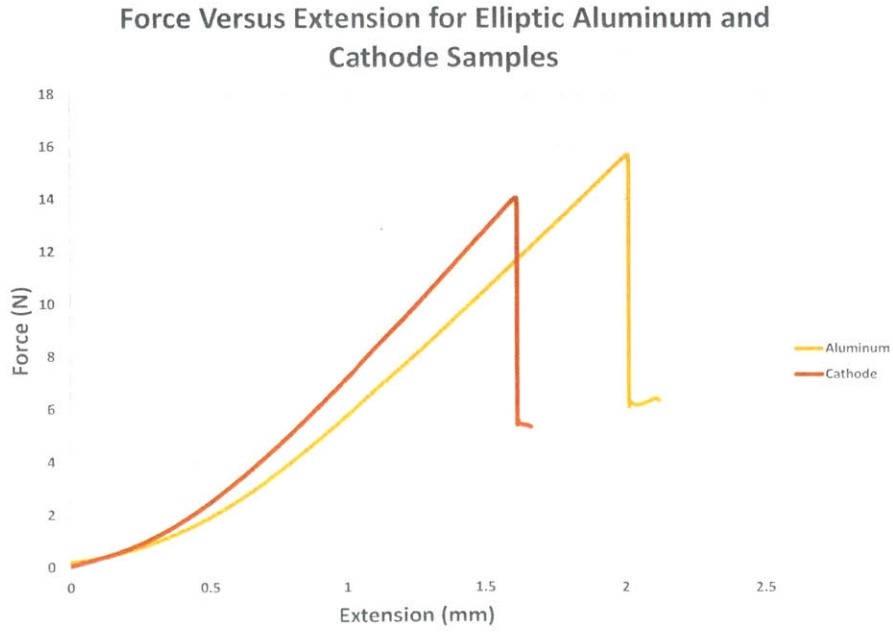

Figure 3-45: Elliptic Aluminum and Cathode Biaxial Test Comparison

The results of the punch test comparison plots were expected to be similar to the uniaxial comparison plots, with the bare metal samples having a higher extension but lower force than the coated metal samples. While the cathode samples had lower maximum force and extension measurements compared with aluminum, they had higher force measurements at each extension before breaking. This corresponds to expectations. However, the copper foil samples have a higher force compared to the anode samples at every extension. Because of this possible discrepancy, the copper punch tests were repeated.

Figure 3-46 shows the results of the repeated copper punch tests. As with the previous bare metal punch tests, only two samples could be used for analysis due to issues with sample loading. The results of the retest have a higher maximum force of 59 N and higher extension of 4.4 mm compared to previous copper punch tests.

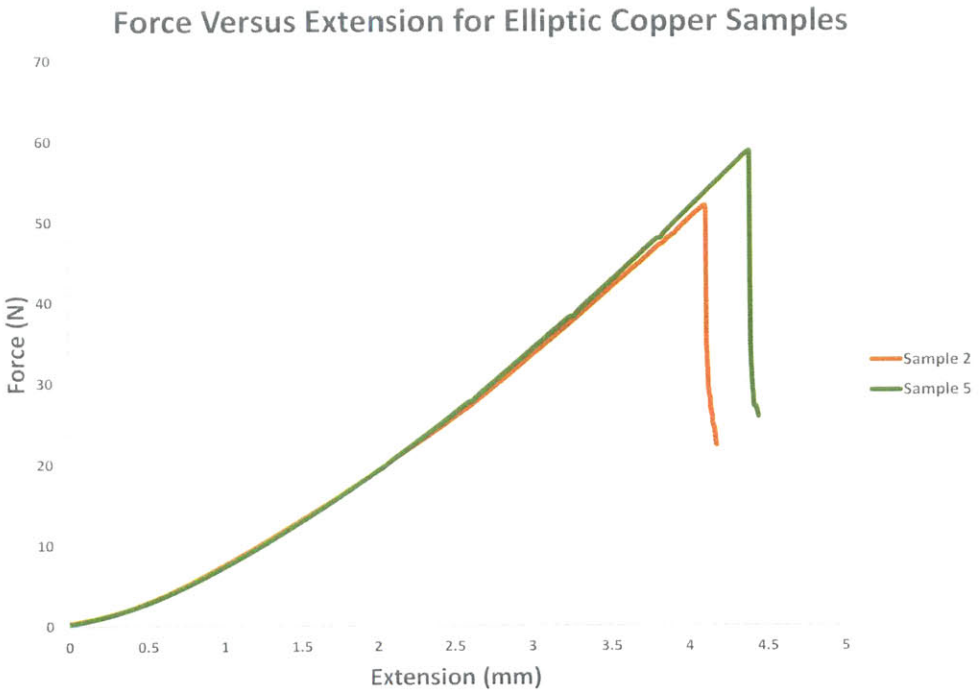

Figure 3-46: Elliptic Copper Biaxial Retest Results

Sample 5 from Figure 3-46 was chosen as the representative elliptic copper sample and plotted with the representative anode sample in Figure 3-47. The copper retest

sample curve is closer to the anode curve than the original copper sample curve. And the results corresponded to expectations with higher anode sample force measurements at every extension compared to the copper sample's force measurements.

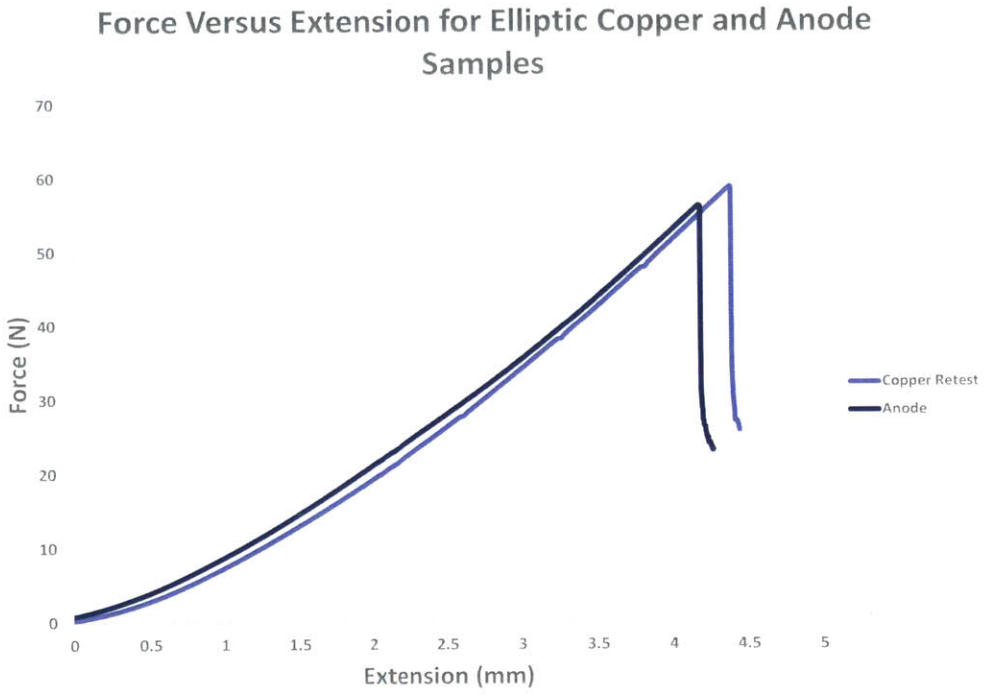

Figure 3-47: Elliptic Copper and Anode Biaxial Retest Comparison

3.2.3 Compression Test Details and Results

Compression test samples were prepared using a 16 mm diameter punch and hammer, with the samples sheets layered between sheets of paper. Twenty samples of each anode and cathode were stacked together and placed in the center of the flat plates on the MTS Loading Frame, as seen in Figure 3-48. The compression tests were conducted at rate of 0.2 mm/min. To ensure an accurate displacement reading, tape with markings was attached to the plates and tracked using DIC.

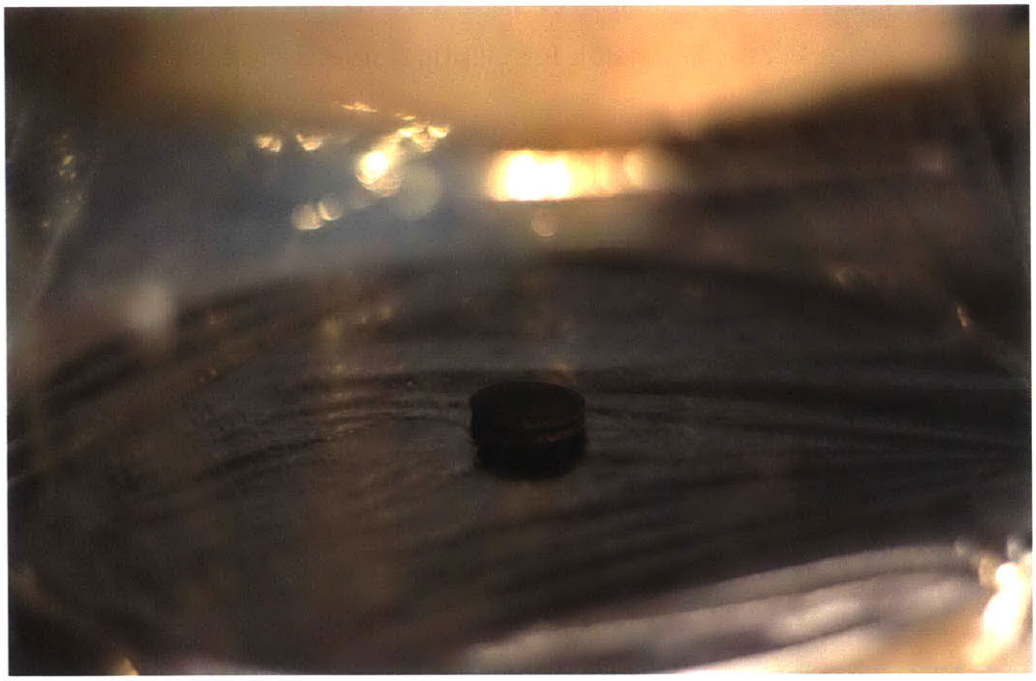

Figure 3-48: Elliptic Coated Metal Compression Test Samples

A starting load of 0.1 kN was chosen as the starting point to ensure no air existed in between the samples. This load corresponded to a stress of 0.5 MPa. But because 0.1 kN was within the accuracy limit of the load cell, and because the samples were difficult to see between the plates, the actual start point was not obvious. The resulting compression test graphs were shifted to the point where the force started increasing.

Figures 3-49 and 3-50 show the results of the compression tests. The anode samples have a maximum force of approximately 24 N with extension of 0.82 mm. And the cathode samples had a higher maximum force at approximately 29 N but with a lower extension of 0.24 mm. When the MTS displacement measurements were compared with the DIC results, both displacement measurements were consistent with one another.

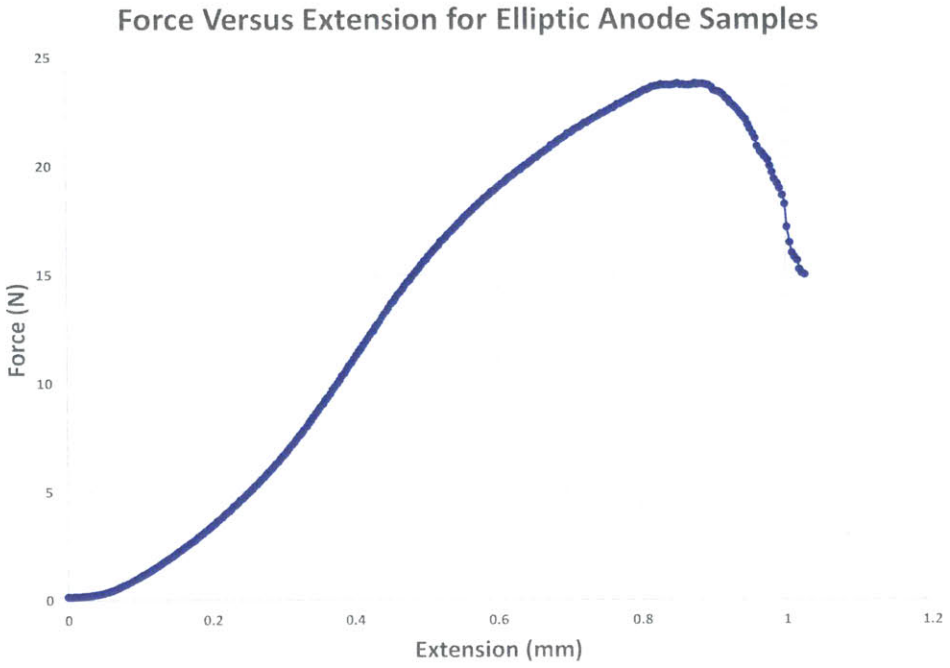

Figure 3-49: Elliptic Anode Compression Test Results

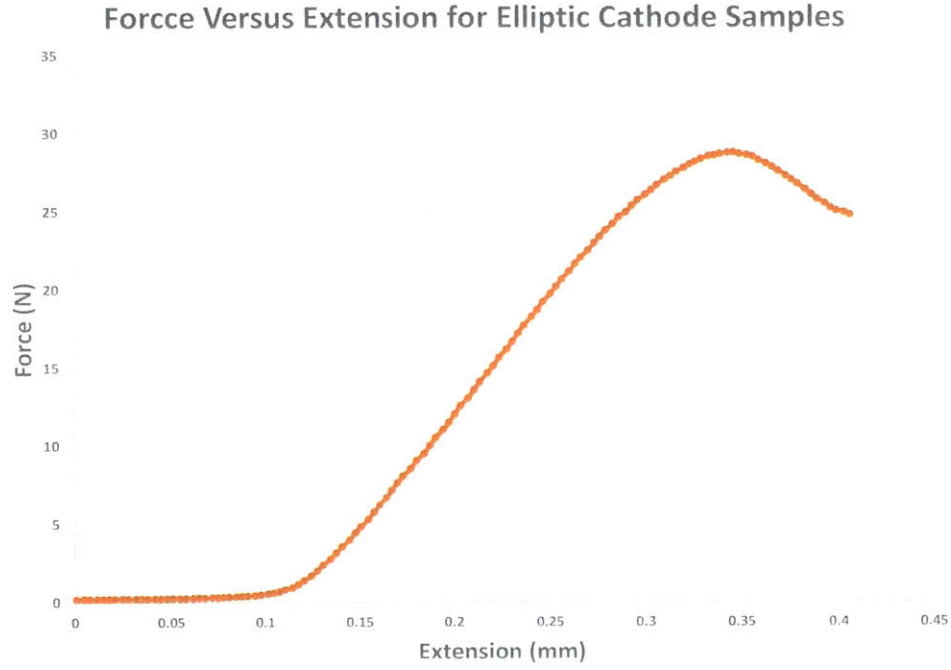

Figure 3-50: Elliptic Cathode Compression Test Results

3.2.4 Summary and Application of Test Results

Table 5.2 shows a summary of the maximum force and crosshead measurements for each cell and test type. For the transverse compression test, the wet cell had a slightly higher maximum force than the dry cell. But for the axial compression and punch tests, the dry cell had a higher maximum force than the wet cell. The maximum force results from the cell punch tests, which were performed twice on each cell type, were consistently higher for the dry cell versus the wet cell. However, the force difference between the dry and wets cells was within the variation seen between cells of the same type.

The differences in maximum force measurements for the wet and dry cells was small for the axial and transverse compression tests and could not be attributed to the presence or absence of polycarbonate. A larger maximum force difference existed between the punch tests of wet and dry cells. But because the amount of polycarbonate in each cell and whether it was consistent between all wet cells or consistent with the amount of electrolyte that would be present in an actual cell was unknown, no conclusions about wet versus dry could be made for the cell punch tests either.

The cell punch test at a speed of 20 mm/min had a lower maximum force than one of the lower speed tests. This result is interesting since the higher strain rate test was expected to have a higher maximum force. But no conclusions could be made from this result because only one test at a higher speed was performed.

One important factor that attributed to the results of the cell tests was the separator type. In the first set of cell tests, the cell housing was removed and separator type was determined. Two types of separators, trilayer and single layer polymers, were observed in the elliptic cells. The compression test results showed a lower maximum force measurement for the wet cell with a single layer separator versus the wet cell with trilayer separator. The cells from the second testing event were instead sent for 3D imaging to observe the interior fracture surfaces, so the separator type was not determined. Therefore, the effect of separator type was not fully captured.

Test Type	Cell Type	Maximum Force (kN)	Crosshead (mm)
Long. Compression	Dry	137	6.5
Long. Compression	Wet	141	6.7
Axial Compression	Dry	10.0	7.0
Axial Compression	Wet	9.6	5.2
Punch at 1mm/min	Dry	8.8	5.4
Punch at 1mm/min	Wet	7.7	5.1
Punch at 20mm/min	Wet	6.7	4.9

Table 3.2: Elliptic Cell Test Results

Table 5.4 shows the approximate maximum force and extension measurements for the interior component tests. Despite the poor condition of the bare metal sheets, some trends were observed. The copper samples had higher maximum force and extension than aluminum samples. Anode samples had higher extension than the cathode samples. The copper and anode samples had more similar force results than the aluminum and anode sample tests. This is expected since graphite, the primary anode coating material, is less stiff than the lithium-cobalt coating of the cathode. And in all of the tests, the bare metal samples had lower force at each extension than the coated metal samples.

Test Type	**Component**	**Maximum Force**	**Extension (mm)**
Uniaxial	Copper	32.2 N	3.0
	Aluminum	30.4 N	1.1
	Anode	35.4 N	1.4
	Cathode	39.4 N	0.3
Biaxial	Copper	58.8 N	4.4
	Aluminum	15.7 N	2.0
	Anode	56.2 N	4.2
	Cathode	14.0 N	1.6
Compression	Anode	23.8 kN	0.8
	Cathode	28.7 kN	0.2

Table 3.3: Elliptic Cell Interior Component Test Results

The elliptic cell and interior component test results were used by other ICL team members to create and validate computational models. These models helped determine possible errors from testing, as in the copper biaxial tests which were repeated due to inconsistencies in modeling and expected results versus testing results. Previous ICL models also validated test results when there were not enough tests performed to reach conclusions.

ICL Research Scientist Elham Sahraei created a numerical simulation model of the elliptic cell. This model, Figure 3-51, was created using three parts: shell casing, jellyroll, and endcaps. The jellyroll was modeled with a modified honeycomb material, while the shell casing and endcaps were created using a material with piecewise linear plasticity. The transverse compression test was used to calibrate the hardening curve for the model. The hemispherical punch test was then used to validate the model, and the resulting damage to the model is shown in Figure 3-52. The simulation and test force-displacement curve correlated closely, as seen in Figure 3-53.

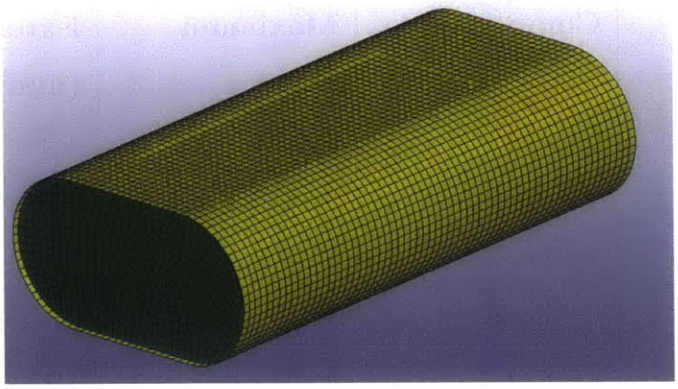

Figure 3-51: Elliptic Cell Model

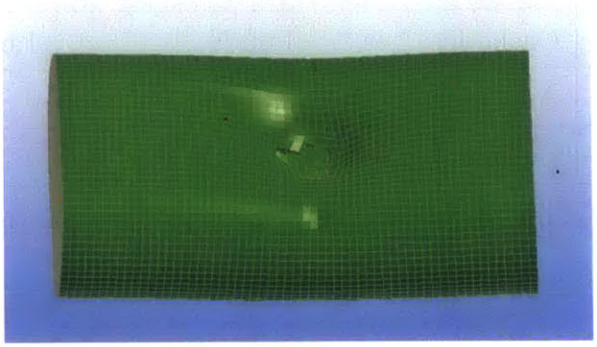

Figure 3-52: Damaged Elliptic Cell Model

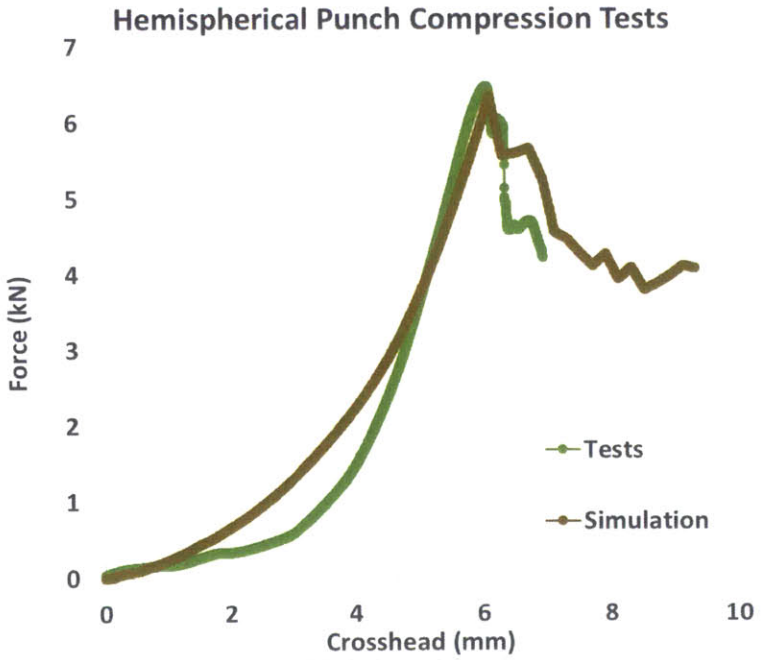

Figure 3-53: Elliptic Cell Hemispherical Punch Simulation and Test Results

At the interior component level, biaxial punch numerical simulation models were created by ICL team member Benjamin Lai. The uniaxial test results were used to create representative stress-strain curves for each material. Because of the varied extension measurements, only the elastic and initial plastic regions of the stress-strain curves were imported into the model. The imported strain at failure was determined from the biaxial punch results. And the coating properties were verified by extracting the coating stress-strain curves from the compression test results.

The biaxial punch numerical simulation model of the elliptic anode sample is seen in Figure 3-54, and Figure 3-57 shows the model of the cathode punch test. The simulated plastic strain contour plots of the anode and cathode biaxial tests at varying strain rates are shown in Figures 3-55 and 3-58. Figures 3-56 and 3-59 show the representative elliptic coated metal biaxial test force-displacement curve with simulation results at varying friction coefficients.

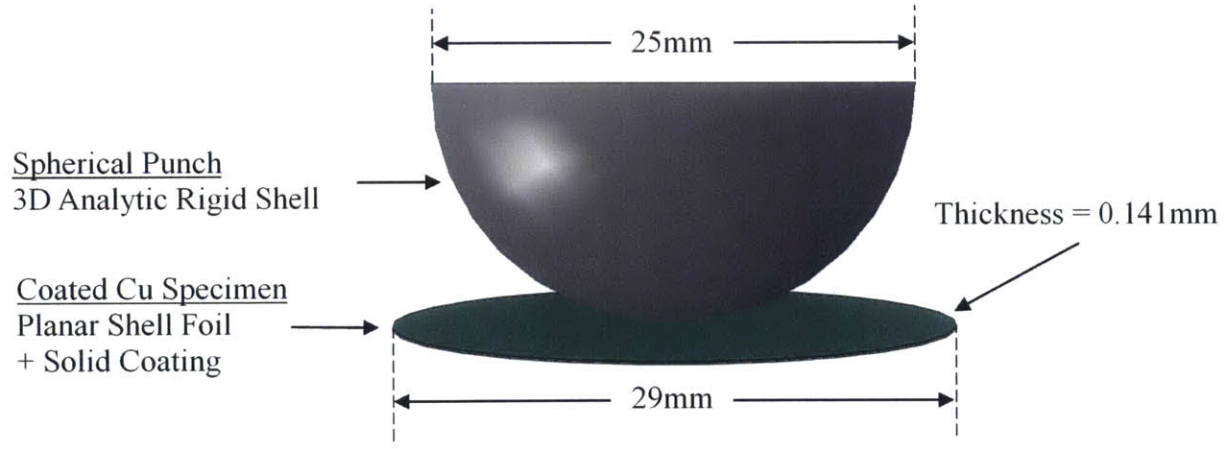

Figure 3-54: Elliptic Anode Biaxial Punch Test Model

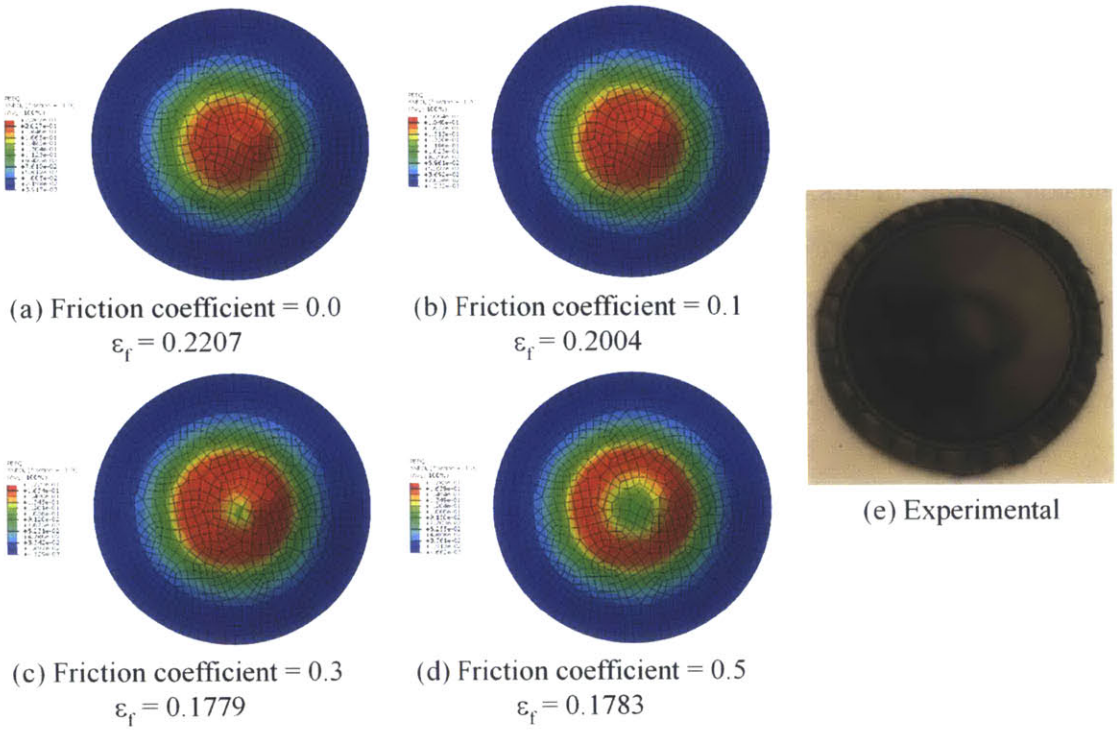

Figure 3-55: Elliptic Anode Biaxial Punch Simulation Contour Plots

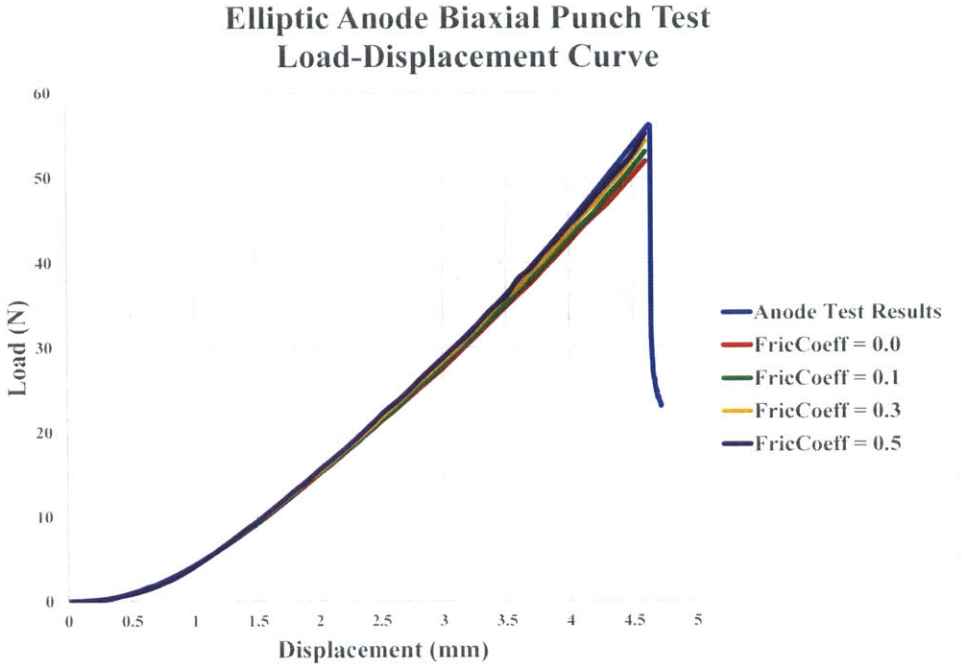

(a) Elliptic Anode Biaxial Punch Simulation and Test Results

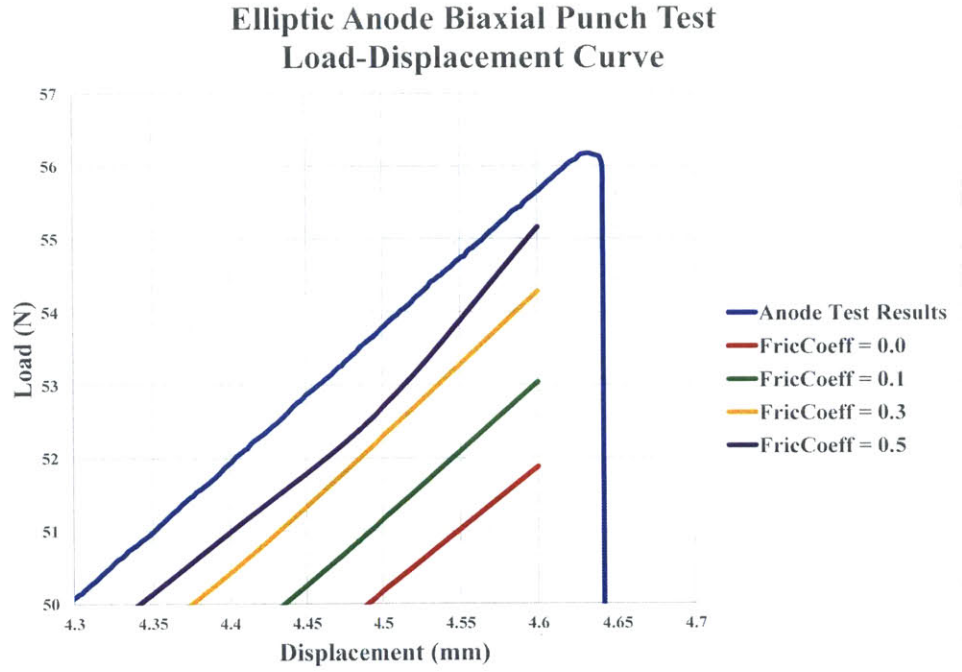

(b) Enlarged View of Graph

Figure 3-56: Elliptic Anode Biaxial Punch Modeling Results

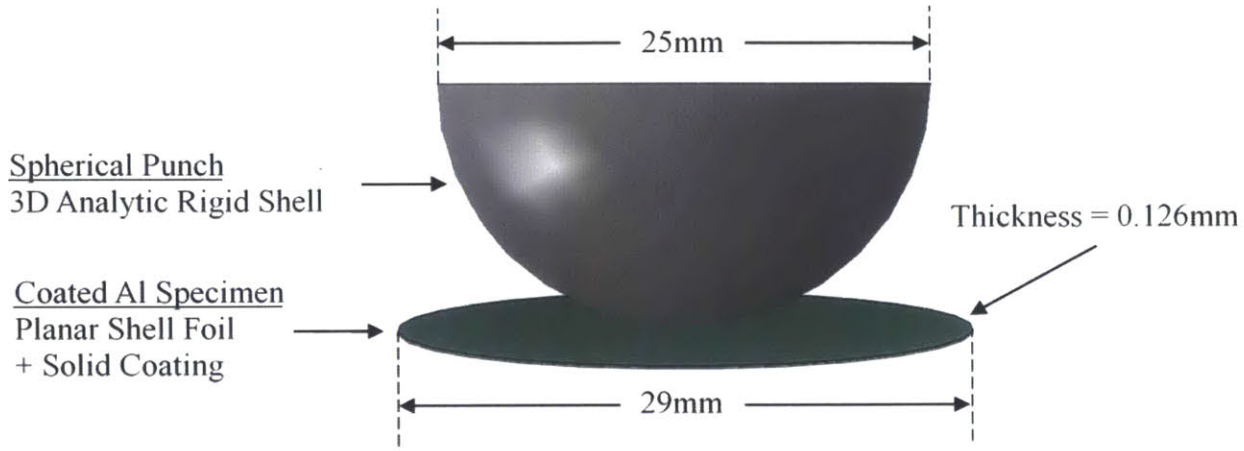

Figure 3-57: Elliptic Cathode Biaxial Punch Test Model

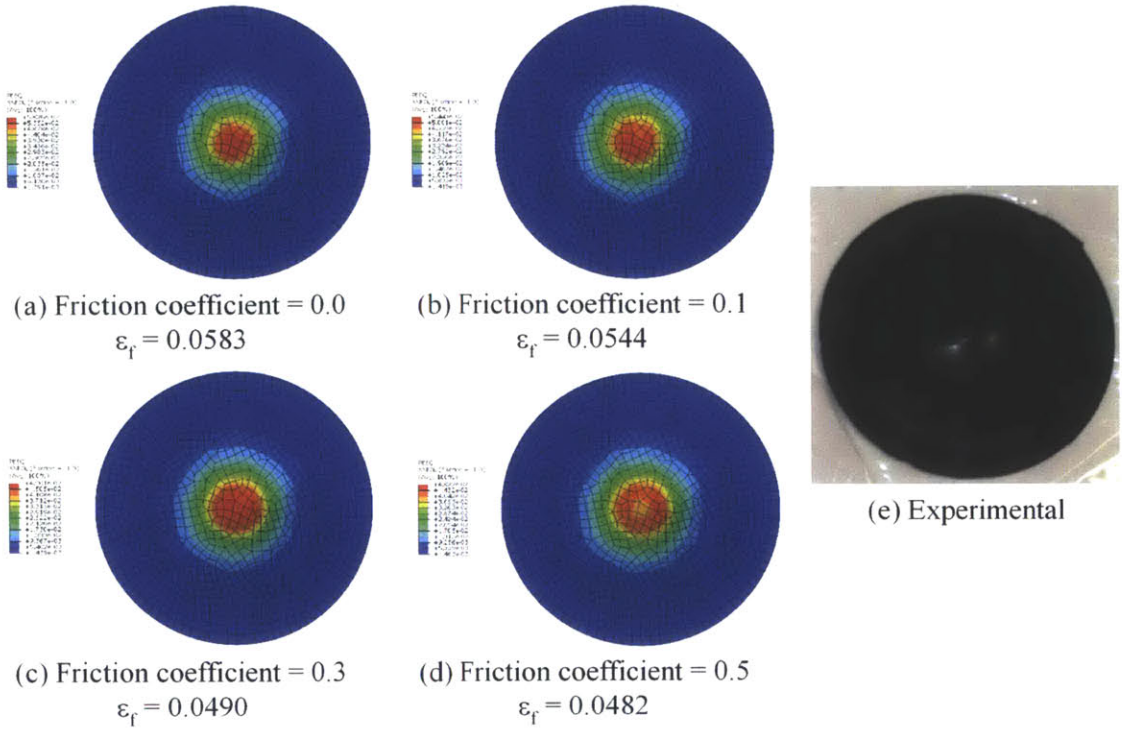

Figure 3-58: Elliptic Cathode Biaxial Punch Simulation Contour Plots

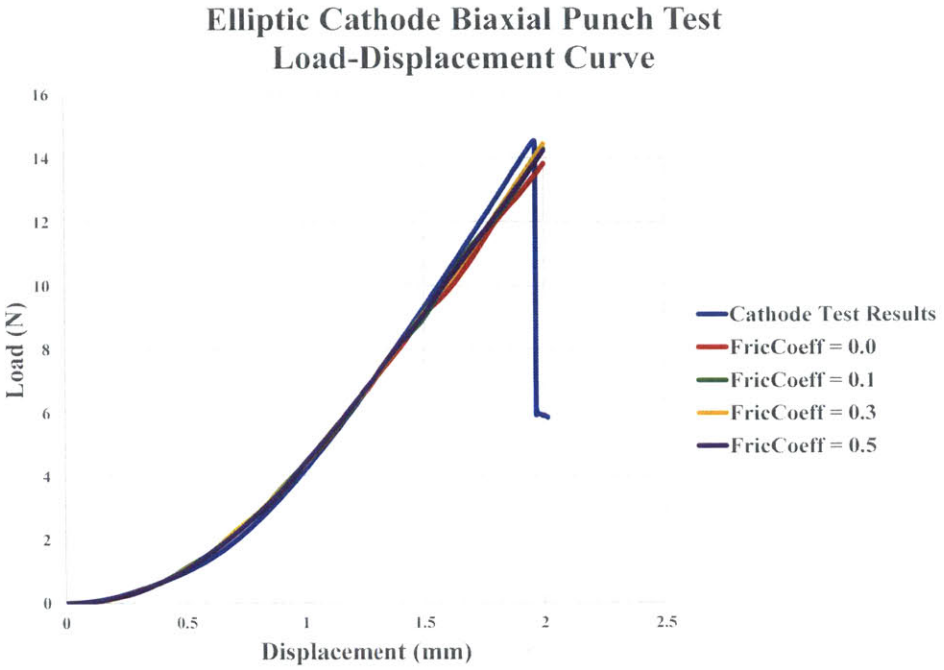

(a) Elliptic Cathode Biaxial Punch Simulation and Test Results

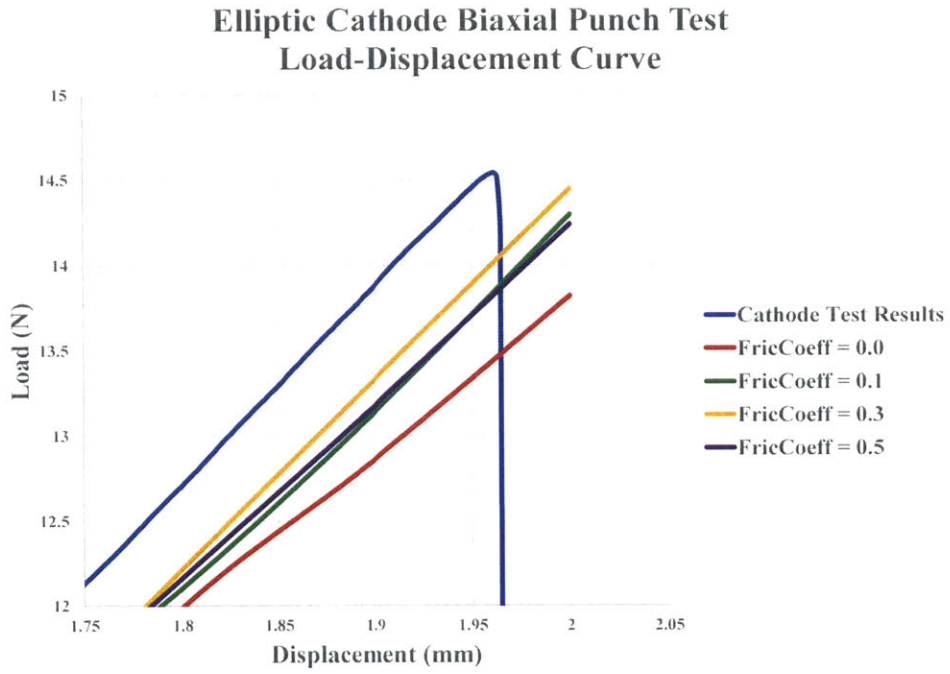

(b) Enlarged View of Graph

Figure 3-59: Elliptic Cathode Biaxial Punch Modeling Results

As seen in Figure 3-56, the anode biaxial test force-displacement curve most closely matched the simulation curve with a friction coefficient of 0.5. Figure 3-59 shows that the curve with a friction coefficient of 0.3 was closest to the cathode biaxial test results. These results were further validated with friction testing conducted by ICL team member Xioawei Zhang[18].

Chapter 4

Pouch Battery Cells

Pouch battery cells have stacked layers of anode, cathode, and separator sheets with a thin flexible enclosure around the stack. ICL sponsors provided both dry pouch cells and charged cells, which were discharged to safe levels for testing in the ICL. One dry cell and one discharged cell were used for compression and hemispherical punch testing. Another dry cell was opened, and the anode and cathode sheets were uniaxial, biaxial, and compression tested. Figure 4-1 shows the battery with approximate dimensions. The battery thickness was measured at 12 mm.

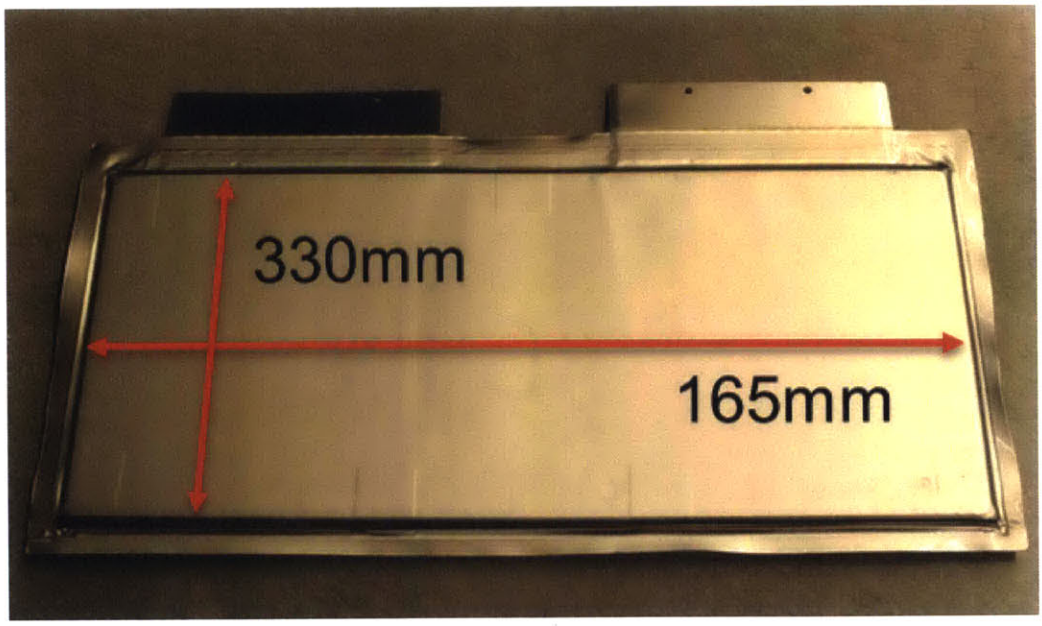

Figure 4-1: Pouch Battery

4.1 Cell Tests

Two pouch cells, one dry and one discharged cell with electrolyte were tested using the MTS Loading Frame. The dry pouch cell was compression and punch tested, and the discharged cell was punch tested. Tape with markings was attached to the MTS fixtures, and the DIC camera tracked the markings for comparison with the MTS displacement results. The voltage and resistance of the cells were recorded using the multimeter. As with the previous dry cell tests, the resistance reading was used as a method to observe cell short circuit.

4.1.1 Pouch Dry Cell

Because the pouch cell was larger than the flat plate fixtures, the dry cell was compression tested using a flat cylinder punch with a diameter of 44.64 mm at a rate of 1 mm/min. Figure 4-2 shows the testing setup, and the results of the test are shown in Figure 4-3. The maximum force of 174 kN occurred at a crosshead of 4.7 mm. The resistance drop was observed at 2.1 mm, well before the maximum force is reached.

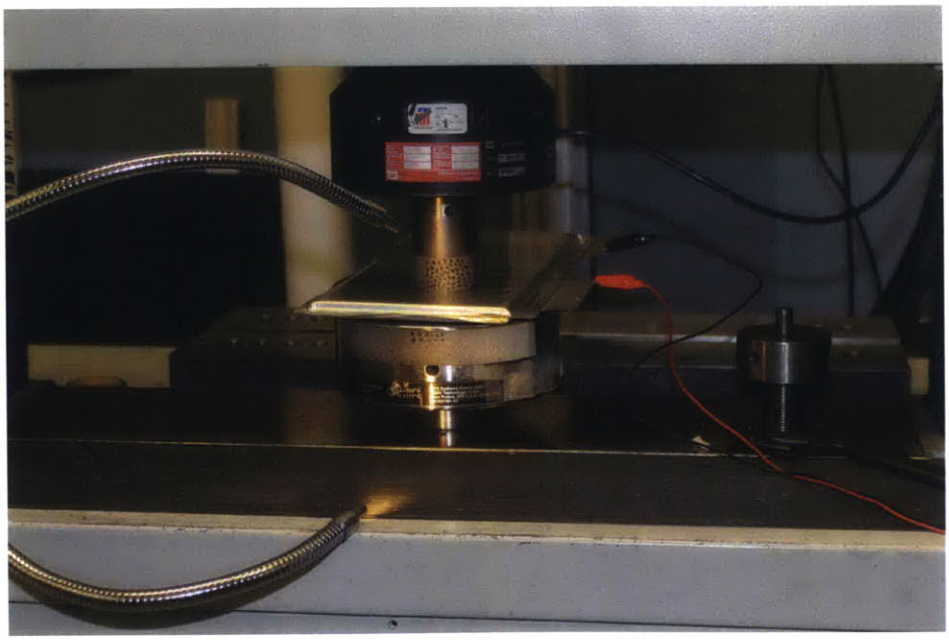

Figure 4-2: Pouch Dry Cell Compression Test Setup

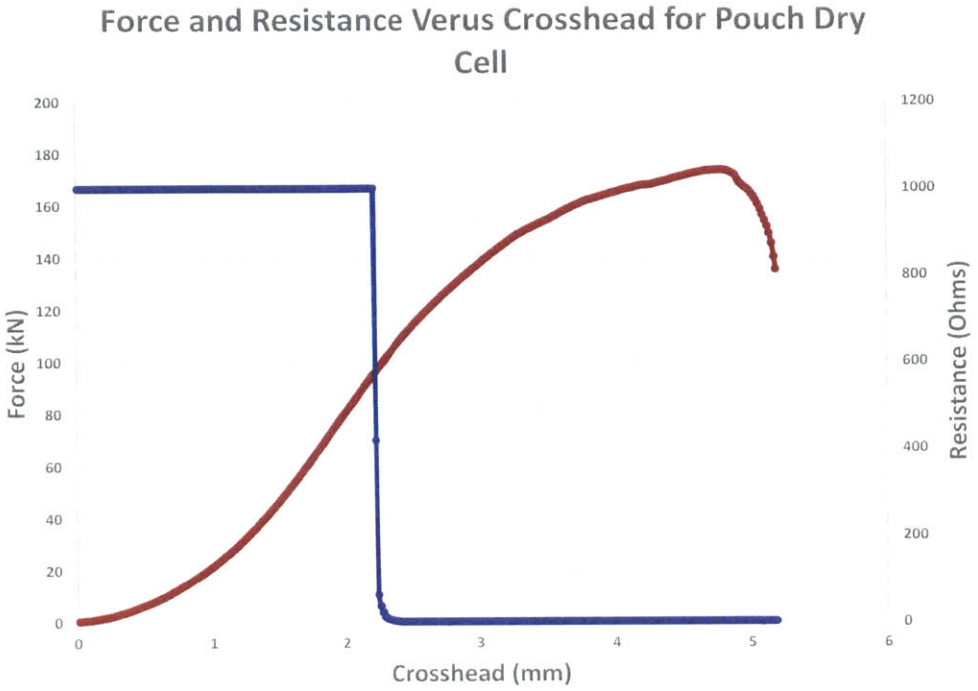

Figure 4-3: Pouch Dry Cell Compression Test Results

Next, the dry pouch cell was hemispherical punch tested with a 12.5 mm diameter punch at a rate of 1 mm/min. The tests were conducted on the opposite end of the cell from the compression test location. Due to the damage from the compression test, no resistance measurements could be obtained, and the resistance was not recorded. Figure 4-4 shows the hemispherical test setup.

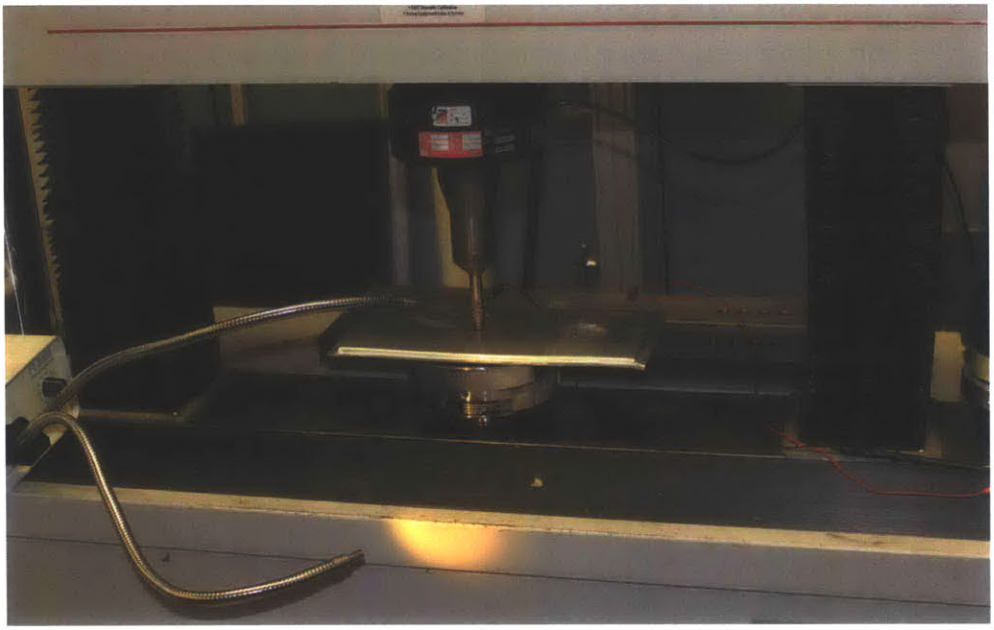

Figure 4-4: Pouch Dry Cell Hemispherical Punch Test Setup

The first series of hemispherical punch tests were performed at varying locations on the dry pouch cell. The first test was located in the center of the cell, approximately 65 mm from the cell's long edge. The second test was 30 mm from the long edge, and the third was 10 mm from the long edge. The fourth test was performed on the edge of the cell. And the fifth test was also on the cell edge, but with the punch centered on the edge. Figure 4-5 shows the third punch test, along with the locations of the first two tests. Figure 4-6 shows the punch indentations of the last two tests.

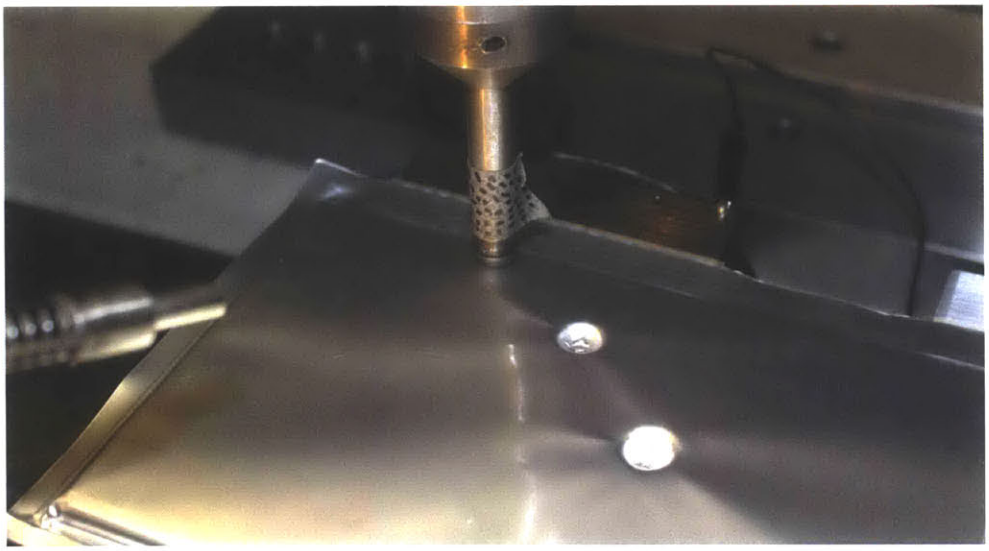

Figure 4-5: Pouch Dry Cell Hemispherical Punch Test 3

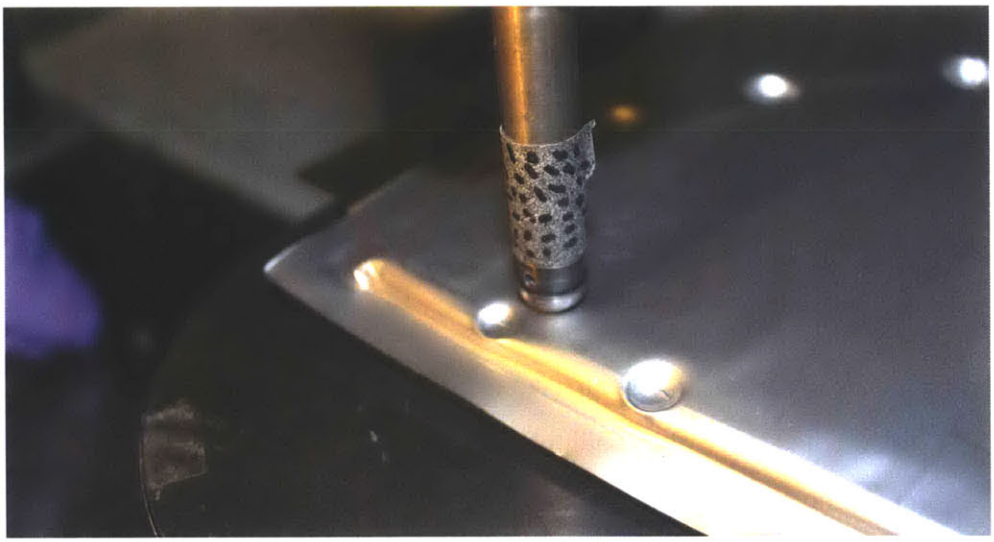

Figure 4-6: Location of Edge Indentations on Pouch Dry Cell

Figure 4-7 shows the results of the punch tests at varying locations on the pouch cell. The plots of three tests that were not on the cell edge were consistent, and all had maximum force measurements around 7.8 kN at a crosshead of 4.1mm. The two tests on the edge had much lower maximum force results. This result was expected since the edge of the cell had less material than the cell interior. The first test performed on the cell edge had a maximum force of 3.1 kN at a crosshead of 2.8 mm, while the second had a maximum force of 1.5 kN at 2.2 mm.

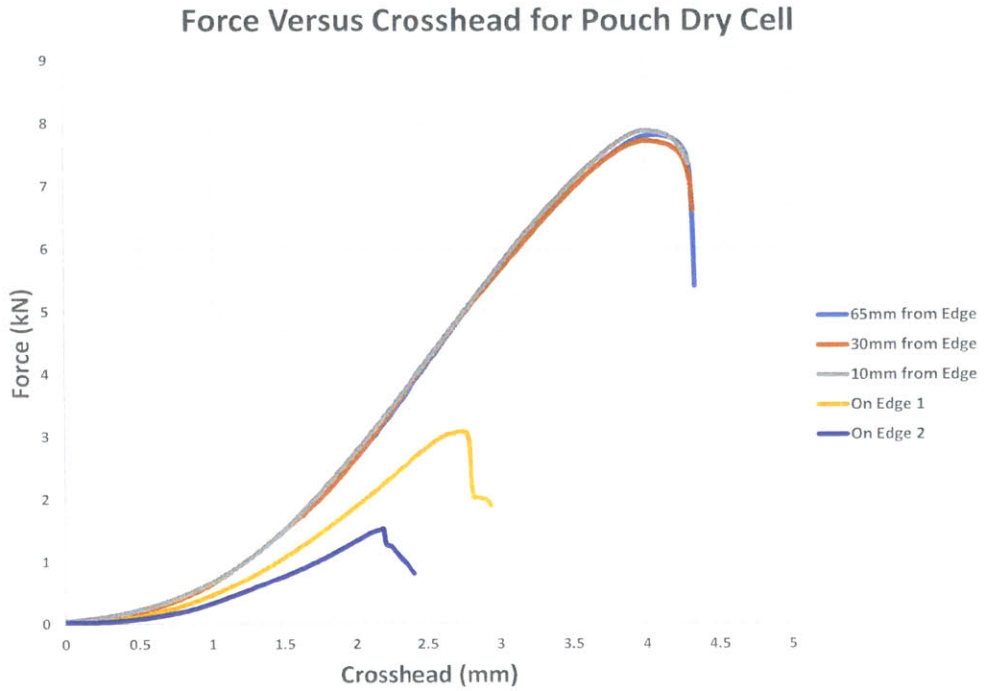

Figure 4-7: Pouch Dry Cell Hemispherical Punch Test Results at Varying Locations

The second set of hemispherical punch tests was performed at varying speeds from 0.2 mm/min to 20 mm/min. To ensure accurate displacement results, the MTS measurements were verified with the displacement data obtained from the DIC analysis. Figure 4-8 shows the test results. Increasing speeds produced increasing maximum force and crosshead measurements. The curves for the 1 mm/min and 2 mm/min tests were extremely close, as were the 10 mm/min and 20 mm/min test curves. Therefore, the 1 mm/min, 5 mm/min, and 10 mm/min curves were removed to show the tests at strain rates of three orders of magnitude in Figure 4-9.

The 20 mm/min punch test had the highest maximum force of 8.4 kN, and the 2 mm/min punch test had a maximum force of 7.7 kN. The 0.2 mm/min test had the lowest maximum force of 7.3 kN. All three maximum force measurements occurred at approximately 4 mm crosshead. This result of increasing maximum force with increasing strain rate was expected.

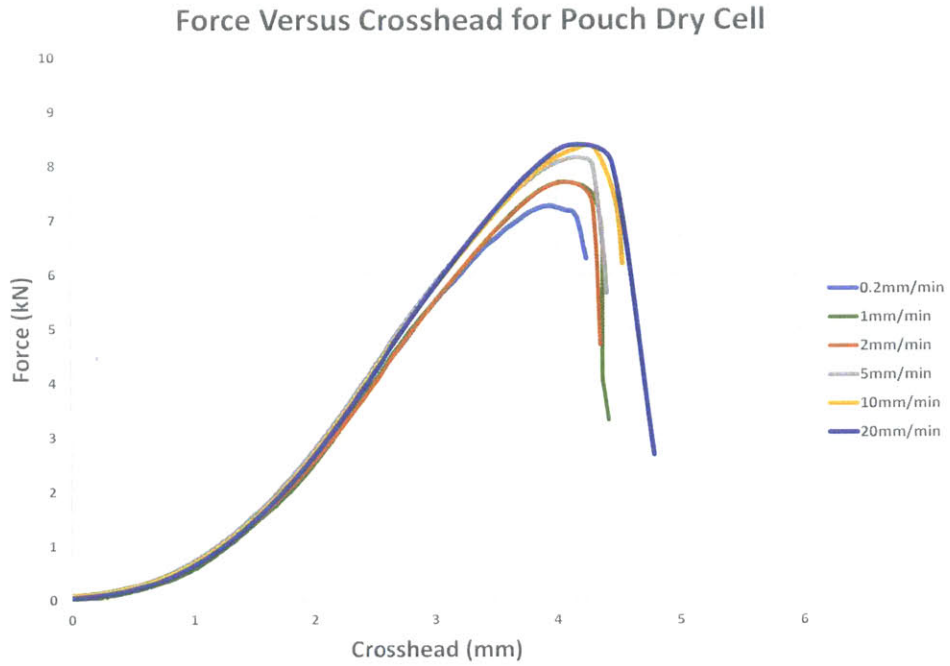

Figure 4-8: Pouch Dry Cell Hemispherical Punch Test Results at Varying Rates

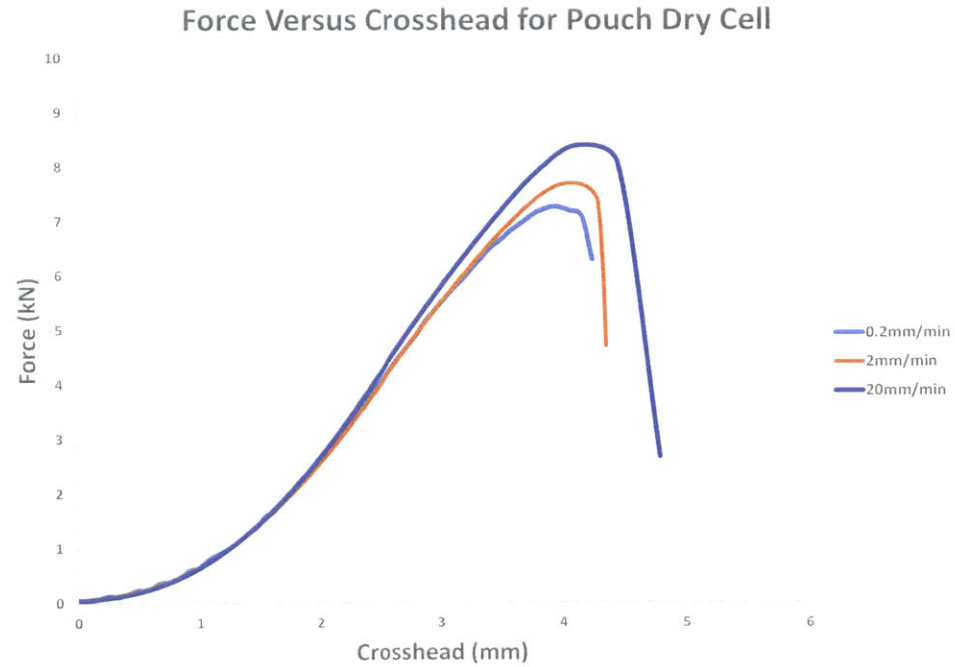

Figure 4-9: Pouch Dry Cell Hemispherical Punch Test Results at Three Strain Rates

Following all tests, the pouch dry cell was opened. Figure 4-10 shows the cell with the top exterior pouch removed. The resulting damage to the top separator layer and location of all indentations was observed.

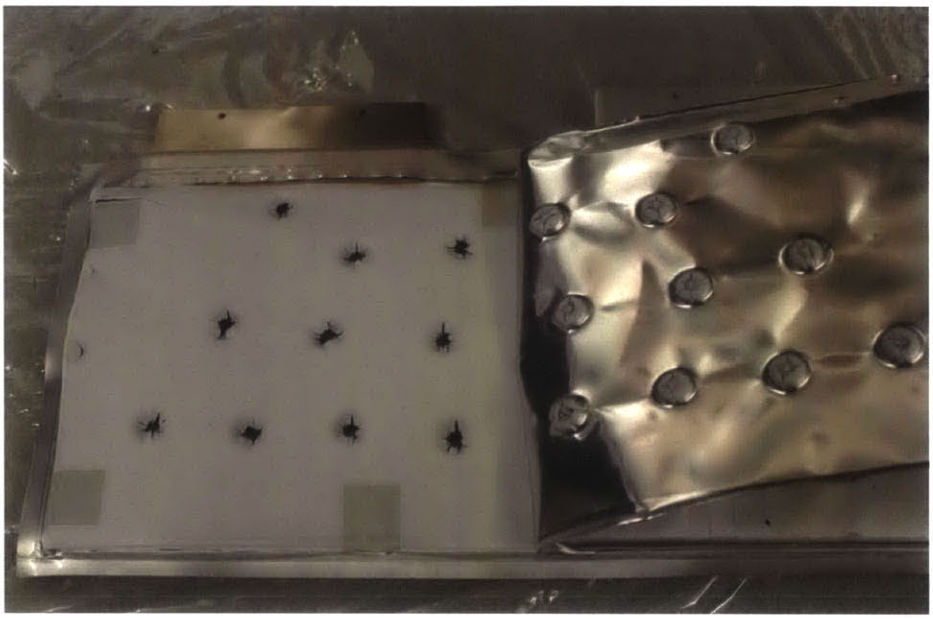

Figure 4-10: Interior Damage to Pouch Dry Cell

4.1.2 Pouch Discharged Cell

The discharged pouch cell was punch tested using the 12.5 mm diameter hemispherical punch at two speeds, 1 mm/min and 5 mm/min. The discharged pouch cell still had a small amount of voltage, around 3 V, so the multimeter was used to measure the voltage of the cell. In addition, the thermometer tracked temperature during the tests. But because the thermocouple was placed on the outside of the cell, away from the punch, the temperature recordings were not useful.

For safety purposes, the pouch cell was placed in an enclosure with attached fan to vent gases. A plastic bag around the cell prevented electrolyte spillage, and SOLUSORB® was available if needed for cleanup. The cell was also marked so that any bulging of the cell due to gas formation would be apparent. Figure 4-11 shows the test arrangement.

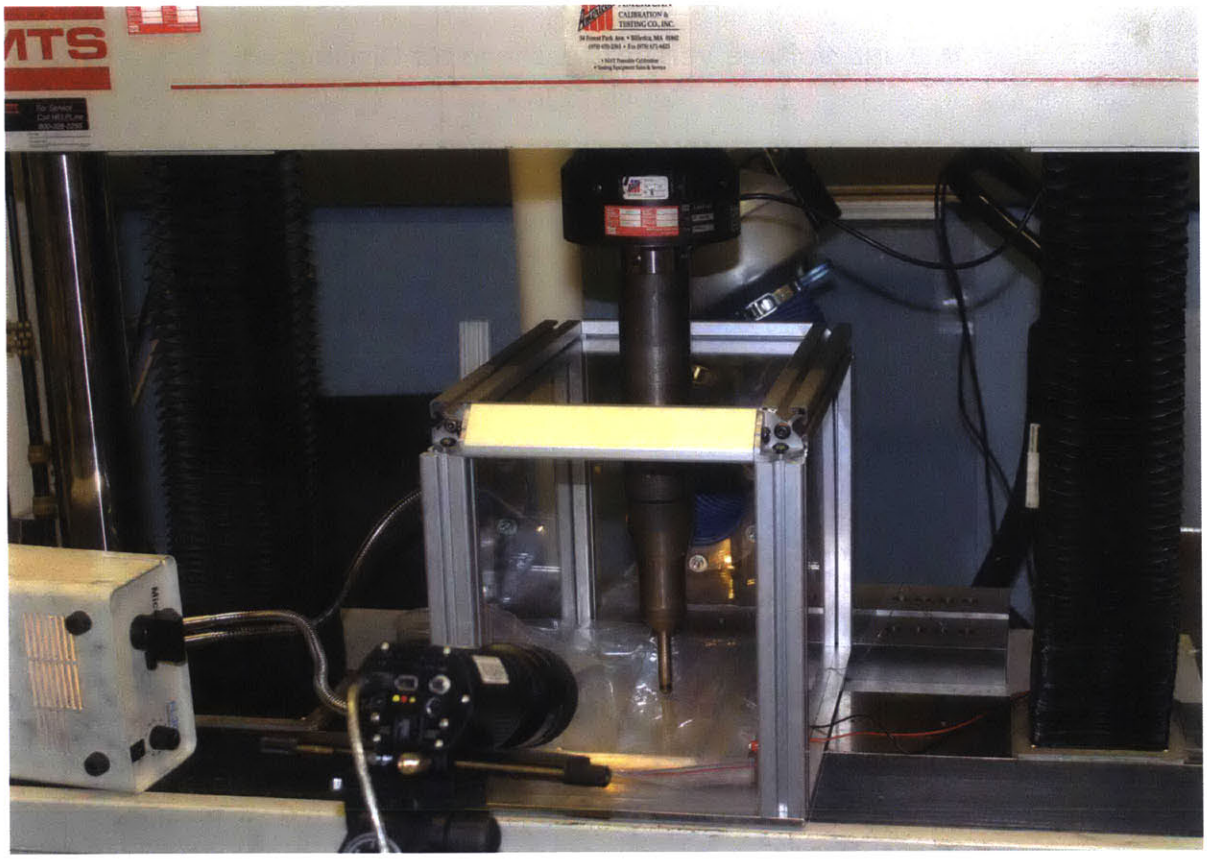

Figure 4-11: Pouch Discharged Cell Hemispherical Punch Test Setup

The first punch test was performed at 1 mm/min, and the results of the force and resistance measurements are displayed in Figure 4-12. The maximum force was 5.3 kN at a crosshead of 3.3 mm. The short circuit of the cell occurs near the maximum force, with the initial voltage drop around 3.1 mm crosshead. No bulging of the cell occurred.

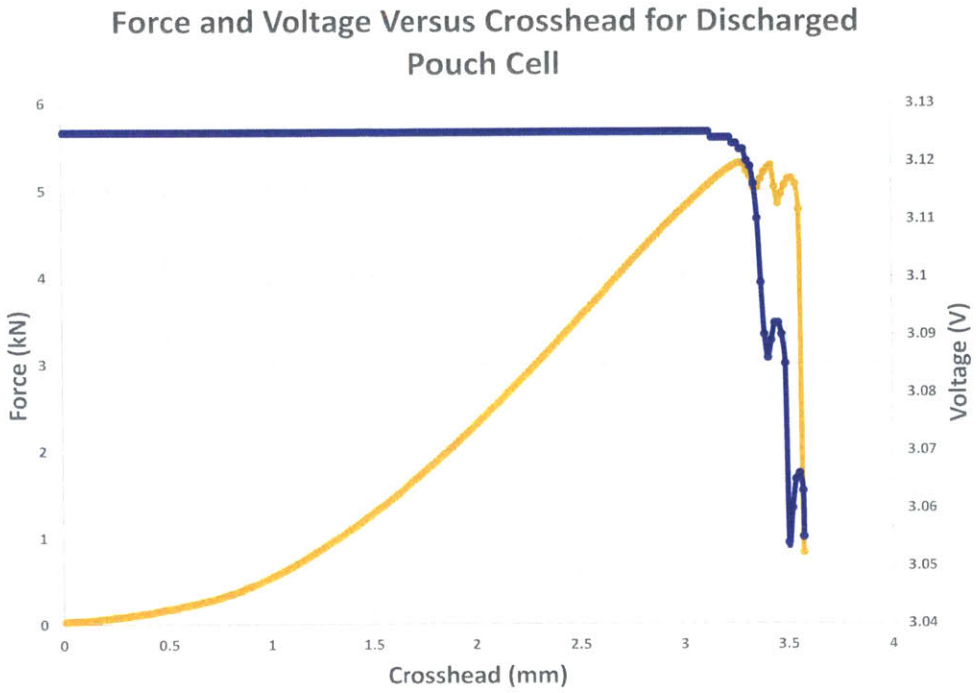

Figure 4-12: Pouch Discharged Cell Hemispherical Punch Test Results

The pouch cell was punch tested three more times. The punch test was repeated at 1 mm/min and conducted twice at 5 mm/min. Due to the short circuit of the cell during the first punch test, the voltage could not be measured for the following tests. Figure 4-13 shows the force results for all four tests.

The two 1 mm/min punch tests had consistent maximum force and crosshead measurements, 5.3 kN at a crosshead of 3.3 mm for the first test and 5.4 kN at 3.5 mm for the second. The two higher speed tests also had consistent results. The first 5 mm/min punch test had a maximum force of 6.0 kN at a crosshead of 3.8 mm, while the second test had a 6.1 kN maximum force at 3.6 mm. The higher speed tests had higher maximum force measurements, which was expected.

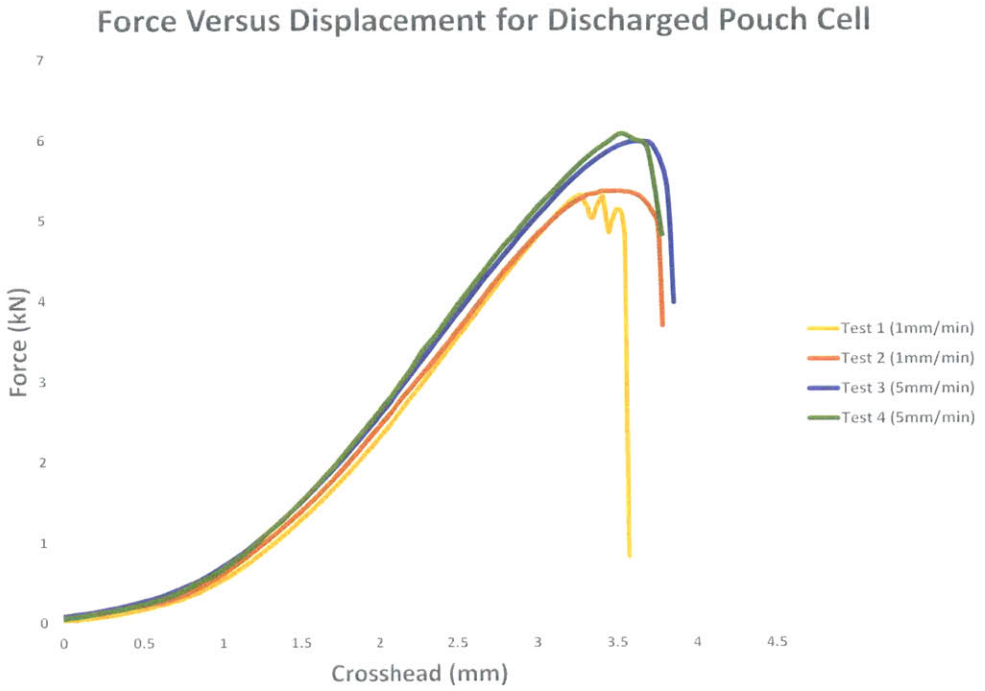

Figure 4-13: Discharged Pouch Cell Hemispherical Punch Test Results at Varying Rates

To compare the results of the dry and discharged pouch cell tests, the the hemispherical punch test plots for both cells at 1 mm/min and 5 mm/min rates were combined in Figure 4-14. Both the dry and discharged pouch cells have higher maximum force measurements at higher test speeds. And the dry cell had higher maximum force and crosshead measurements than the discharged cell at both rates.

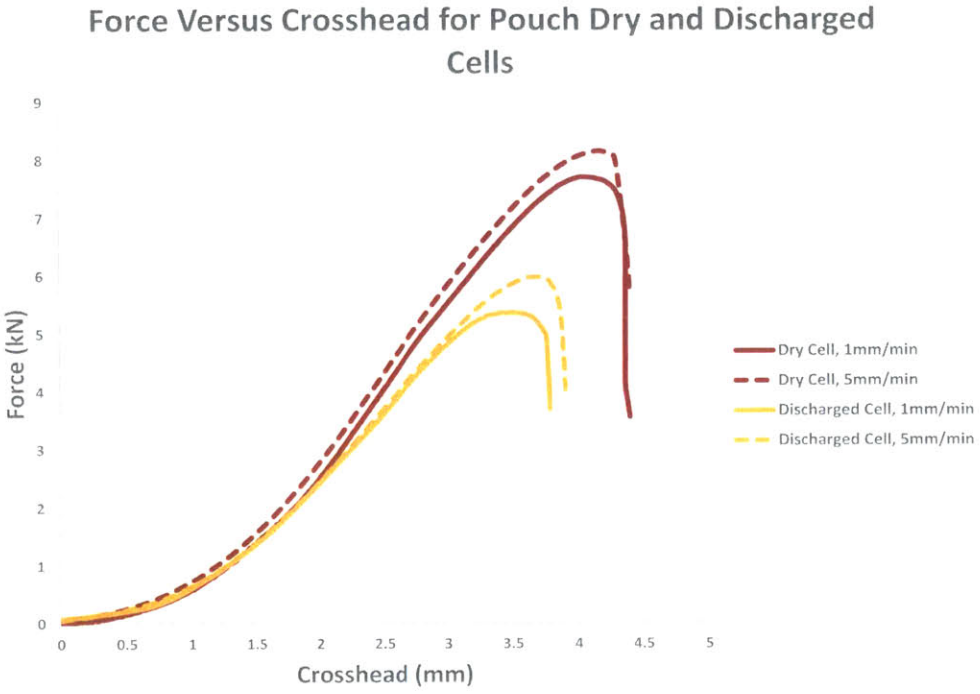

Figure 4-14: Dry and Discharged Pouch Cell Hemispherical Punch Test Results at Varying Rates

4.2 Interior Component Tests

One dry pouch cell was provided for interior component testing. This cell was opened, and sheets of anode and cathode were removed for testing. Figure 4-15 shows the dry cell before and after the outer shell was removed. The separator is the first layer seen in the opened cell photographs. The thicknesses of the bare copper, bare aluminum, and anode and cathode sheets were measured and are displayed in Table 4.1.

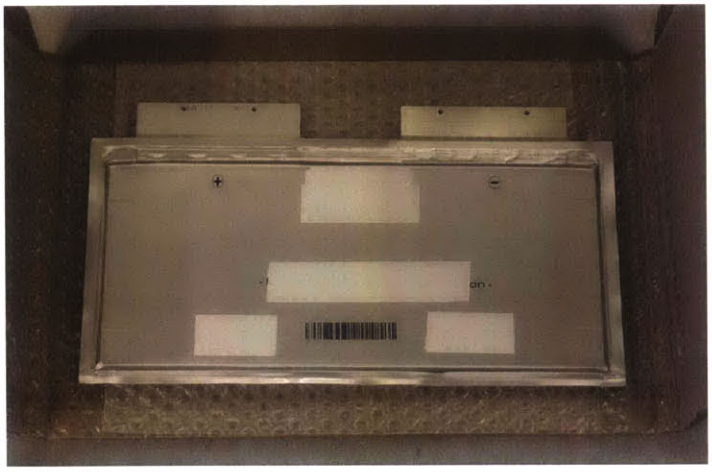

(a) Dry Pouch Cell

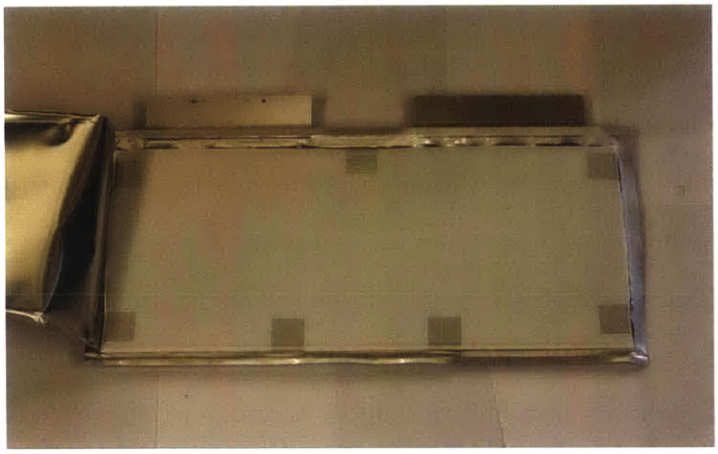

(b) Opened Pouch Cell

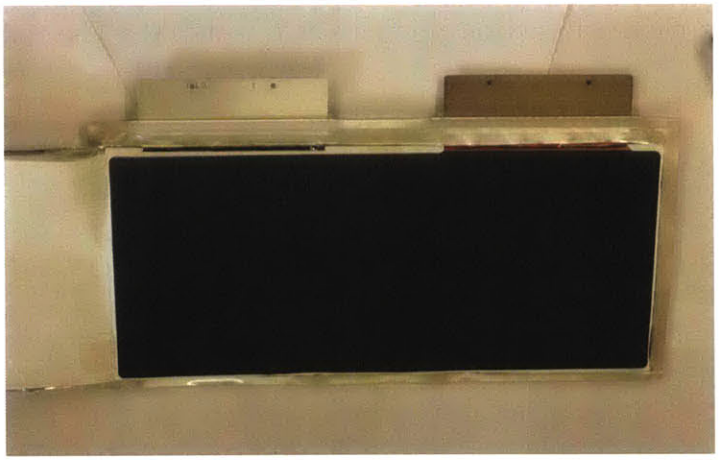

(c) Opened Pouch Cell with Separator Layer Removed

Figure 4-15: Dry Pouch Cell Before and After Outer Shell Removal

Component	Thickness (μm)
Copper	16
Aluminum	24
Anode	149
Cathode	134

Table 4.1: Pouch Cell Sheet Thicknesses

4.2.1 Uniaxial Test Details and Results

The sheets of anode and cathode were carefully removed from the cell, and uniaxial test samples were prepared using lined paper and an X-Acto© knife. Each sample was 85 mm long and 10 mm wide. Paper tape was applied to the samples in the same manner as the elliptic coated metal samples to prevent sample damage from machine grip pressure. The uniaxial tests were conducted using the Instron machine fitted with the pneumatic grips at a rate of 0.2 mm/min.

The anode and cathode samples were cut in both the rolling and 90° direction. The rolling direction of the metal foil of the anode and cathode sheets was not obvious, so a direction was chosen based on previous ICL tests[11]. The rolling direction is illustrated in Figure 4-16.

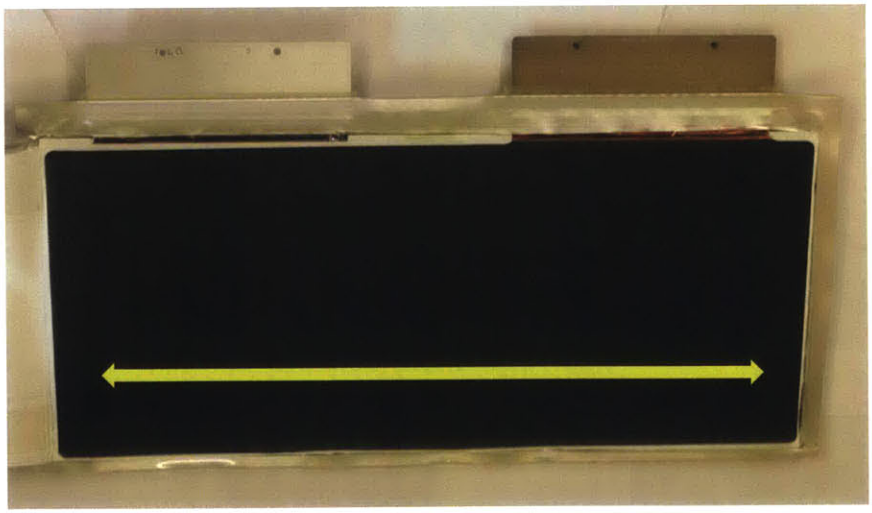

Figure 4-16: Machine Direction of Coated Sheets from Pouch Cell

The results of the anode tests are shown in Figures 4-17 and 4-18. In the rolling direction, the anode samples had a maximum force of 15 N at an extension of 0.6 mm, while the maximum force for the anode samples in the 90° direction was 20 N at 0.6 mm. Therefore, the anode samples were anisotropic. In addition, tearing occurred in all uniaxial tests of anode samples. Figure 4-19 shows the anode uniaxial test samples.

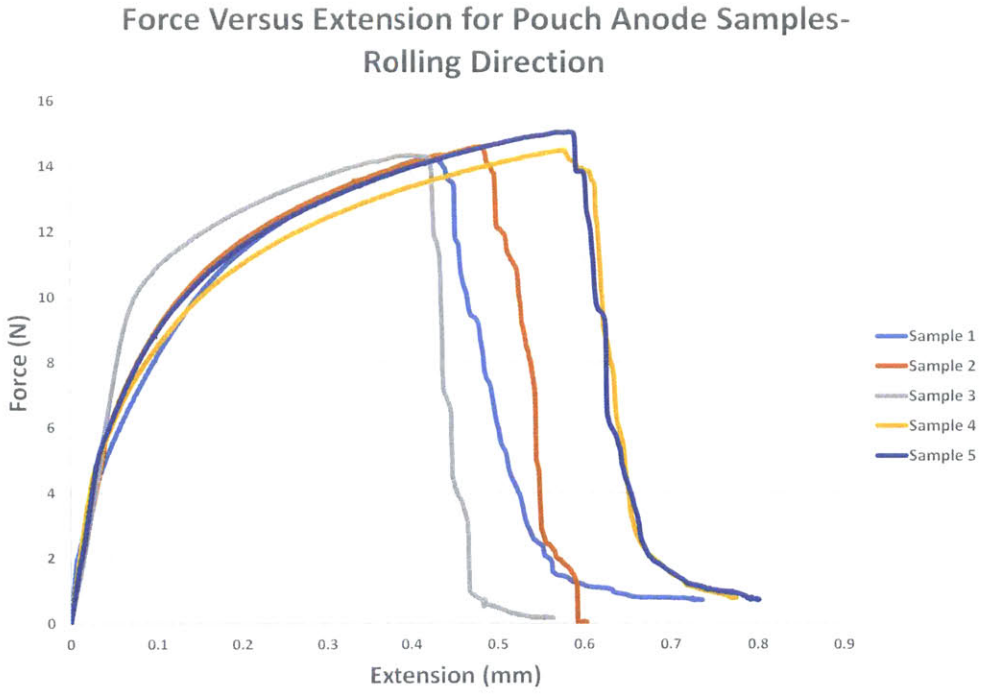

Figure 4-17: Pouch Anode Uniaxial Test Results- Rolling Direction

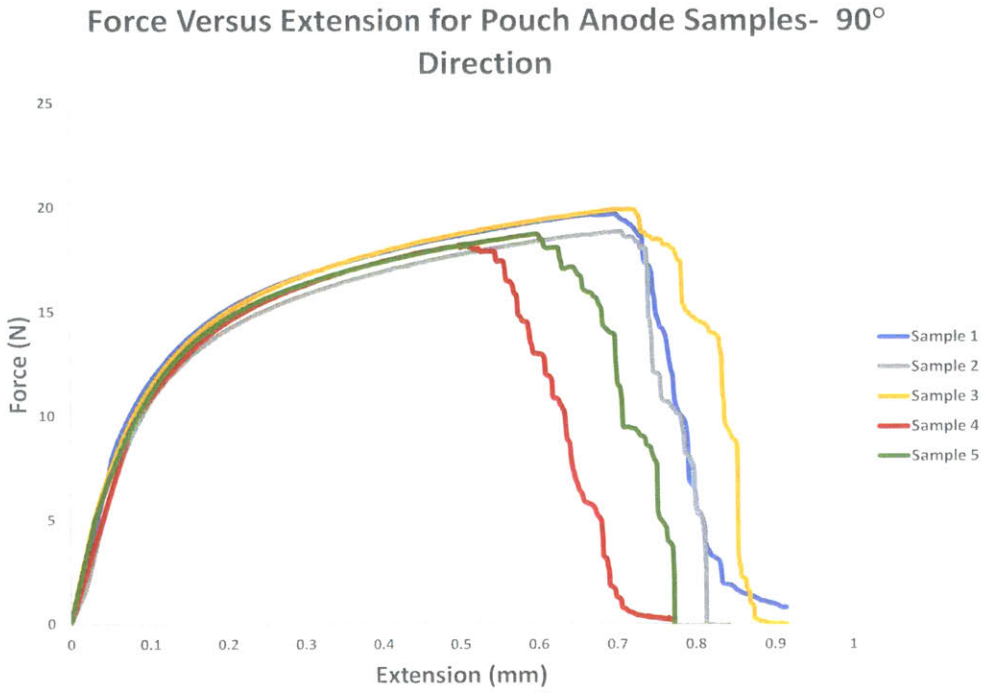

Figure 4-18: Pouch Anode Uniaxial Test Results- 90° Direction

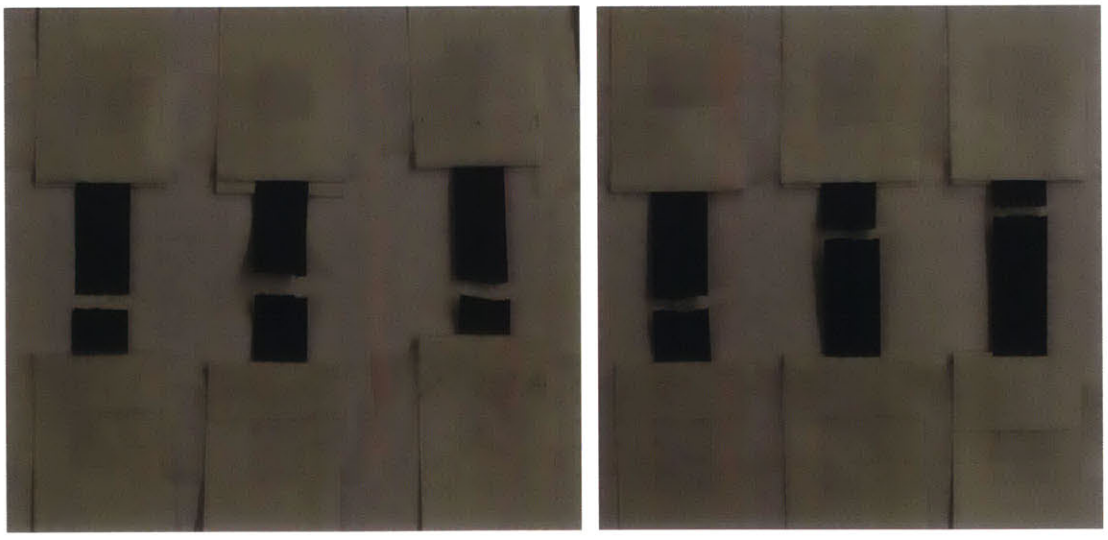

(a) Machine Direction (b) 90° Direction

Figure 4-19: Pouch Anode Uniaxial Test Samples

The cathode uniaxial test results are displayed in Figures 4-20 and 4-21. The cathode samples in the rolling direction had a maximum force of 37 N at an extension of 0.7 mm. In the 90° direction, the maximum force of the anode samples was also 37 N, and the maximum extension was 0.7 mm. The cathode samples were therefore isotropic. Figure 4-22 shows the samples following uniaxial testing.

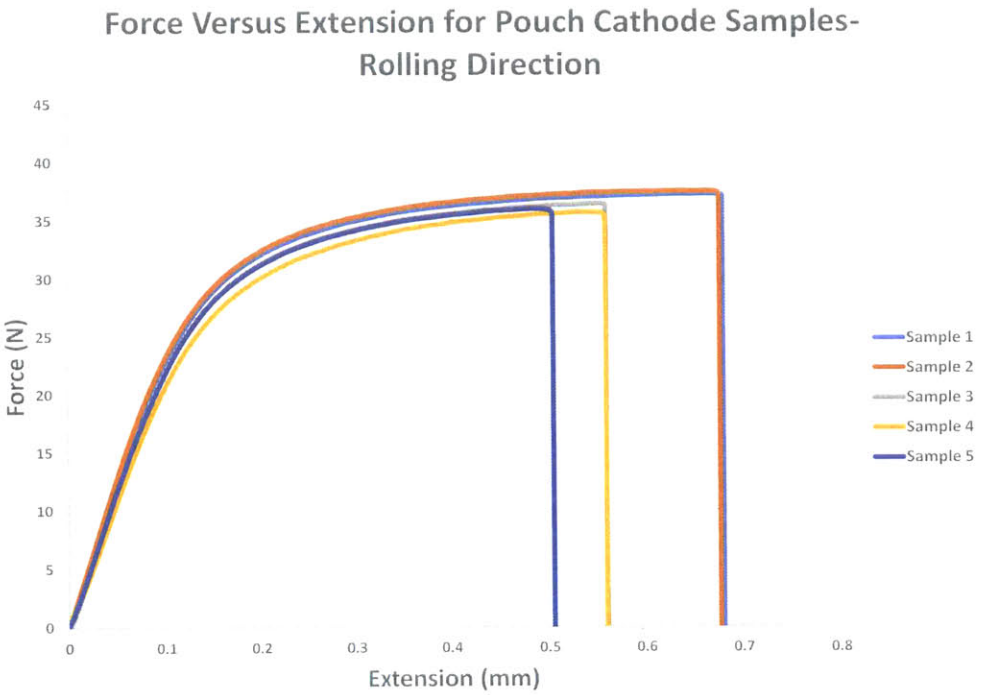

Figure 4-20: Pouch Cathode Uniaxial Test Results- Rolling Direction

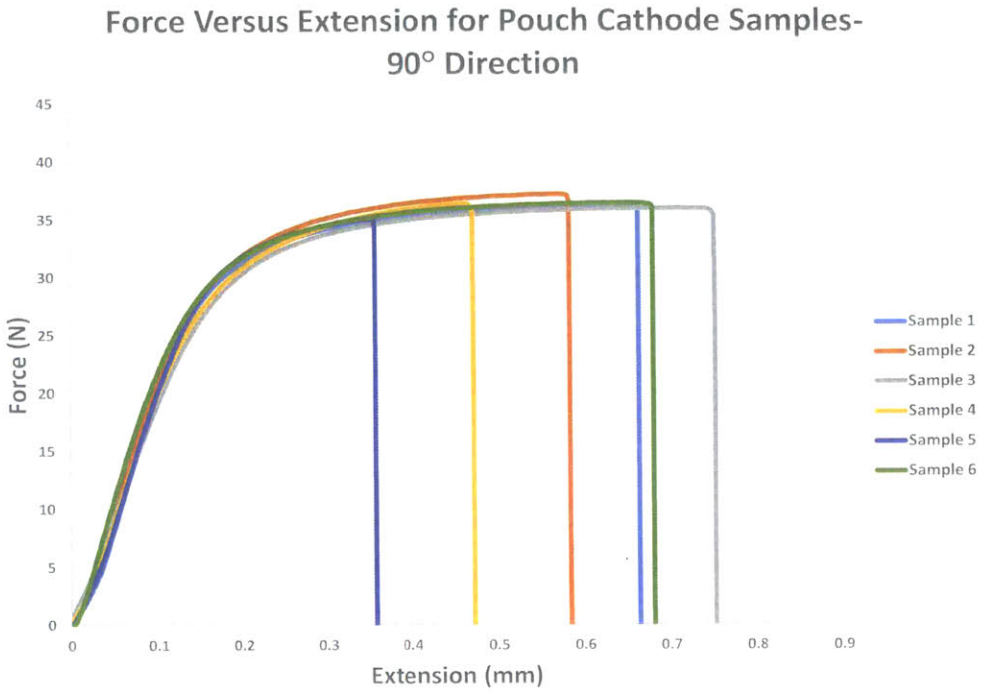

Figure 4-21: Pouch Cathode Uniaxial Test Results- 90° Direction

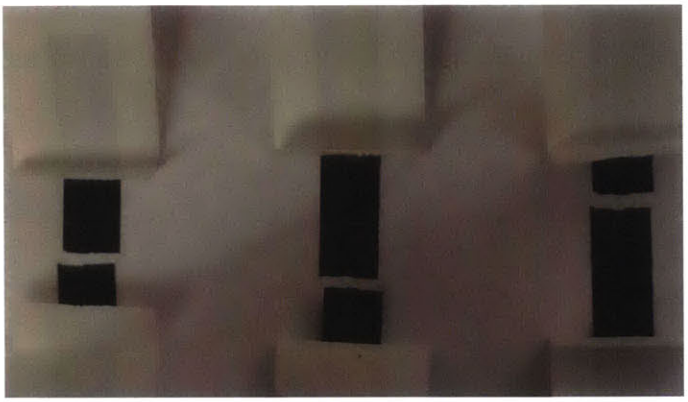

(a) Machine Direction

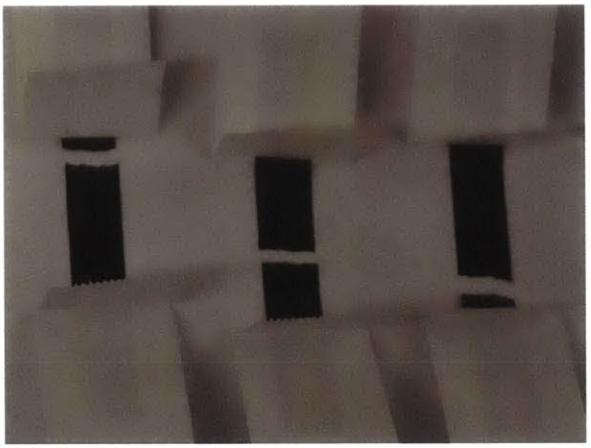

(b) 90° Direction

Figure 4-22: Pouch Cathode Uniaxial Test Samples

4.2.2 Biaxial Test Details and Results

Circular samples were cut from the pouch cell anode and cathode sheets using a metal punch with diameter of 45 mm. The biaxial punch test was conducted using the Instron machine fitted with a spherical punch at a rate of 1 mm/min. The samples were placed in a mount, which consisted of two circular metal plates that hold the sample and were tightened together with screws.

Figure 4-23 shows the punch test results for the pouch anode sheets. During the testing, issues with sample loading occurred, and only three samples were used for further analysis. The maximum force for the pouch anode samples was 12 N at an extension of 2.4 mm. Sample 6, shown in Figure 4-24, had an off-center fracture point, indicating a non-zero friction coefficient between the anode sample and the punch.

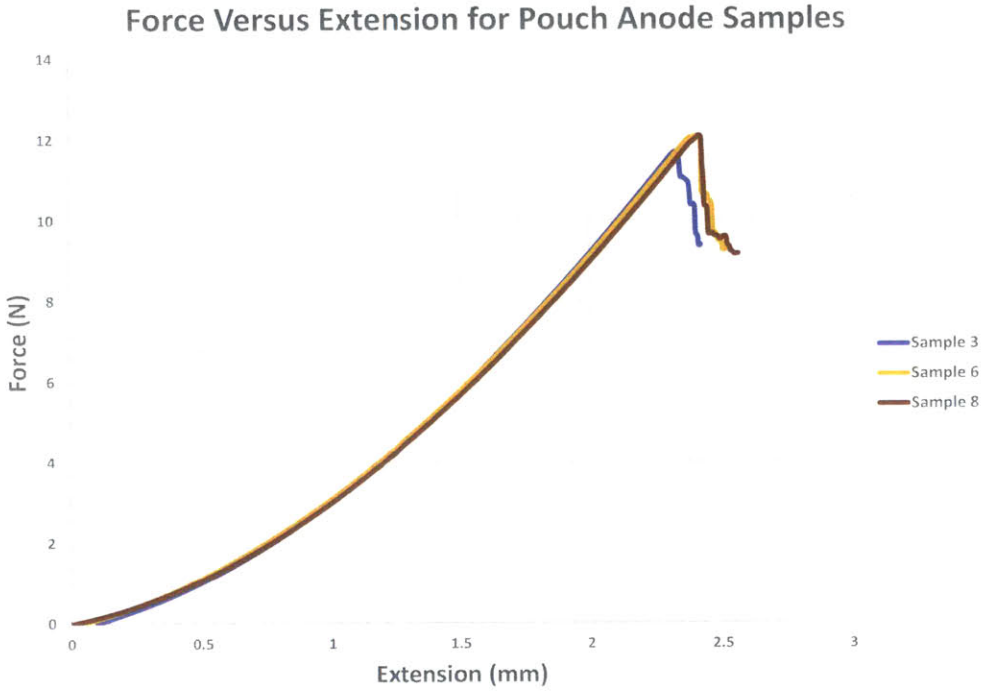

Figure 4-23: Pouch Cathode Biaxial Punch Test Results

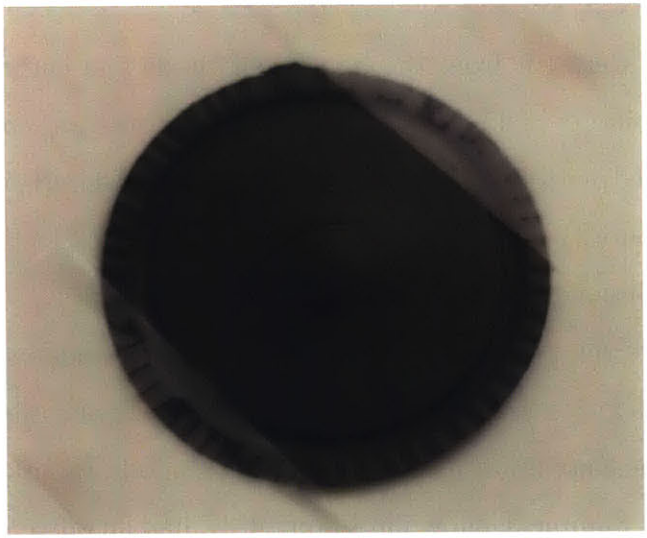

Figure 4-24: Pouch Anode Biaxial Test Sample 6

The punch test results for the pouch cathode samples are displayed in Figure 4-25. Fewer loading issues occurred with the cathode samples, so more samples were available for further analysis. The maximum force for the biaxial punch test was 25 N at an extension of 2.3 mm. Figure 4-26 shows the cathode sample with the highest force measurement, Sample 1. The crack in Sample 1 was not in the center of the sample, and this indicated that the cathode and punch also had a non-zero friction coefficient.

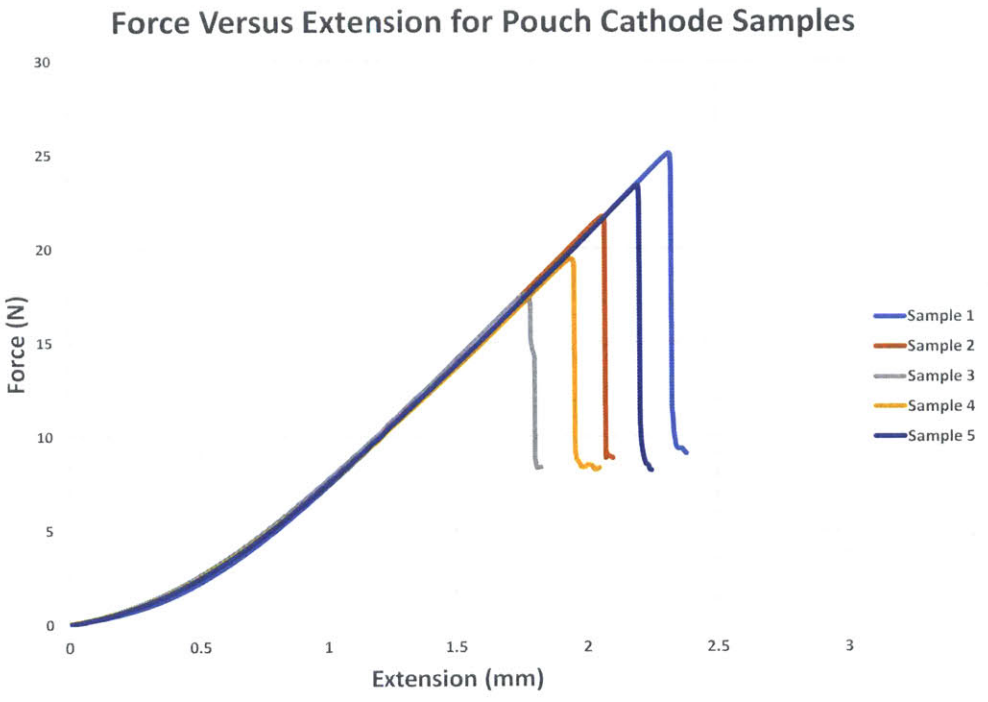

Figure 4-25: Pouch Cathode Biaxial Punch Test Results

Figure 4-26: Pouch Cathode Biaxial Test Sample 1

4.2.3 Compression Test Details and Results

Pouch anode and cathode compression test samples were prepared using a metal punch with a diameter of 16 mm. Twenty samples of each material were stacked, and the MTS Loading Frame fitted with flat plate fixtures was used to conduct the tests at a rate of 0.2 mm/min. Tape with markings was applied to the plates and tracked using DIC to compare with the MTS displacement readings.

Figure 4-27 shows the compression test results for the pouch anode samples, and the cathode compression test results are displayed in Figure 4-28. The maximum force of the anode samples was 23 kN at a crosshead of 1.1 mm. The maximum force of the cathode samples was not reached due to safety concerns.

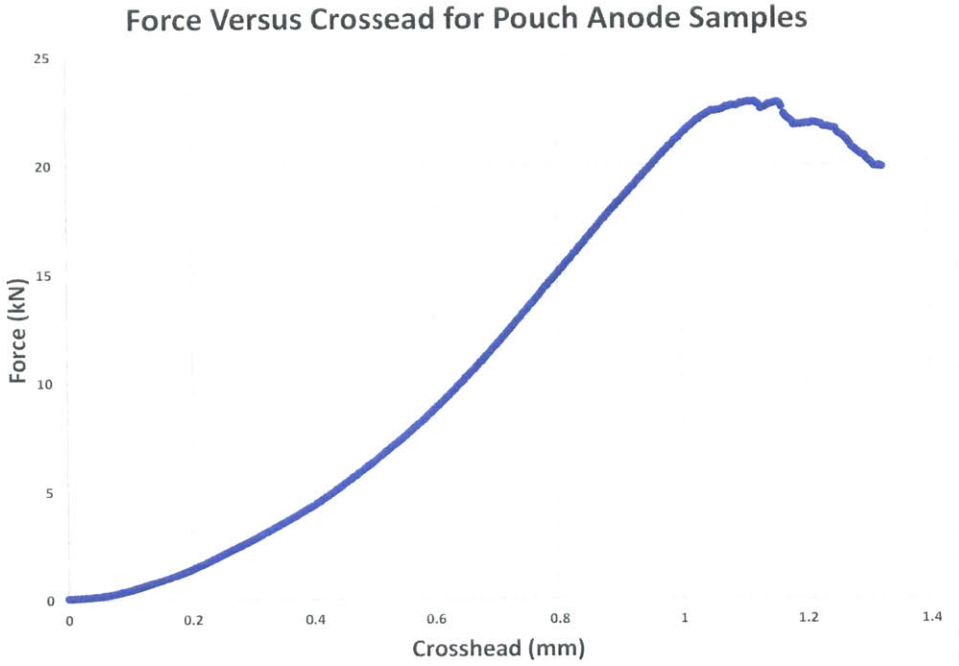

Figure 4-27: Pouch Anode Compression Test Results

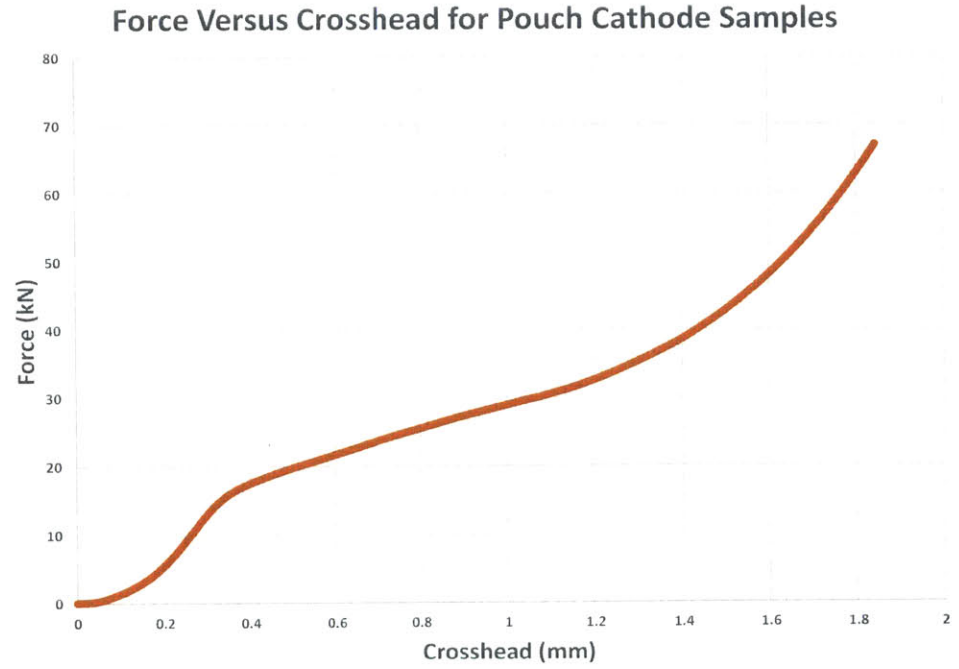

Figure 4-28: Pouch Cathode Compression Test Results

4.3 Summary and Application of Test Results

Table 5.3 shows a summary of the maximum force and corresponding crosshead measurements for each cell and test type. The dry cell had a higher maximum force for all punch tests. No comparison could be made for the compression test since a discharged cell was not tested in this manner.

Test Type	**Cell Type**	**Maximum Force (kN)**	**Crosshead (mm)**
Compression	Dry	173.6	4.8
Punch at 1 mm/min	Dry	7.9	4.0
Punch at 1 mm/min	Discharged	5.4	3.5
Punch at 5 mm/min	Dry	8.1	4.1
Punch at 5 mm/min	Discharged	6.1	3.6

Table 4.2: Pouch Cell Test Results

The summary of interior component test results, Table 5.5, shows that the cathode samples consistently had higher maximum force measurements compared to the anode samples. The anode samples had similar extension measurements as the cathode samples.

Test Type	**Component**	**Maximum Force**	**Extension (mm)**
Uniaxial	Anode	19.9 N	0.7
	Cathode	37.5 N	0.7
Biaxial	Anode	12.1 N	2.4
	Cathode	25.1 N	2.3
Compression	Anode	22.9 kN	1.1
	Cathode	>66 kN	>1.8

Table 4.3: Pouch Cell Interior Component Test Results

The pouch cell and interior component test results were used by other ICL team members to create and validate computational models. Interior component models were not yet completed at the conclusion of this research. These models will be completed and presented in future ICL articles.

ICL Research Scientist Elham Sahraei created the numerical simulation model for the pouch cell in Figure 4-29. The model consisted of one part, the electrode stack, created with a modified honeycomb material. Based on previous testing and modeling of small pouch cells, the contribution of the pouch was negligible and not modeled. The model's hardening curve was calibrated using the flat cylinder compression test. The model was then validated with the hemispherical punch test. The resulting damage to the model is shown in Figure 4-30, and the simulation and test force-displacement curve is shown in Figure 4-31.

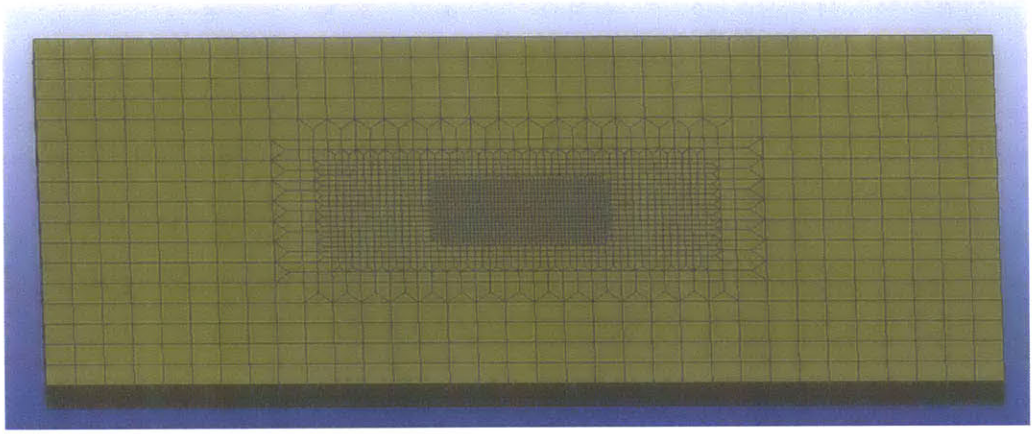

Figure 4-29: Pouch Cell Model

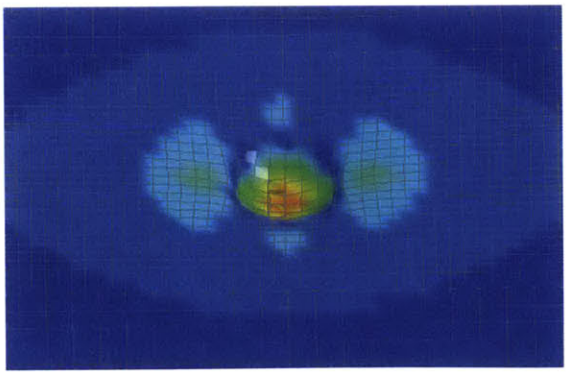

Figure 4-30: Damaged Pouch Cell Model

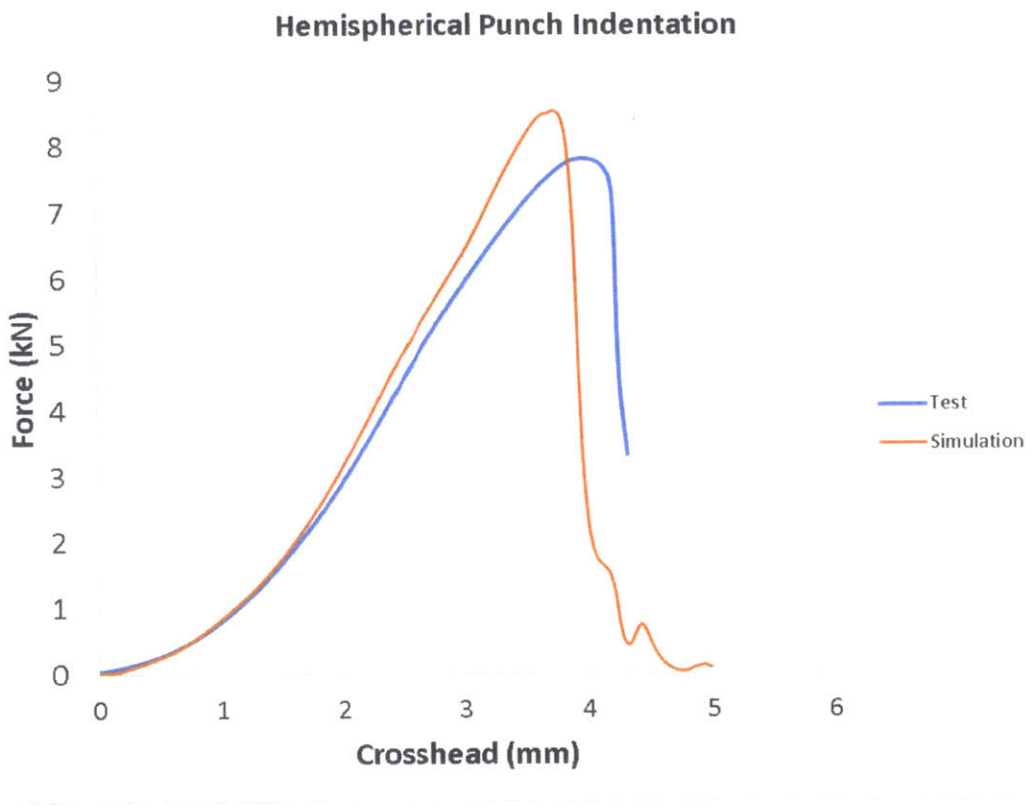

Figure 4-31: Pouch Cell Hemispherical Punch Simulation and Test Results

To further validate the pouch cell model, the hemispherical punch test on the edge of the cell was simulated. Figure 4-32 shows the simulation setup and resulting damage to the model. The force-displacement curve for the simulated edge punch test corresponded to the test results, as seen in Figure 4-33.

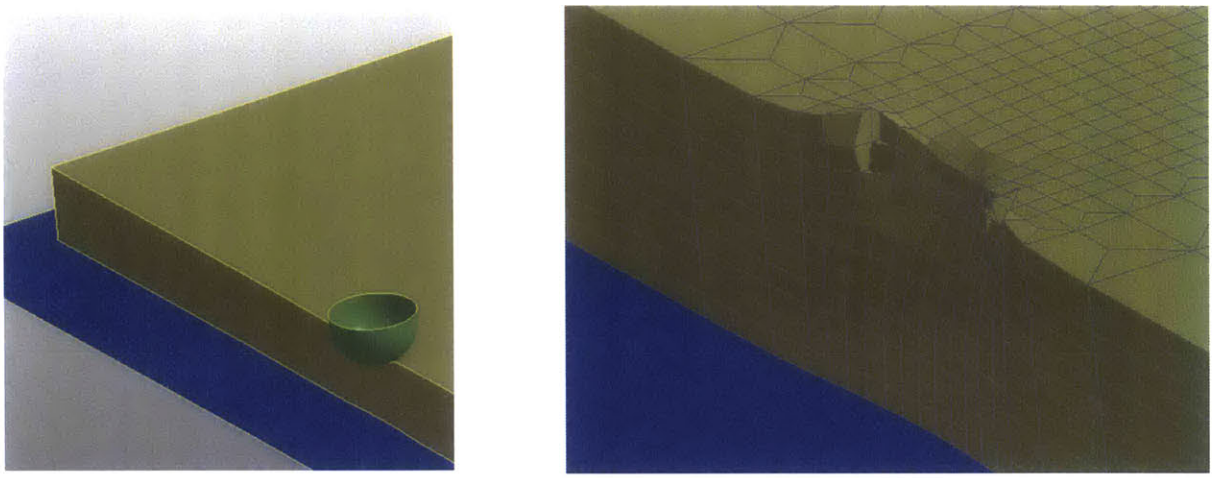

(a) Model Setup

(b) Damaged Pouch Cell Model

Figure 4-32: Pouch Cell Hemispherical Punch Simulation on Cell Edge

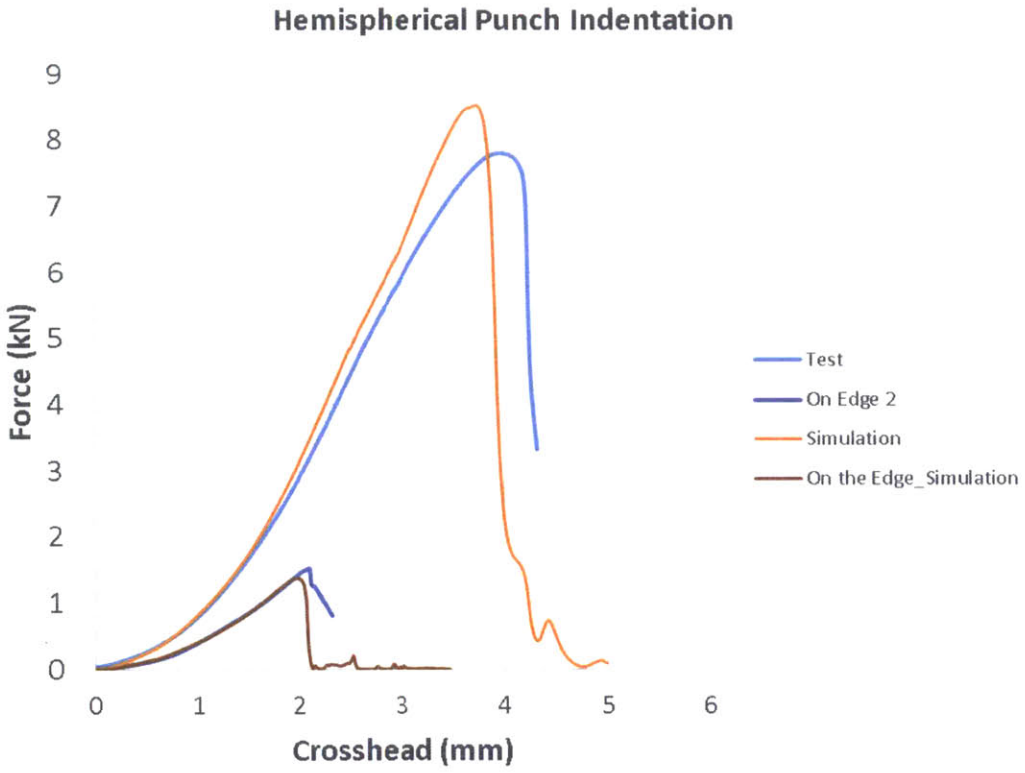

Figure 4-33: Pouch Cell Hemispherical Punch Simulation and Test Results

Chapter 5

Conclusion

The objective of this research was to characterize the mechanical properties of three types of lithium-ion batteries through cell and interior component testing. Prismatic, elliptic, and pouch cells were tested using hemispherical punches to obtain load-displacement curves. Elliptic and pouch cells were also compression tested. The interior components of elliptic and pouch cells were uniaxial, biaxial, and compression tested. Testing results were then used by ICL team members to create, validate, and refine computational models.

5.1 Summary of Results

The results of the hemispherical tests on prismatic cells are summarized in Table 5.1. The results of elliptic cell tests are in Table 5.2, and Table 5.3 is a summary of pouch cell results. Direct comparison of the cell test results is not possible since different tests were performed on each cell type. In addition, elliptic cells were not actual battery cells, but instead dummy cells for testing. Trends were noted, however, between cell types. First, the transverse compression tests had the highest maximum force measurements and were the same order of magnitude for both the elliptic and pouch cells. Second, all tests had maximum force measurements of the same order of magnitude for the 12.5 mm diameter hemispherical punch tests.

Punch Diameter	Maximum Force (kN)	Crosshead (mm)
12.5 mm	4.7	5.3
28.575 mm	13.8	6.8
44.45 mm	29.5	8.1

Table 5.1: Prismatic Cell Hemispherical Punch Test Results

Test Type	Cell Type	Maximum Force (kN)	Crosshead (mm)
Long. Compression	Dry	137	6.5
Long. Compression	Wet	141	6.7
Axial Compression	Dry	10.0	7.0
Axial Compression	Wet	9.6	5.2
Punch at 1mm/min	Dry	8.8	5.4
Punch at 1mm/min	Wet	7.7	5.1
Punch at 20mm/min	Wet	6.7	4.9

Table 5.2: Elliptic Cell Test Results

Test Type	Cell Type	Maximum Force (kN)	Crosshead (mm)
Compression	Dry	173.6	4.8
Punch at 1 mm/min	Dry	7.9	4.0
Punch at 1 mm/min	Discharged	5.4	3.5
Punch at 5 mm/min	Dry	8.1	4.1
Punch at 5 mm/min	Discharged	6.1	3.6

Table 5.3: Pouch Cell Test Results

Tables 5.4 and 5.5 summarize the results of the anode and cathode testing for the elliptic and pouch cells. The elliptic cell anode had higher maximum force measurements compared with the pouch cell anode for all three test types. However, the

elliptic cell cathode had lower maximum force and extension measurements than the pouch cell cathode for the biaxial and compression tests. Both pouch and elliptic cell cathode samples had similar maximum force measurements for the uniaxial tests. The maximum extension measurements for elliptic anode biaxial tests were 75% larger than those for the pouch anode. These results were interesting and showed the large differences in material properties of the coated metal samples from each cell type. These results also contradicted the initial assumption that the bare metal samples from the ellptic cell could be used in pouch interior component micro-models.

Test Type	**Component**	**Maximum Force**	**Extension (mm)**
Uniaxial	Anode	35.4 N	1.4
	Cathode	39.4 N	0.3
Biaxial	Anode	56.2 N	4.2
	Cathode	14.0 N	1.6
Compression	Anode	23.8 kN	0.8
	Cathode	28.7 kN	0.2

Table 5.4: Elliptic Cell Interior Component Test Results

Test Type	**Component**	**Maximum Force**	**Extension (mm)**
Uniaxial	Anode	19.9 N	0.7
	Cathode	37.5 N	0.7
Biaxial	Anode	12.1 N	2.4
	Cathode	25.1 N	2.3
Compression	Anode	22.9 kN	1.1
	Cathode	>66 kN	>1.8

Table 5.5: Pouch Cell Interior Component Test Results

5.2 Conclusions

This research resulted in many conclusions involving the lithium-ion cells, their interior components, and efforts to model the failure of cells. At the cell level, the effect of liquid presence, strain rate, separator type, and test location was studied. The level of experience in sample preparation and testing methods was an important factor for interior component material characterization, as was the varied force-displacement results for different cell types.

The goal of this research, to demonstrate that the material characterization of lithium-ion battery cells through mechanical testing could be used to create, calibrate, and validate cell numerical simulation models, was accomplished. These models successfully predicted load displacement and onset of failure in the jellyroll or electrode stack for both elliptic and pouch cells. Material characterization of cell interior component sheets was also successfully used to create and validate micro-models.

Another notable conclusion from this research was the effect of liquid on cell tests. For the elliptic cells, the addition or omission of polycarbonate from the cells did not significantly effect the load-displacement results. However, the pouch cells with electrolyte had lower force and crosshead measurements compared with dry pouch cells.

The strain rate effect was an important observation during the cell tests. The higher strain rate tests of the pouch cells showed a higher maximum force and crosshead measurements. While the elliptic cell test at higher strain rate did not have a higher maximum force measurement compared with one of the lower strain rate tests, this test was only performed once and could have been related to the difference in interior components between cells.

The influence of separator type in elliptic cell tests was another interesting result. The magnitude of the maximum force difference between elliptic cells with different separator types was significant. The testing results showed that elliptic cells with trilayer separator had higher maximum force measurements.

The effect of testing location was explored through pouch cell hemispherical punch

tests. The resulting force-displacement curves were consistent for all tests except those conducted on the edge of the cell. The edge tests showed a significant decrease in maximum force and crosshead.

For interior component testing, sample preparation and testing procedure was extremely important in obtaining consistent, reliable results. The cutting of samples for uniaxial testing had to be completed in a specific manner, and the application of paper tape was required for coated metal samples. These lessons were learned through testing different methods and carefully documenting the results. In addition, alignment of uniaxial samples and mounting of biaxial samples required focus and experience.

Finally, the varied results of elliptic and pouch cell interior component testing was an important conclusion. Because the anode and cathode materials had very different results, the interior component testing for one cell could not be substituted in the modeling of another cell type. This was significant for creating models and showed that a robust testing program must be completed in conjunction with modeling to capture the full material characterization of the cell and generate reliable results.

Bibliography

[1] Hooked on lithium. *The Economist*, June 2002.

[2] Instron 5940 Series Brochure, 2013.

[3] 653450 Samsung prismatic cell lithium ion battery 3.7v 1230mah, 2014.

[4] Hitachi's High Functional Materials, 2014.

[5] Lenovo Recalls Battery Packs for ThinkPad Notebook Computers Due to Fire Hazard, March 2014.

[6] Lithium-ion Batteries Enhanced by Nanomaterials, April 2014.

[7] Sony Recalls VAIO Flip PC Laptops Due to Fire and Burn Hazards, July 2014.

[8] Li-Polymer 3.7v 3000mah (506090) Battery, 2015.

[9] H. J. Bergveld, W. S. Kruijt, and Peter H. L. Notten. *Battery Management Systems: Design by Modelling.* Springer Science & Business Media, September 2002.

[10] Isidor Buchmann. *Batteries in a portable world: a handbook on rechargeable batteries for non-engineers.* Cadex Electronics Inc., Bristish Columbia, 3rd edition, 2011.

[11] Kyle Miller. Mechanical Characterization of Lithium-Ion Battery Micro Components for Development of Homogenized and Multilayer Material Models. Master's thesis, Massachusetts Institute of Technology, May 2014.

[12] Elham Sahraei, John Campbell, and Tomasz Wierzbicki. Modeling and short circuit detection of 18650 Li-ion cells under mechanical abuse conditions. *Journal of Power Sources*, 220:360–372, December 2012.

[13] Elham Sahraei, Rich Hill, and Tomasz Wierzbicki. Calibration and finite element simulation of pouch lithium-ion batteries for mechanical integrity. *Journal of Power Sources*, 201:307–321, March 2012.

[14] Elham Sahraei, Joseph Meier, and Tomasz Wierzbicki. Characterizing and modeling mechanical properties and onset of short circuit forÂăthree types of lithium-ion pouch cells. *Journal of Power Sources*, 247:503–516, February 2014.

[15] Azadeh Sheidaei, Xinran Xiao, Xiaosong Huang, and Jonathon Hitt. Mechanical behavior of a battery separator in electrolyte solutions. *Journal of Power Sources*, 196(20):8728–8734, October 2011.

[16] Tomasz Wierzbicki and Elham Sahraei. Homogenized mechanical properties for the jellyroll of cylindrical Lithium-ion cells. *Journal of Power Sources*, 241:467–476, November 2013.

[17] Yong Xia, Tomasz Wierzbicki, Elham Sahraei, and Xiaowei Zhang. Damage of cells and battery packs due to ground impact. *Journal of Power Sources*, 267:78–97, December 2014.

[18] Xiaowei Zhang. personal communication.